MYELOPEROXIDASE-MEDIATED BIO-ACTIVATION OF NSAIDS IN LEUKEMIA CELLS: POTENTIAL SELECTIVE CYTOTOXICITY

By

Andrew Morgan

A thesis submitted in partial fulfillment of the requirements for the degree of

DOCTOR OF PHILOSOPHY
IN
PHARMACEUTICAL SCIENCES

Faculty of Pharmacy and Pharmaceutical Sciences
University of Alberta

ABSTRACT

Several lines of evidence have pointed to the potential benefit of anti-inflammatory drugs (NSAIDs) in cancer therapy due to the well-established correlation between cancer and chronic inflammation. Acute myeloid leukemia (AML) cells overexpress myeloperoxidase (MPO), which has been studied for its ability to bio-activate xenobiotics into reactive species with little research done on its potential to be a target in treating leukemic cells. Our main hypothesis is that MPO bio-activation of NSAIDs produce pro-oxidant species that will cause oxidative damage and induce leukemic cell death. To test our hypothesis, a number of biochemical and *in vitro* studies were conducted. In the first two studies, we included four different NSAIDs, namely diclofenac, naproxen, indomethacin and mefenamic acid and we also included their hepatic metabolites and chemical analogues for comparative purposes. We found that MPO was capable of oxidizing certain NSAIDs and their metabolites/analogues to reactive species, which have cytotoxic potential to HL-60 leukemia cell lines through oxidizing GSH and dropping mitochondrial membrane potential and inducing leukemic cell death. Interestingly, even a few structural changes between metabolites and the parent NSAIDs exhibited significant differences in the reactivity of the results species and in their cytotoxic potential *in vitro*. These studies suggest a potential novel approach of modulating leukemia cells oxidative balance and viability by taking advantage of the high expression of MPO and its oxidizing capacity of NSAIDs. Further studies are needed to evaluate the role of MPO expression levels in leukemia cells' response to NSAIDs by using leukemia cells with different levels of MPO expression and to investigate the effect of combining the clinically used chemotherapy

agents with NSAIDs on the potency of the former in eradicating leukemia cells. In our third study, the cell culture pH indicator, phenol red, was found to be oxidized by MPO into free radical species as well as halogenated metabolites that depleted HL-60 cells' glutathione but did not significantly affect cell viability. Phenol red is a phenolic compound that was structurally similar to hydroxylated NSAID metabolites. The latter suggests potential interference of phenol red-containing cell culture media with oxidative stress studies done in MPO expressing cell lines, which mandates cautious selection of cell culture media depending on the nature of the studies.

PREFACE

This thesis is an original work by Andrew Morgan under the supervision of Dr. Arno G. Siraki at the faculty of Pharmacy and Pharmaceutical Sciences, University of Alberta. Parts of this thesis have been previously published, (which is indicated at the beginning of such chapters). The majority of experiments were carried out by Andrew Morgan in Dr. Siraki's lab under his direct supervision. Certain experiments were carried out by other collaborating lab members (Dr. Karim Michail – clinician postdoctoral fellow, Md. Saifur Khan- former PhD graduate, Dr. Dinesh Babu – Postdoctoral fellow, Lindsey Yeon Kyoung Suh – Masters' student, Harunur Rashid – PhD student). Chapter 2 of this thesis has been published as Andrew Morgan *et. al.*, "An evaluation of myeloperoxidase-mediated bio-activation of NSAIDs in promyelocytic leukemia (HL-60) cells for potential cytotoxic selectivity", Toxicology Letters, volume 280, pages 48-56. Chapter 4 of this thesis has been published as Andrew Morgan *et. al.*, "Caution for the routine use of phenol red – It is more than just a pH indicator", Chemico-Biological Interactions, volume 310, 108739. I was responsible for designing and carrying out most of the experiments, data collections and analysis, as well as the manuscripts' write-ups under the supervision of Dr. Arno G. Siraki.

ACKNOWLEDGMENTS

I am so grateful to have completed my PhD studies under the supervision of Dr. Arno Siraki. I was fortunate to work with Dr. Siraki who has been a very supportive, patient and knowledgeable mentor. He provided a unique, friendly work environment that allowed to freely share ideas and suggestions throughout the course of research to continuously improve the quality of our studies. He was a competent leader who was providing guidance and encouraging his lab members to work as a team through giving advice and support on a daily basis, setting an example of a dedicated scientist.

I am thankful to Dr. Ayman El-Kadi and Dr. Dion Brocks, my supervisory committee members for their continuous help and support as well as their interest in my work. Their valuable guidance, discussions and inputs throughout all the committee meetings and the candidacy exam had made it possible to complete my studies in a timely manner.

I also would like to thank and show my appreciation to my former and present colleagues and lab members, Dr, Karim Michail, Dr. Saifur Khan, Dr. Naif Aljuhani, Dr. Dinesh Babu, Lindsey Yeon Kyoung Suh and Md Harunur Rashid for helping me out along the way whenever possible by sharing their expertise and providing all the support and care.

I also would like to acknowledge Alberta Innovate and Natural Sciences and Engineering Research council (NSERC) and University of Alberta for their support. Finally, I owe a debt of gratitude to all my family members and friends for all their support, motivation, encouragement and inspirations.

Andrew Morgan

TABLE OF CONTENTS

ABBREVIATIONS

AML	Acute Myeloid leukemia
ATP	Adenosine triphosphate
CCCP	carbonyl cyanide *m*-chlorophenyl hydrazine
CLL	Chronic lymphocytic leukemia
COX	Cyclooxyegnase
Coxib (s)	Selective COX-2 inhibitor (s)
DMBI	O-desmethyl-N-deschlorobenzoylindomethacin
DMI	O-desmethylindomethacin
DMPO	5,5-dimethyl-1-pyrroline N-oxide
DTPA	Diethylenetriamine-penta acetic acid
EPR	Electron paramagnetic resonance
FAB	The French-American-British classification of AML
FAP	Familial adenomatous polyposis
FBS	Fetal bovine serum
G/GOx	Glucose and glucose oxidase
$GS^{\cdot}$	Glutathionyl radical
GSH	Glutathione
HBSS	Hank's balanced salt solution
HRP	Horseradish peroxidase
HSCs	Hematopoietic cells
MFA	Mefenamic acid
MMP	Mitochondrial membrane potential
Mn-SOD	Manganese-dependent superoxide dismutase
MPO	Myeloperoxidase
NADPH	Nicotinamide adenine dinucleotide phosphate
NEM	N-ethylmaleimide
NSAIDs	Non-steroidal anti-inflammatory drugs

ODN	O-desmethylnaproxen
4'-OHD	4'- hydroxydiclofenac
5-OHD	5-hydroxydiclofenac
OPA	*o*-Phthaldehyde
PBS	Phosphate buffered saline
PR	Phenol red
ROS	Reactive oxygen species
SDS	Sodium dodecyl sulfate
TC1,4-BQ	Tetrachloro-1,4-benzoquinone
UV	Ultraviolet
WBCs	White blood cells

CHAPTER 1

INTRODUCTION

1.1. THE CORRELATION BETWEEN CANCER AND CHRONIC INFLAMMATION

Extensive data have been generated over the years, exploring the longstanding hypothesis that the presence of chronic inflammation at different anatomical sites contributes to the initiation and progression of different types of cancer. This issue was raised after the first observation by Rudolf Virchow in 1863 that neoplastic tissues are infiltrated by leucocytes and the sites of chronic inflammation could be the origin of cancer. In fact, Virchow's work has since then sparked an entire field of cancer research. Later, it was also found that many chronic inflammatory conditions such as pancreatitis, prostatitis and ulcerative colitis can significantly increase the risk for developing pancreatic, prostate and colorectal cancers respectively[1]. Also, chronic inflammation is the common component between cancers that are caused by infectious agents, like *Helicobacter Pylori* and hepatitis B and C. In fact, epidemiological evidence has showed conclusively that chronic infection and other types of chronic inflammation are involved in 15% of all cancers[2]. Both malignant and chronically inflamed tissues have some common hallmarks or transformations that take place in them during tumorigenesis and inflammation processes. These hallmarks include the accumulation of peripheral blood mononuclear cells[3], constitutively induced angiogenesis (formation of new blood vessels, described below), inhibition of apoptosis, increased tissue destruction, DNA damage with unsuccessful DNA repair machinery, and hence genomic instability. It is also believed that in order for growing tumours to survive, they need the macrophages and granulocytes to infiltrate them and release cytokines that would activate the angiogenesis required for acquiring oxygen and nutrients. Not only that, but inflammation is found to promote metastasis and increase the resistance to chemotherapy[4]. Sustained inflammation

can also predispose cells for oncogenic transformation through upregulating of cytokines and chemokines, reactive oxygen species (ROS), overproduction and increased cyclooxygenase-2 (COX-2) and nuclear factor kappa B [5]. Not surprisingly, the unique role of chronic inflammation in the pathogenesis and survival of leukemia has also been the subject of intensive research for the last two decades. It has emerged that for instance, serum levels of pro-inflammatory cytokines, including tumour necrosis factor α (TNF-α), interleukin 6 (IL-6), IL-10 and IL-8 were found to be significantly elevated in chronic lymphocytic leukemia (CLL) patients[6,7,8]. CLL cells are highly dependent on the interactions with its microenvironment for their survival, and that's through a complex network of adhesion molecules, chemokine receptors, and tumour necrosis factor (TNF)[9]. Moreover, constitutive activation of the pro-inflammatory pathways, such as NF-kB and STAT3 in B lymphocytes from CLL patients, have been reported[10]. Similarly, cytokines have a critical role in the proliferation of acute myeloid leukemia (AML). Interleukin-1α (IL-1α) and IL-1β were found to have the most significant effect on *ex vivo* cell growth of AML patients' samples *ex vivo* cell growth. Importantly, the effect was seen in the majority of the samples irrespective of the AML subtypes[11]. Accumulating evidence has led to an increasing interest in evaluating the therapeutic effect of inhibiting various inflammatory pathways in cancer chemoprevention or as an adjuvant to standard chemotherapy[12].

1.2. POTENTIAL THERAPEUTIC BENEFITS OF NSAIDS IN CANCER THERAPY

Interconnections between chronic inflammation and development of different types of cancer have stimulated a huge interest to test the hypotheses that NSAIDs can prevent

the growth of cancer if used prophylactically and/or treat cancer that has already formed if combined with chemotherapeutic agents.

Using NSAIDs for prevention of colorectal carcinoma, in particular, had attracted a lot of attention since high concentrations of prostaglandins were found in colorectal cells but not in the surrounding mucosa [13]; as a result, an expected question was whether or not inhibiting prostaglandin synthesis by NSAIDs could compromise the proliferation of colorectal cancer cells.

Experimental models of chemically-induced colorectal cancer in rats and mice have been used to answer that question, and it was consistently shown that numerous NSAIDs, namely, aspirin, piroxicam, indomethacin, sulindac, ibuprofen, ketoprofen, and celecoxib inhibit the growth of the adenomatous polyps and cancers at early stages of cancer development. Selective COX-2 inhibitors (coxibs) showed superiority by continuing to inhibit tumour development during progression stages. Randomized clinical trials have shown that 6 month of daily use of celecoxib in either low dose of 100 mg twice a day or high dose of 400 mg twice a day significantly reduces the number of the colorectal polyps in patients with familial adenomatous polyposis (FAP) compared to the placebo group[14]. Another shorter trial done on children for 3 months showed that both high and low doses of celecoxib were well tolerated, but only the high dose significantly reduced the number of colorectal polyps[15].

Coxibs, generally, have the advantage of less gastrointestinal toxicity than long-term use of non-selective NSAIDs. Despite the effectiveness, reports of dose-dependent increases in cardiovascular toxicity, including myocardial infarction, stroke, or heart failure had prevented celecoxib from becoming indicated for this use[16]. Likewise, long-

term cohort studies showed that sulindac not only decreases the recurrence of polyps but also suppresses the existing polyps, but was associated with hepatotoxicity[17,18,19]. Moreover, given the potential toxicities associated with the use of NSAIDs, few studies have turned to aspirin as a candidate for chemoprevention in FAP. Aspirin showed moderate chemoprotective effects against colorectal adenomas in the large bowel when used at the cardio-protective oral daily dose of 81 mg, but not the high 325 mg dose [20,21]. In 2011, a larger clinical study was conducted using aspirin 600 mg a day in combination with resistant starch (RS) in patients with FAP; there was no significant reduction in the count of polyps in the colon , but there was a trend towards reduction in the size of the polyps in patients treated with the high dose aspirin versus no aspirin[22]. Overall, despite the appeal of using aspirin given its favourable toxicity profile, the evidence for its effectiveness in FAP is currently not very strong.

In general, NSAIDs can have one of two main modes of action when used in cancer: chemoprotection or chemosensitization. With respect to chemoprotection, several studies have demonstrated that the therapeutic combination of NSAIDs with the conventional chemotherapeutic agents could significantly decrease the toxicity of the latter. For instance, co-administration of celecoxib with docetaxel had resulted in a significantly low incidence of hematological toxicities in hormone-refractory prostate cancer patients[23]. Similarly, celecoxib was shown to decrease capecitabine associated toxicities, hand and foot syndrome and diarrhea, in metastatic breast cancer patients[24]. A more recent study reported a strong association between inflammation and the severity of somatic symptoms, including fatigue, sleep disturbances, drowsiness, dry mouth, lack of appetite,

and pain during remission induction chemotherapy in AML patients[25], suggesting that inflammation is the underlying mechanism[26,27].

With respect to chemosensitization, NSAIDs may act additively or synergistically or sensitize cancer cells to treatment by the conventional chemotherapeutic agents. Celecoxib was found to potentiate cytotoxic effects when combined with doxorubicin, etoposide, irinotecan and etoposide[28]. Aspirin also was reported to sensitize human breast cancer cells to chemotherapy[29]. Also, combining erlotinib with celecoxib was reported to be an effective chemopreventive approach for patients at high risk of developing head and neck cancer[30]. Concurrent use of aspirin, but not other NSAIDs, with the fludarabine-cyclophosphamide-rituximab (FCR) regimen was associated with improved progression-free survival (PFS) and overall survival (OS) in patients with relapsed CLL[31].

A significant amount of research has been done to delineate the underlying pharmacology of the anti-cancer actions of NSAIDs. Mechanistic studies suggested two mechanisms by which NSAIDs could repress tumorigenesis. These are restoring cell apoptosis and inhibiting angiogenesis. Apoptosis is an intrinsic, highly complex programmed cell death that is essential to maintain cell homeostasis by disposing of damaged cells in an orderly manner. Apoptosis acts as a natural barrier to cancer development , and for that, tumour cells have to evolve numerous strategies during tumorigenesis to hinder apoptosis in order to gain replicative immortality[32]. Selective COX-2 inhibitors were found to stimulate apoptosis and suppress growth in many cultured human cancers of colon, stomach, tongue, pancreas, brain and lung. Despite the evident findings of this effect in different cancer cell lines, the precise mechanism by which apoptosis is induced by NSAIDs is not completely understood. Although several

studies pointed towards the inhibition of prostaglandin synthesis to be the possible main mechanism, other studies indicate the involvement of other COX-2 independent pathways[33,34,29]. For example, sulindac sulfone was found to inhibit colon cancer both *in vitro* and in rats without inhibiting prostaglandin synthesis[35,36].

The second cellular mechanism by which NSAIDs may inhibit tumour proliferation is by inhibiting angiogenesis. Angiogenesis is the formation of new blood vessels from existing ones, a process that is continuously overactive in tumour tissues[32]. Angiogenesis is essential for cancer since the proliferation, as well as metastatic spread, depends on an adequate supply of oxygen and nutrients and the removal of waste products[37]. COX-2 is highly expressed in angiogenic vasculature of colorectal adenomatous polyps and in carcinomas of colon, lung, breast, esophagus, and prostate[38]. Selective COX-2 inhibitors suppress the growth of human tumours transplanted into mice[39]. Such findings suggest that COX-2 may be essential for tumour neovascularization. Cell cycle arrest is the third mode of action of NSAIDs in cancer cells, suggested in more recent studies of celecoxib in nasopharyngeal carcinoma cells and in head and neck squamous cell carcinoma[40,41].

At this present time, the real clinical debate is whether to use NSAIDs for chemoprevention for a long period of time or to use it for treatment, which would be for a shorter time. The last studies showed that the risk of cardiovascular and kidney disease, accompanied by the long-term use of coxibs outweigh the potential benefit. Moreover, high-risk patients (good candidates for the chemoprevention) only represent a small fraction of all cases of cancer. In other words, the vast majority of people would not benefit if treated prophylactically by coxibs. For those reasons, some NSAIDs may be better suited to be used as adjuvants in treating cancer, rather than preventing it, because

there would be fewer side effects associated with the short-term use, and then the risks would be minor compared to the benefit of improving patient prognosis and clinical outcomes. Nevertheless, health organizations have been appropriately withholding any recommendation regarding the use of NSAIDs for prevention or treatment of cancer until answering fundamental questions about their safety and efficacy, and optimal regimens.

1.3. BACKGROUND ON ACUTE MYELOID LEUKEMIA (AML)

1.3.1. AML Pathophysiology

Leukemia encompasses a heterogeneous group of cancers that starts in the bone marrow causing overproduction of abnormal blood cells (called blasts or leukemia cells) that rapidly accumulate and overtake the healthy bone marrow leading to a reduction in the production of normal blood cells. In healthy bone marrow during hematopoiesis, the bone marrow makes hematopoietic stem cells (HSCs), (also called pluripotent hematopoietic stem cells), and HSCs give rise to all different types of blood cells. Generally, the early blood-forming cells could be either one of two main lineages, lymphoid or myeloid. Lymphoid stem cells differentiate into lymphocytes, which can be further classified into T cells, B cells and natural killer cells. Myeloid cells, on the other hand, give rise to a variety of cells, including red blood cells, platelets and WBCs (neutrophils, monocytes, eosinophils, and basophils). Leukemia develops as a result of maturation arrest of HSCs at their earliest stages of development, resulting in clonal expansion and accumulation of those immature progenitor cells without further terminal differentiation and apoptosis as seen in normal blood cells.

Leukemia can broadly be classified into four types, acute lymphocytic leukemia (ALL), acute myelogenous leukemia (AML), chronic lymphocytic leukemia (CLL) and chronic myelogenous leukemia (CML). Whether leukemia is lymphocytic or myelogenous depends on which stage the bone marrow cells were at when the cancerous transformation took place, and each type of leukemia can be acute or chronic depending on how fast the disease progresses. In acute leukemia, the majority of cells are immature (blasts), and they multiply more rapidly, which makes the disease worsen quickly. Acute leukemia, therefore, requires more aggressive, timely treatment. Chronic leukemia, however, involves more mature blood cells that accumulate more slowly and could still function normally for a period of time[42]. AML patients range from newborns to elderly, but the prevalence increases with age with the median age of onset being 70 years old. AML is overall a rare disease (representing 1% of all cancers according the American Cancer Society), but it is still one of the most common types of leukemia in adults, representing about 32% of adult leukemia cases[43].

At the point of diagnosis, cytopenias are often seen in AML patients due to low number of normal blood cells, which explains the signs and symptoms of fatigue, anemia, fever and signs of infections due to neutropenia, despite the apparent elevated total WBC count, also easy bleeding and bruising as a result of thrombocytopenia are common. WBC count can sometimes be extremely high (>100,000 cells/μl) at the time of diagnosis and patients can then present with symptoms of leukostasis (i.e. respiratory and neurological distress) which is caused by leukocytes plugs that block delivery of oxygen to critical body tissues[44]. The work up to diagnose leukemia and first differentiate AML from ALL and to classify subtypes of AML is usually based on a combination of

morphologic, cytochemical, immunogenic, and cytogenic criteria. A presumptive diagnosis of AML can be made when circulating blasts in the peripheral blood smear are beyond 20%, then a confirmatory diagnosis usually requires bone marrow aspiration and biopsy[45]. Although the precise mechanism of HSC's maturation arrest that happens in leukemia is not fully understood, it is believed that accumulation of DNA lesions and inefficient DNA repair mechanisms in HSCs and progenitor cells over time play a major role in acquiring key mutations and altering the differentiation fate of these stem cells [46,47,48,49]. Furthermore, these mutations have a high prognostic value and are used in identifying high-risk patients, and hence, requiring more aggressive therapeutic interventions[50,51]. It is well known that HSCs are found in the bone marrow in specialized niche microenvironments that are critical for their maintenance and functions[52].

In addition to HSCs, bone marrow contains mesenchymal stem cells, which generate bone, cartilage, muscle, and fat cells. Recent studies showed that genetic mutations in the mesenchymal stem cells located in the bone marrow tumor microenvironment can induce malignant changes in HSCs, increasing the risk of leukemia in mice. RNA sequencing of mesenchymal cells from mice and leukemia patients with pre-leukemic syndromes revealed that mesenchymal cells, in these disorders, are under stress, and secrete inflammatory molecules called S100A8 and S100A9, which drive mitochondrial and DNA damage in HSCs and progenitor cells[53]. Interestingly, a correlation was found between activation of this inflammatory pathway in mesenchymal cells and the development of leukemia as well as clinical outcomes in human patients[54]. Such findings are of major clinical relevance to the pathogenesis of leukemia and bone marrow failure and are further evidence of inflammation in the

malignant transformation of HSCs. Although whole genome sequencing revealed that AML genomes have only a total of 23 genes that were significantly mutated[55], many mutations have not been characterized because of the heterogeneity in the genetic abnormalities driving AML, which also has been posing a major challenge to the clinical translation of selective inhibitors to the pathways affected by these genetic perturbations. Therefore, an ideal scenario is to target a critical unifying mechanism(s) required for AML progression, irrespective of the diverse genetic and molecular abnormalities.

1.3.2. AML classification

AML is a variable and complex disease with different subgroups based on how mature the leukemic blasts are at the time of diagnosis and how different they are from normal cells. These leukemic groups are not only different in the clinical and laboratory findings, but also in the patient response to therapy and their prognosis. That is why it was critical to have an objective system that unifies the definitions of AML subclasses that were, at the time, not distinctly characterized. The first proposed system of classification was published in 1976 by the French-American-British (FAB) group[56]. The FAB proposal was widely accepted by clinicians as it had a quantitative element that introduced some objectivity to the AML workup after being regarded as mostly subjective, and it was mainly based on the morphological appearances, cytological features (percentage of maturing myeloid cells and monocytic component) in films of peripheral blood and bone marrow aspirates. Three subtypes of ALL (L1, L2 and L3) and six types of AML (M1 to M6) were characterized. Briefly, the first three subtypes (M1, M2 and M3) all predominately have granulocytic differentiation, yet differ from one

another in the nature and extent of granulocytic maturation. M4 shows both granulocytic and monocytic differentiation. M5 is dominated by monocytic differentiation and usually requires cytochemical confirmation. Finally, M6 (erythroleukemia) has the majority of the blasts (more than 50%) show evidence of erythropoietic differentiation. A few essential cytochemical tests were of diagnostic value and were recommended to be used routinely in the investigation of every new case of acute leukemia. These are MPO and Sudan Black B (SBB) and non-specific esterase (NSE) staining. MPO is synthesized in the azurophilic granules of myeloid cells during the early stages of differentiation. Therefore, MPO is only present in cells descending from the myeloid lineage. MPO has a key diagnostic value to distinguish between AML and ALL cells that lack MPO. More precisely, the presence of more than 3% MPO-positive blasts is diagnostic of acute myeloid leukemia (AML). Moreover, the MPO test is used to establish the identity of AML subtype as the percentage of MPO positive blasts would vary from one subtype to another[57].

Subsequent revisions then followed the initially introduced FAB proposal and two more forms of AML were added. In 1985, M7 (megakaryoblastic leukemia) was characterized[58], this subtype has that the majority of the leukemic cells originating from the megakaryocyte (platelet-forming) lineage. Then in 1987, a criterion for M0 was added to the FAB list of AML[59]. It is called AML with minimum differentiation since the blasts in M0 cannot usually be recognized as myeloid by the morphological or cytochemical features, but it requires verification by using antibodies to MPO and antibodies to CD13, CD33 and CD34. Immunophenotyping, therefore, has become

another essential diagnostic tool for AML due to its accuracy and efficiency in defining the hematological lineage involved in the malignancy[60,61].

Another commonly used scheme for AML classification is the one proposed by the World Health Organization (WHO). Although the FAB system is still widely used, the WHO classification might be more clinically useful in terms of providing more meaningful prognostic tools[62]. The WHO system not only includes morphologic, cytochemical and immunophenotypic features but is also increasingly based on identifying recurrent genetic criteria in different AML subgroups that highly correlate them to patient's prognosis and risk stratification[63]. According to WHO, the diagnosis of AML is established if 20% of the blood and/or bone marrow cells have been replaced by leukemic myeloblasts, whereas the FAB criteria require a blast percentage of at least 30% AML diagnosis to be considered. Most recently updated WHO classification in 2016 has 7 subtypes of AML, and they are as follows: AML with recurrent genetic abnormalities (gene or chromosome changes), AML with myelodysplasia-related changes, therapy-related myeloid neoplasms, myeloid sarcoma, myeloid proliferations related to Down syndrome and mixed phenotype acute leukemias (MPALs).

1.3.3. Current pharmacotherapy & challenges

Cytotoxic chemotherapy has remained the standard of care of AML treatment over the years. Treatment of AML is divided into two phases: induction and consolidation (or postremission). The goal of therapy during induction is to achieve remission by reducing the number of leukemia cells to an undetectable level. The induction standard regimen is called "7+3" and it is a combination of a continuous infusion of cytarabine for seven

consecutive days with the co-administration of anthracycline on the cycle first three days as IV bolus[64]. Within days, chemotherapy can remarkably lower the leukemic cell burden in the circulation, but in case of patients presenting with symptoms of leukostasis (as described in section 1.3.1.), leukapheresis (the separation of white blood cells from whole blood) might be needed before starting chemotherapy as a life-saving measure. The remission achieved during induction is not curative and neither does it mean the complete elimination of leukemia cells. So, consolidation has to follow the induction to destroy the residual leukemia cells and help prevent relapse. For young patients (<60 years old), a consolidation regimen consists of 3 or 4 cycles of high doses of cyatarabine given over 5 days and repeated every 4 weeks. Whereas, for older patients with comorbid medical conditions, they either still cautiously receive the high cytarabine monotherapy (but not as high as in young patients) or get a combination of a standard cytarabine dose along with an anthracycline (e.g. idarubicin or daunorubicin or mitoxantrone). For very frail patients, chemotherapy induction and consolidation regimens are more conservative and often use low-intensity chemotherapy such as low-dose cytarabine, azacitidine or glasdegib. Leukemia is considered in remission if the blasts in the bone marrow biopsy, done a week after the chemotherapy round, are no more than 5% of bone marrow cells. 70% of AML patients (with favourable risk) achieve remission after the first round of chemotherapy. However, patients who fail to achieve remission after primary induction chemotherapy might need another chemotherapy round or hematopoietic stem cell transplantation[65].

The major challenge of the currently used chemotherapeutic regimens is the large number of adverse effects. The majority of agents target rapidly proliferating cells,

causing collateral damage in various host tissues, primarily the gastrointestinal tract and bone marrow. Other toxicities arise as a result of the accumulation of the agent in a particular anatomic region (e.g. cardiovascular system or liver). These side effects limit the dose that can be given, and significantly reduce the patient's quality of life. Other challenges include that 10 to 40% of AML patients have a treatment-resistant disease[66]. Relapse is unfortunately common, and long-term survival is rare. Another challenge is that despite the growing knowledge of AML biology, its genetic heterogeneity, and its distinct subclasses, there is no subtype-specific or tailored AML therapy for every case, but instead, treatment protocols are uniform irrespective of the classification. That is why there is a need for innovations that target the vulnerabilities that are applicable across AML subtypes.

1.4. NSAIDS PHARMACODYNAMICS AND PHARMACOKINETICS

1.4.1. General mechanism of action of NSAIDs

NSAIDs are among the most widely prescribed class of medications for pain and inflammation[67]. They are used for symptomatic relief of painful inflammatory conditions including osteoarthritis, rheumatoid arthritis, gout, headaches, dental and postoperative pain and dysmenorrhea. NSAIDs exert their anti-inflammatory activity by the inhibition of the cyclooxygenase (COX) enzyme, also known as prostaglandin-endoperoxide synthase, which is the key enzyme that mediates the biosynthesis of prostaglandins from arachidonic acid[68]. Arachidonic acid is a 20-carbon unsaturated fatty acid, which, under normal conditions, is found embedded in cell membranes. Free arachidonic acid is

released from the plasma membrane in response to a wide variety of inflammatory stimuli by the action of the membrane-bound enzyme phospholipase A_2 (PLA_2) and then metabolized in two steps by the bifunctional COX enzyme. First, arachidonic acid is oxidized to the cyclic endoperoxide PGG2, which is then reduced to PGH_2 by the enzyme's peroxidase activity. Those are the two common initial steps from which different prostanoids are then metabolized by terminal synthases and isomerases in various tissues into biologically active prostaglandins[69] (Fig.1).

There are five primary bioactive prostaglandins (PGs): prostaglandin D_2, prostaglandin E_2, prostaglandin $F_{2\alpha}$, prostaglandin I_2 and thromboxane A_2. The letters of prostaglandins stand for different intermediates along the biosynthesis process, and the number indicates the number of double bonds in the molecule. Prostaglandins are degraded rapidly and therefore have a short half-life, and their actions are limited only to the nearby cells as autocrine lipid mediators to maintain local homeostasis. Even though PG functions are not fully understood, they are known to be involved in the induction of inflammation, pain signals and fever as well as platelet aggregation and smooth muscle contraction and relaxation. It is believed that they can either exert actions by activating G- protein-coupled surface receptors or by activating nuclear receptors and modulating gene transcription[70]. PG levels are usually very low in uninflamed tissues. However, both their biosynthesis and activity dramatically increase during acute inflammation and due to their vasodilation effect, they play a major role in developing four out of the five cardinal signs of inflammation (pain, heat, redness and swelling)[71].

In humans, there are two distinct isoforms of COX enzymes, namely COX-1 and COX-2, each produced by a different gene. COX-1 gene is located on chromosome 9,

whereas COX-2 on chromosome 1. Both have a molecular weight of 70 kDa and similar Km and Vmax values for their reaction with arachidonic acid. COX-1 is a constitutive enzyme that is constantly synthesized in most tissues. It is believed to be responsible for the production of PGs that do "housekeeping" functions. COX-1 is primarily found in blood platelet and gastrointestinal tract. In platelets, it mediates the synthesis of thromboxane A_2 that is responsible for platelet aggregation. So, inhibition of COX-1 would lead to loss of the platelet aggregation function. Mucosaprotective prostaglandins in the gastrointestinal tract were long believed to be produced exclusively by the action of COX-1, and thus inhibition of COX-1 and prostaglandins production in gastric mucosa is considered responsible for the most common side effect of NSAID, which is gastric ulceration[72]. Lastly, COX-1 produces the prostaglandins in the kidney that are responsible for total renal blood flow, Na^+ and water reabsorption and renin release. That explains NSAIDs' renal adverse effects of lowering the glomerular filtration rate and opposing the pharmacological effects of blood pressure medications due to Na^+ and water retention. In contrast, COX-2 is an inducible enzyme that plays a major role in the production of PGs associated with inflammation, tissue damage and malignant transformation[73]. Although constitutive expression of COX-2 had been observed in kidneys and central nervous system[74,75], its expression in other tissues only greatly increases in response to cytokines, hormones, growth factors or hypoxia. A third isozyme, COX-3, was discovered in 2002[76]. It is a product of the same gene as COX-1, but it retains an intron that is not found in COX-1[76].

NSAIDs can be classified based on their relative inhibition of each of the COX isozymes into selective COX-1 inhibitors, non-selective COX inhibitors, and selective

COX-2 inhibitors. In general, the extent to which the NSAID inhibits a particular COX affects its activity and toxicity. A classic example of selective COX-1 inhibitors in platelets is aspirin. When given at a low dose (75 to 81 mg/day), it irreversibly acetylates serine-530 of the COX-1 active site, which sterically prevents the arachidonic acid oxidation. Aspirin provides an antithrombotic effect for the life span of the platelet (7-10 days) by inhibiting the production of thromboxane A_2, which is used prophylactically for the prevention of cardiovascular events. However, aspirin inhibits both COX-1 and COX-2 at higher doses of 650 mg to 4 g/day providing analgesic and antipyretic effects due to inhibition of prostaglandin production[77]. Non-selective NSAIDs inhibit both COX-1 and COX-2. This class causes both platelet aggregation and gastrointestinal and renal side effects[78]. The non-selective class is comprised of conventional NSAIDs, e.g. diclofenac, indomethacin, piroxicam, ibuprofen, naproxen as well as high-dose aspirin. COX-1 and COX-2 enzymes are different in their structure, where three amino acid differences result in COX-2 having a larger hydrophobic channel at the active site. These differences include: a) the presence of valine at positions 523 and 434 in COX-2 instead of the bulkier isoleucine in COX-1; b) the exchange of histidine for arginine at position 513 of COX-2, which allows interaction with more polar substrates. These differences allow for the selective inhibition since drugs with large substituents would only access the COX-2 active site and not COX-1 whose active site is more restricted[79]. Selective COX-2 inhibitors are relatively newer developed NSAIDs, designated “coxibs” by the WHO[80]. They were developed to suppress prostanoid formation by blocking COX-2 induction in response to inflammation while sparing the protective effect of COX-1 on gastric epithelium and kidney and thus reducing the side effects associated with the nonselective

NSAIDs. Even though large scale clinical trials showed a significant reduction of gastrointestinal side effects in patients using coxibs compared to non-selective NSAIDs[81,82], the major problem with these medications was that their use was associated with a significant increase of cardiovascular risk[83]. The pharmacological effects of NSAIDs are therefore complicated by the diverse functions of prostanoids in different tissues and hence, variable effects on COX inhibition.

NSAIDs can also be classified based on their chemical structure into five major chemical classes, salicylate derivatives (e.g. aspirin and diflunisal), acetic acid derivatives (e.g. diclofenac, indomethacin, etodolac, ketorolac and sulindac), propionic acid derivatives (e.g. ibuprofen, S-naproxen, ketoprofen, fenoprofen and flurbiprofen), anthranilic acid derivatives or fenamates (e.g. mefenamic acid, meclofenamic acid) and enolic acid derivatives (oxicams) (e.g. piroxicam and meloxicam). Generally, for an NSAID to be an effective competitive inhibitor of COX enzymes, it has to mimic the natural substrate (arachidonic acid) in being highly lipophilic and acidic. So, the general structure of NSAIDs has to have an acidic moiety, either carboxylic acid or enol, attached to an aromatic group, which makes most NSAIDs strong organic acids with pKa ranging from 3 to 5. The presence of the acidic group is essential for binding to the COX active site. It also serves as a major site for ionic binding with plasma proteins and for phase II metabolism by glucuronidation[84]. The acidic group in NSAIDs structure is partly responsible for the irritation of the gastric mucosa, commonly associated with the use of this class. Lots of research has been done to develop NSAIDs' prodrugs where the carboxylic group is masked by conjugation or esterification to lower the gastrointestinal side effect, while sparing the pharmacological activity[85]. In general, NSAIDs have many

common pharmacokinetic properties but they still have considerable differences in some of the clinically important disposition parameters. NSAIDs are well absorbed orally and rectally, but only small amounts are absorbed topically. However, their rate of oral absorption is quite variable, and it slows down if the dose is taken with meals. Like many acidic drugs, NSAIDs are highly bound to plasma proteins (>90%), and thus have a relatively small volume of distribution (V_d). Most NSAIDs are eliminated through extensive hepatic metabolism by CYP2C9 and glucuronidation into inactive metabolites, followed by renal excretion. NSAIDs, however, are variable in two main aspects. First is their half-lives ($T_{1/2}$), which is the time required for the plasma concentration of the drug to be reduced by half of its original value. NSAIDs can either have a short half-life (less than five hours) or a long half-life (more than five hours)[86].

1.4.2. Diclofenac

Diclofenac is an acetic acid derivative NSAID indicated as an analgesic and anti-inflammatory agent for osteoarthritis and rheumatoid arthritis, and it is also used in dysmenorrhea, ocular inflammation and ankylosing spondylitis. It is a non-selective inhibitor of both COX-1 and COX-2, which leads to the peripheral inhibition of prostaglandins[87]. It is available as sodium or potassium salts as oral tablets or solutions. Its sodium salt is also available as a suppository, topical gel, and ophthalmic solution. When given orally, it is completely absorbed from the gastrointestinal tract. However, due to first-pass metabolism, only 50% of the dose will be systemically bioavailable. Like other NSAIDs, it is highly bound to plasma proteins (more than 99%), mainly to albumin resulting in a volume of distribution of 1.3 L/Kg. The elimination half-life of diclofenac is 1.8 h. Diclofenac is metabolized by the liver by oxidation mainly by

CYP2C9 and CYP3A4 to a lesser extent, producing two major inactive metabolites, 4'-hydroxydiclofenac (4'OHD) and 5-hydroxydiclofenac (5-OHD) and other minor metabolites as 4',5-dihydroxydiclofenac and 3'-hydroxydiclofenac and 3'-hydroxy-4'-methoxydiclofenac may also result. 4'-OHD and 5-OHD can then be further metabolized to reactive quinone imines that can form protein adducts which were proposed to be implicated in the rare liver injury associated with diclofenac use[88,89]. Diclofenac can also readily undergo glucuronidation at the carboxylic group to form diclofenac acyl glucuronide, which is also a reactive metabolite that could be involved in diclofenac induced hepatotoxicity[90]. Plasma clearance of diclofenac is 263 ± 56 mL/min[91].The urinary and biliary excretion of glucuronide conjugates of metabolites also occurs. The diclofenac dose excreted in the urine is 65%, and 35% in the bile as glucuronide conjugates of the parent molecule or the metabolites. Little to no free unchanged diclofenac is excreted in the urine[92].

1.4.3. Indomethacin

Indomethacin is an indole-acetic acid derivative with the chemical name 2-[1-(4-chlorobenzoyl)-5-methoxy-2-methylindol-3-yl] acetic acid. It is indicated to treat mild to moderate pain and inflammation in rheumatoid arthritis, ankylosing spondylitis, osteoarthritis as well as gout acute attacks. It acts mainly by inhibiting the peripheral biosynthesis of the inflammatory mediators, prostaglandins, from arachidonic acid. Indomethacin is a nonselective reversible inhibitor of both COX-1 and COX-2, with greater selectivity towards the constitutive COX-1, which accounts for its higher incidence of gastric adverse events relative to other NSAIDs, which makes it less

favourable for chronic use unless a cytoprotective agent (e.g. proton pump inhibitor or misoprostol) is co-prescribed. In addition to its primary mode of action, Indomethacin was also found to inhibit phospholipase A2, thus inhibiting the release of AA from cell membrane in response to inflammatory stimuli. Moreover, indomethacin has an additional mode of action for relieving migraine headaches by causing vasoconstriction of intracranial capillaries[93]. Indomethacin is available as an oral capsule or rectal suppository. After oral administration, indomethacin is completely absorbed and follows a linear pharmacokinetic profile where its plasma concentrations and area under the curve (AUC) change by changing the dose. Indomethacin reaches the peak concentration of 2 to 3 μg/ml after only 2 h with more than 90 % of the dose absorbed after 4 h[94,95]. Indomethacin has a volume of distribution ranging from 0.34 to 1.57 L/Kg due to its strong ionic binding to plasma albumin. Plasma clearance of indomethacin ranges from 0.044 to 0.109 L/kg/hr[96]. Indomethacin undergoes extensive hepatic metabolism mediated mainly via CYP2C9 and glucuronosyl transferases. Major phase I metabolites are O-desmethyl-indomethacin (DMI), N-deschlorobenzoyl-indomethacin and desmethyldeschlorobenzoylindoemthacin (DMBI). These metabolites then get conjugated via glucuronidation into pharmacologically inactive, easily excreted conjugates[97]. Indomethacin metabolism also involves direct glucuronidation of the carboxylic group. DMBI was reported to be bioactivated into a reactive iminoquinone that could be implicated in indomethacin-induced idiosyncratic adverse events[98]. Glucuronide metabolites are then excreted into the bile where they get hydrolyzed followed by the reabsorption of the indomethacin parent through enterohepatic circulation[99]. The other main route of excretion is through the kidneys, which is responsible for excreting 60% of

indomethacin oral dose, while the remaining 40% is excreted in feces after biliary secretion. Indomethacin disposition in the plasma was reported to be biphasic, with an initial phase of 1 h half-life followed by a second phase with a much longer half-life ranging from 2.6-11.2 hours second phase. The mean half-life of oral indomethacin is estimated to be 4.5 h which increases in the elderly population.

1.4.4. Naproxen

Naproxen is a popular over-the-counter (OTC) NSAID. It belongs to the 2-arylpropionic acid (profen) family. It is widely used in the management of rheumatoid arthritis, osteoarthritis, ankylosing spondylitis, polyarticular juvenile idiopathic arthritis, tendinitis, bursitis, acute gout and primary dysmenorrhea. Like other NSAIDs, the pharmacological activity of naproxen can be attributed to the inhibition of COX, The α-methyl substituent in naproxen structure increases its cyclooxygenase inhibitor activity[100]. Naproxen structure possesses one chiral center, which results in two optically active isomers and it was found that the S-enantiomer is more pharmacologically active than the R-enantiomer, which led to marketing the pure S-enantiomer[101]. Naproxen is available as a free acid and a sodium salt (naproxen 500 mg equals to 550 mg naproxen sodium). Both forms are similar in their pharmacokinetic profiles, and only differ in their rate of absorption. Naproxen sodium dissolves more rapidly in the stomach, which makes it reach peak plasma concentration after only 1 h compared to 2 h with naproxen free acid[102,103]. Naproxen is lipid soluble, and thus rapidly and completely absorbed after oral administration, it follows linear pharmacokinetic, as its area under the curve (AUC) is directly proportional with the administered dose. Naproxen is a nonselective inhibitor that blocks both COX-1 and COX-2[104]. Naproxen has a volume of distribution of 0.16 L/Kg

because of the high protein binding. Clearance of naproxen is 0.13 mL/min/kg[105]. Naproxen is heavily metabolized in the liver and undergoes phase I and II metabolism. The first step is demethylation of naproxen via CYP 1A2, 2C8 and 2C9 into 6-O-desemthyl naproxen. Both parent and desmethyl naproxen proceed to form acyl and phenolic glucuronide conjugates. Desmethyl naproxen also undergoes conjugation by sulphation. After oral administration, almost all of naproxen and its oxidative desmethyl metabolite and their corresponding conjugates can be recovered in the urine. Less than 3% of naproxen is excreted in the feces. The half-life of naproxen is reported to be 12-17 h, allowing once or twice daily regimens. Steady state plasma concentration is usually reached in 4 to 5 days.

1.4.5. Mefenamic acid

Mefenamic acid (MFA) is an anthranilic acid derivative. It is used for symptomatic treatment of mild to moderate pain in arthritis and postoperative and post-traumatic pain, dental pain and also for the treatment of primary dysmenorrhea and associated migraine headache[106]. It exhibits anti-inflammatory, analgesic, and antipyretic activity through potent nonselective inhibition of both COX-1 and COX-2. MFA is typically orally administered as capsules; it is rapidly absorbed after oral administration, attaining its peak plasma concentration in 1-2 h. MFA has been reported to be more than 90% bound to albumin, resulting in a volume of distribution of 1.06 L/kg. CYP2C9 mainly metabolizes MFA in the liver into 3-hydroxymethyl MFA that could be further oxidized to 3-carboxymefenamic acid. MFA can also be glucuronidated directly. Plasma clearance of mefenamic acid is 21.23 L/h[107]. MFA and its metabolites are primarily excreted through the kidneys. About half of a MFA acid dose is excreted into the urine primarily

as MFA glucuronides (6%), 3-hydroxy MFA (25%) and 3-carboxy MFA (21%). The fecal route of elimination accounts for up to 20% of the dose, mainly in the form of unconjugated 3-carboxymefenamic acid. The elimination half-life of MFA is approximately two hours[108].

1.5. ROLE OF MYELOPEROXIDASE IN THE IMMUNE SYSTEM AND XENOBIOTICS METABOLISM

Myeloperoxidase (MPO) is a heme peroxidase, most abundantly present in neutrophils, monocytes, and under pathological conditions, in macrophages. Neutrophils play a critical role in defending against microbial attacks as part of the innate immune system[109]. Neutrophils, as granular phagocytes, ingest bacteria into phagosomes, where they direct an arsenal of antibacterial proteins. MPO is the most abundant antimicrobial protein in the neutrophils, representing 5 % of cellular dry weight[110]. MPO is stored in the primary azurophilic granules in neutrophils. During phagocytosis, MPO is released from the activated neutrophils into the phagosomes through a process called degranulation. When MPO was initially purified, it was called verdoperoxidase due to its intense green colour. MPO biosynthesis takes place during the early stages of neutrophil development, particularly starting at the promyelocytic stage up until the myelocyte stage. Human monocytes also contain MPO that only comprises 0.9% by their dry weight. MPO is usually lost during the maturation of monocytes into macrophages. However, MPO was found in macrophages in some pathological conditions[111,112]. Eosinophils also have another peroxidase in their cytoplasmic granules, eosinophil peroxidase, and it is structurally and functionally distinct from MPO despite the

similarity in about 70% of their amino acids' sequence[113]. MPO has a molecular mass of 150 kDa. It consists of two light chains and two heavy chains bound to a prosthetic heme group. MPO on its own has no antimicrobial activity until its catalytic cycle gets triggered by H_2O_2; then it exerts its antimicrobial activity through the production of different reactive oxygen and nitrogen species. MPO has two catalytic cycles, peroxidation and halogenation (Fig. 2). In the presence of H_2O_2, the ferric form of the native enzyme (MPO-Fe^{3+}) is oxidized into the reactive MPO compound I (MPO$^{\bullet+}$-Fe^{4+}=O) (reaction 1, Fig.2). Compound I can be recycled back to the native enzyme through two pathways, one is the halogenating cycle, where it catalyzes the oxidation of halide ions (Cl^-, Br^-, I^-) to the corresponding hypohalous acid (HOCl, HOBr and HOI) (reaction 2, Fig.2). Hypochlorous acid (HOCl) is an extremely efficient antimicrobial agent [114,115] that was also found to bio-activate several biological molecules into free radicals, a process that was believed to contribute to different pathological conditions[116]. Alternatively, in the presence of an electron donor substrate (AH) (e.g. tyrosine, ascorbate, urate or aromatic xenobiotics), MPO compound I could also be turned into compound II (MPO-Fe^{4+}-OH), by catalyzing one-electron oxidation of AH forming A$^{\cdot}$ radicals (reaction 3, Fig.2). Compound II does not contribute to hypohalous acids' formation, but it can cause another one-electron oxidation of AH with the regeneration of the native enzyme (reaction 4, Fig.2)[116]. Whether MPO compound I proceeds into the halogenation or the peroxidase cycle would be dictated by the concentration of halide and the reducing substrates (AH) present in the vicinity of the enzyme. H_2O_2 required for the MPO-mediated antimicrobial activity may come from several sources, including most significantly NADPH oxidase. NADPH oxidase is an enzyme bound to the neutrophil

membrane. Neutrophils undergo a respiratory burst, caused by the NADPH oxidase complex, present at the phagosomal membrane. NADPH oxidase transfers electrons across the wall from NADPH to oxygen forming superoxide ($O_2^{-\cdot}$), which kills bacteria directly or dismutates to form H_2O_2 and generates other reactive oxygen and reactive nitrogen species[117,118]. The dismutaion reaction could either occur spontaneously or via the superoxide dismutase (SOD) enzyme. H_2O_2 could either then be converted into water via the action of catalase or trigger the MPO catalytic cycle. The respiratory burst is essential for fighting infections. Inefficient respiratory burst activity due to defective NADPH oxidase had been identified as the main etiology for the low immune system capacity in patients with chronic granulomatous disease (CGD)[119]. MPO is also known to oxidize tyrosine into tyrosyl radical that is believed to play a role in both killing bacteria and tissue injury and pathogenesis of different diseases[120]. MPO's antimicrobial role was demonstrated when enzyme inhibitors such as azide decreased the antimicrobial activity of neutrophils with no effect on the MPO-deficient neutrophils.[110] Moreover, patients with MPO deficiency were found to have significantly low immunity against the opportunistic infection by *Candida albicans*[121].

In addition to MPO metabolism (bio-activation) of various endogenous substrates, extensive research data pointed at MPO as an important bio-activation pathway for many medications and toxins into pro-oxidant reactive species. That particular metabolic activation pathway has been proposed to be implicated in idiosyncratic adverse drug events, including drug-induced agranulocytosis, liver injury and methemoglobinemia [122,123,124,125]. It has also been proposed that MPO catalyzes bio-activation of different chemotherapeutic agents, which could be an essential secondary mode of antitumor

activity. For instance, Mitoxantrone has been shown to be oxidized by MPO and H_2O_2 to a metabolite that binds covalently to DNA and RNA. Moreover, mitoxantrone metabolism by MPO was also detected in the urine of patients treated with mitoxantrone, implicating its metabolism by MPO in humans[126,127,128]. Similarly, etoposide, which is another topoisomerase II poison, was reported to be metabolized by MPO *in vitro* into a reactive quinone, that oxidized GSH and protein thiols[129]. Another example is ellipticine, which is a potent antineoplastic agent whose primary mode of action is based on DNA intercalation and inhibition of topoisomerase II. Ellipticine was shown to be oxidized by human MPO and results in adduct formation between 12-hydroxyellipticine and 13-hydroxyellipticine and deoxyguanosine. Identical adducts were also formed in human leukemia HL-60 cells where ellipticine covalently binds to DNA after its activation by MPO[130,131]. Another study demonstrated that the herbal medicine, parthenolide, targeted apoptosis in AML cells, highly expressing MPO while sparing normal hematopoietic cells through MPO-dependent significant increases in ROS production and apoptosis[132,133]. Moreover, several observational studies showed that myeloperoxidase genotypes in different cancers, including breast cancer and leukemia, increase the efficacy of chemotherapy and patient prognosis[134].

1.6. FREE RADICAL DETECTION METHODS

1.6.1. Basic principles of electron paramagnetic resonance

Electron paramagnetic resonance (EPR), also known as electron spin resonance (ESR), is a spectroscopy method that was discovered by Yevgeny Zavoisky in 1944. EPR spectroscopy is predominantly based on the interaction of magnetic properties of the

unpaired electrons in the sample with an external magnetic field. An isolated electron, without any external forces, still has an intrinsic angular momentum called spin, and because of its charge, this angular motion generates a magnetic field. If electrons occur in pairs, t the net magnetic moment is zero (Pauli's exclusion principle) (Fig.3). However, if an unpaired electron is present, its unopposed magnetic moment can then suitably interact with a magnetic field, in such case, the electron would be called paramagnetic, which means that it has a net spin value $\neq 0$.

Because of their magnetic moment, single electrons would act as a compass when placed in a magnetic field (Fig.3). The unpaired electron will have a state of lowest energy when the moment of the electron is aligned with the magnetic field and a state of highest energy when aligned against the magnetic field. This is called the Zeeman effect (Fig.3). The two states are labeled by the projection of the electron spin, M_S, on the magnetic field, where M_S=-1/2 is parallel and M_S=+1/2 is antiparallel state. The energy states of the unpaired electron can be defined as

$$E = g\,\mu_\beta\,B_0\,M_S = \pm\,1/2\;g\,\mu_\beta\,B_0$$

Where E is the energy state, μ_β is the Bohr magneton, which is the natural unit of electronic magnetic moment, g is the g-factor, which is a proportionality constant approximately equal to 2 for most samples. From the equation, we could conclude that the two spin states have the same energy in absence of a magnetic field (no energy difference to measure), and the energy difference increases linearly as the magnetic field increases. In EPR, sample is exposed to microwaves at a fixed frequency, while scanning the magnetic field. A peak in the absorption will occur when the magnetic field "tunes" the two spin states so that their energy difference matches the energy of the radiation.

This field is called the "field for resonance", thus an EPR spectrum of an unpaired electron alone consists of one peak. In EPR spectrometers, a phase-sensitive detector is used which converts the normal absorption signal to its first derivative (Fig.3)[135]. Thus, the EPR spectrum typically consists of the magnetic field on the x-axis and $d\chi/dB$, the derivative of the imaginary part of the molecular magnetic susceptibility with respect to the external static magnetic field in arbitrary units is on the y-axis (http://webhome.auburn.edu/~duinedu/epr/1_theory.pdf.)

1.6.2. Hyperfine interactions

EPR data does not only provide direct evidence for the presence of free radical species but also gives very important information about their chemical composition. The magnetic field surrounding an unpaired electron interacts with nuclei with non-zero spin ($I \neq 0$), that are located typically not more than three bonds away, causing the single peak of the unpaired electron to split. Such interaction is called the hyperfine interaction. The splitting pattern, therefore, gives important information about the identity and number of atoms as well as proximity from the unpaired electron in a given sample. If the interacting nucleus has no spin, the spectrum would still be a single line. However, if the interacting nucleus has a spin ($I \neq 0$), the single peak of the unpaired electron would split into a set of lines (peaks), where the number of lines in the set equals $2I+1$. Generally, nuclear spin values are determined by the number of protons and neutrons within an atom, and there are general rules that could be applied. For instance, a nucleus that has an even atomic number and even mass number, which means an even number of both protons and neutrons, the resulting net spin would be zero, e.g. spin for ^{16}O nucleus is

zero. Whereas in a nucleus with odd numbers of both protons and neutrons, the spin number would be a positive integer, e.g. spin in ^{14}N is 1, but all remaining nuclei with odd atomic number and even mass number or vice versa would have spins of half integral, e.g. spin for ^{1}H is ½. Thus, the hydrogen nucleus would cause splitting of the peak into two lines (2×½ +1), whereas interaction with ^{14}N (I = 1) would give three lines (2×1 +1) (Fig.4). If there are two equivalent spin nuclei with same hyperfine coupling, the lines would further split because of the equal hyperfine splitting, and two of the EPR signals will overlap. For instance, n nuclei of non-zero spin with equal hyperfine couplings, the number of lines would be $2n+1$[136].

1.6.3. Spin trapping

One major challenge to directly detect paramagnetic species by EPR is the short half-life of those reactive centers that tend always to look to form more chemically stable bonds. To overcome this obstacle, the EPR spin trapping technique is often used. It is basically an indirect detection of the short-lived free radicals by addition to chemical traps called spin traps, that covalently bind to the radicals and result in a relatively persistent radical trap adducts. There are two major classes of traps; nitrones and nitroso compounds. In our studies, we use DMPO (5,5-dimethyl-1-pyrroline N-oxide), a nitrone spin trap. In general, nitrones have the advantage of their ability to react with a variety of different free radicals ($RC^{\cdot}$, $RO^{\cdot}$, $RS^{\cdot}$, and in some cases $RN^{\cdot}$) to form nitroxide stable adducts (Fig.5). In addition, they are not toxic, which makes them a useful tool for *in vivo* spin trapping. The unpaired electron in DMPO is located in a π-orbital on the nitrogen and oxygen atoms; the spin of the unpaired electron would interact with both nuclei, but

since the oxygen nucleus has no spin, only the interaction with the nitrogen (I=1) nucleus will be EPR visible. Therefore, three equally intense lines (2×1 +1) is expected for DMPO attached to groups consisting of atom with no spin. However, attachment of paramagnetic atoms to DMPO nitrogen would lead to further splitting due to hyperfine interaction phenomenon explained in section 2.6.3.

1.7. IN VITRO LEUKEMIA CELL LINES: HL-60 CELLS

In our studies, we used the human promyelocytic leukemia cell line HL-60. This cell line is a human cell line derived from peripheral blood of a 36-year old woman with acute promyelocytic leukemia (M3). It was the first myeloid leukemic cell line that was successfully made to grow continuously in a cell culture suspension to be used as a model by researchers [138]. HL-60 cells are mostly neutrophilic promyelocytes that can be induced with chemicals to differentiate *in vitro*[139], which made it an attractive model to study proliferation and differentiation of human myeloid cells [140,141]. HL-60 cells have also been used in cancer research projects to study development and progression of various cancers[142] or to understand the synergistic role of chemotherapy agents in the treatment of leukemia[143]. HL-60 cells represent a useful model for our studies since these cells have abundant amounts of MPO[144], and in the presence of H_2O_2, intracellular MPO catalyzes one-electron oxidation of xenobiotics through its peroxidation cycle (as explained under section 2.5).

1.8. RATIONALE AND HYPOTHESES

According to the Leukemia and Lymphoma Society of Canada, between 2014 and 2016, there was a 3% increase in Canadians that died from leukemia, lymphoma and myeloma[145]. Due to advances in diagnosis and treatment, there has been a decrease in age-standardized mortality rates for blood cancers. However, blood cancers still are the third leading cause of cancer death in Canadian men and fourth in women. For leukemia, the standardized five-year survival rate is less than 60% in both genders, a significantly lower figure compared to other cancers like thyroid cancer, prostate or breast cancer. Acute myeloid leukemia (AML) is the most common type of acute leukemia in adults, and one of the current major therapeutic challenges is the collateral damage that results from using intensive chemotherapy regimen cycles. Chemotherapy attacks normally rapidly dividing cells like those in the mouth, intestinal lining, hair and bone marrow; this causes patients to lose their hair, develop mouth sores, anemia, bleeding, infection and suffer nausea and vomiting. With such increasing trends of blood cancer incidence and poor safety of the used chemotherapy regimens, there has always been a need to explore the utility of new medications. Such drugs should possess anti-cancer activity with a more favourable safety profile. Studies have been done on either using these drugs alone or in combination with chemotherapeutic agents in an attempt to improve clinical outcomes with a lower dose of chemotherapeutic agent and thus lower toxicity. One approach is to look at medications that are already used clinically for repurposing. The advantage of the latter approach is that it could help with the translation of research findings into clinical use since these medications have already passed the basic pre-clinical and clinical toxicity screening. In some cases, there could be a significant amount

of data available from post-marketing surveillance on their safety when used in larger populations. Taken together, all of these parameters would save precious time and money spent in drug development stages of brand new molecules.

As discussed earlier in the introduction, NSAIDs have drawn much attention of many researchers, especially over the last few decades, and that was mostly driven by the widely accepted role that acute and chronic inflammation play in tumorigenesis and cancer development[146]. NSAIDs have been shown to reduce the risk of colon cancer, breast cancer, prostate cancer, and head and neck cancers. However, very limited studies, if any, have investigated the utility of NSAIDs use in AML. Moreover, most of these were focusing mainly on celecoxib, sulindac, and, to a lesser extent, aspirin. The rationale behind these studies was that COX-2 plays the major role in vascularization and proliferation of certain tumors. However, other studies demonstrated that some NSAIDs exert potent anti-tumor activity *in vitro* and *in vivo* (animal studies) without inhibiting COX-2 e.g. sulindac sulfone and 2,5 dimethyl celecoxib[34,33,147,148].These findings open up the horizon for studying the conventional non-selective NSAIDs, and other anti-inflammatory agents that have not been examined yet for their possible chemoprotective or chemosensitizing effects in cancer cells. A number of studies that have been done are either epidemiological studies that conclude only an association between the use of NSAID and the resulting cancer risk reduction or findings of efficacy *in vitro* or in animal models without knowing the precise mechanism involved. The question remains: what other mechanisms could be involved other than the inhibition of prostaglandins' biosynthesis.

As discussed earlier, MPO has been considered a golden biomarker for the diagnosis of AML in the French-American-British and World Health Organization classifications[149]. MPO was also demonstrated to metabolize a small number of chemotherapeutic agents (e.g. etoposide[150], mitoxantrone[127], ellipticine[131]) into reactive species, which had detrimental consequences on cell viability and its oxidative state. However, this concept has not been applied to other drug classes, including NSAIDs. Our studies focused on studying the metabolic activation of different non-selective NSAIDs, namely diclofenac, indomethacin, naproxen and mefenamic acid via MPO (in Chapters 2 and 3 of this thesis). We used a combination of *in vitro*-biochemical approaches to test our hypotheses. In our biochemical studies, we used purified MPO enzyme from human neutrophils, and for our *in vitro* studies, we used the human promyelocytic leukemia HL-60 cell line that highly expresses MPO. We hypothesized that MPO bio-activation of NSAIDs produces pro-oxidant species that will cause oxidative damage and induce leukemic cell death.

The HL-60 cell line is a suspension cell line cultured in RPMI medium that contains all the amino acids, vitamins and nutrients necessary for growth, and also contains phenol red (PR) that acts as a quick check for the culture health. As a pH indicator, PR changes the color of the medium into yellow once it becomes acidic due to accumulation of waste products produced by old cells or contaminants that change the culture pH. Some previous studies indicated the production of ROS from cell-free culture medium RPMI after addition of horseradish peroxidase[151], which has a similar activity as MPO that is present in HL-60 cells. PR has been used in various protocols to detect H_2O_2 from macrophages using horseradish peroxidase[152], and also in peroxidase activity

protocols (e.g. bromoperoxidase[153], eosinophil peroxidase[154]). These studies led us to our last study (chapter 4), where we hypothesized metabolism of PR that is present in the culture media via MPO, expressed in HL-60 cells could result in reactive metabolite(s) that could modulate cell viability and compromise the oxidative state of the cell culture. This is important because caution should be taken when doing *in vitro* oxidative stress studies assuming that the cells in the culture are in a perfect oxidant-free condition, when the truth might be that the growth medium itself could have promoted the production of reactive species that interfere with the results.

1.9. HYPOTHESES AND OBJECTIVES

1.9.1. Hypothesis 1

MPO bio-activation of diclofenac, indomethacin and naproxen and their hepatic metabolites cause oxidative damage and induce leukemic cell death**.**

Specific objectives:

1) To evaluate the effect of MPO-mediated metabolism of NSAIDs and their hepatic metabolites on ascorbate co-oxidation rate.
2) To evaluate free radical production from NSAIDs metabolism by purified human neutrophil MPO through EPR spectroscopy.
3) To evaluate the effect of MPO-mediated metabolism of NSAIDs on HL-60 cell viability using Trypan blue exclusion assay.
4) To assess the effect of MPO-mediated metabolism of NSAIDs on cellular ATP levels.

5) To assess the effect of MPO-mediated metabolism of NSAIDs on cellular glutathione levels.
6) To assess the effect of MPO-mediated metabolism of NSAIDs on mitochondrial membrane potential.

1.9.2. Hypothesis 2:

MPO bio-activation of mefenamic acid (MFA) and its chemical analogues results in reactive metabolites that induce cell death in HL-60 leukemia cell line.

Specific objectives:

1) To evaluate the UV spectral changes as a result of peroxidation of MFA and its analogues and the effect of glutathione addition on these changes.
2) To evaluate free radical production from peroxidation of MFA and its analogues and the detection of resulting glutathionyl radicals.
3) To analyze peroxidase-mediated metabolism of MFA and its analogue and the formation of MFA-GSH adducts by LC/MS.
4) To evaluate the effect of MPO-mediated metabolism of MFA and its analogues on HL-60 cell viability.

1.9.3. Hypothesis 3*:*

MPO metabolism of PR via MPO-expressing HL-60 cells could result in PR metabolite(s) that could modulate cell viability.

Specific objectives:

1) To evaluate PR UV spectral change due to its oxidation by MPO/H_2O_2/Cl^- by using UV-VIS spectrophotometry.

2) To carry out LC-MS analysis of phenol red (PR) metabolism by MPO.
3) To evaluate the effect of PR on MPO catalyzed chlorination activity.
4) To evaluate the production of gluathionyl radicals by MPO metabolism of PR.
5) To evaluate the uptake of PR by HL-60 cells.
6) To evaluate the effect of MPO-mediated metabolism of PR on cellular ATP levels in HL-60.
7) To evaluate the effect of MPO-mediated metabolism of PR on glutathione and oxidized glutathione dimer contents in HL-60 cells.

1.10. FIGURES

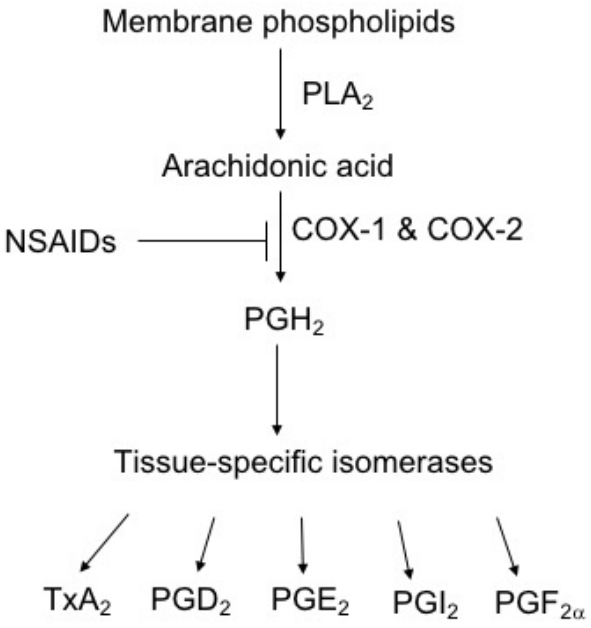

1.10.1. Figure 1: General mechanism of action of NSAIDs

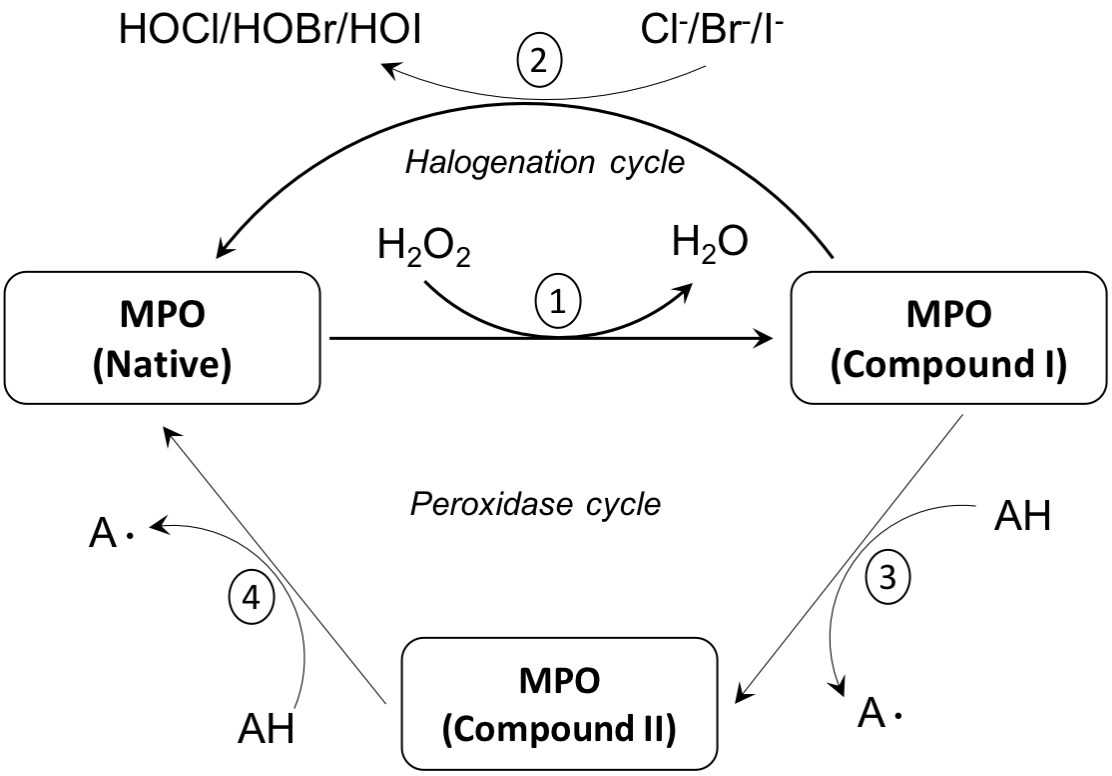

1.10.2. Figure 2: MPO catalytic cycle

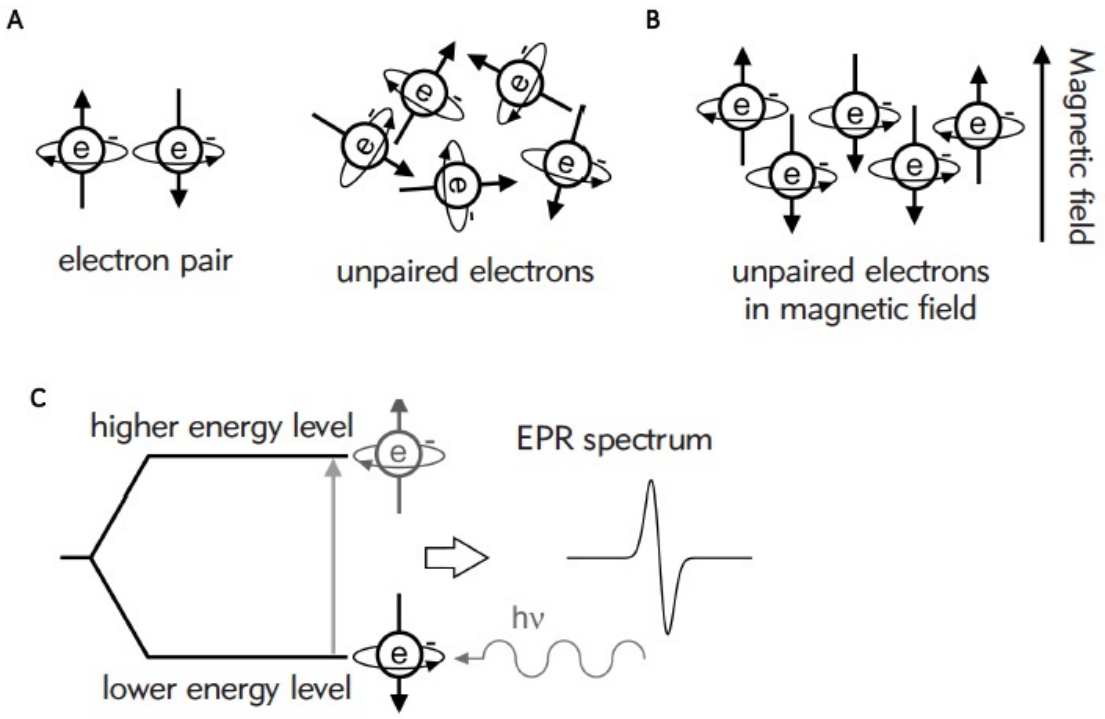

1.10.3. Figure 3: Basic principles of electron paramagnetic resonance[135]. (A) represents opposite spin of paired electrons according to Pauli's exclusion principle. (B) represents the interaction between unpaired electrons and external magnetic field. (C) represents Zeeman effect.

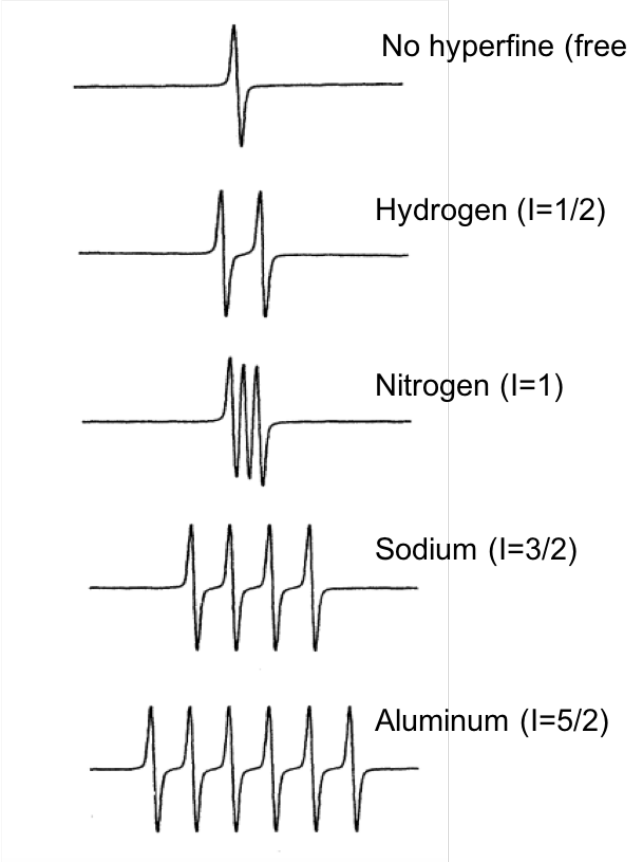

1.10.4. Figure 4: EPR spectra that result from hyperfine interactions of unpaired electron with different atoms or nuclei that have spin (I≠0). Adapted from a publication by Janzen et.al[137].

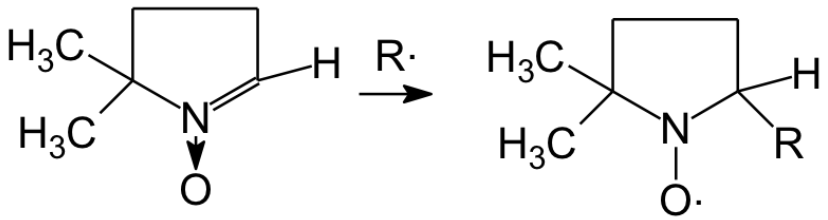

1.10.5. Figure 5: A general reaction between DMPO spin trap and a free radical.

CHAPTER 2

EVALUATION OF MPO BIO-ACTIVATION OF DICLOFENAC, INDOMETHACIN AND NAPROXEN AND THEIR HEPATIC METABOLITES IN HL-60 CELLS

[A version of this work has already been published as Morgan, A. G. M., D. Babu, K. Michail, and A. G. Siraki. 2017. An Evaluation of Myeloperoxidase-Mediated Bio-Activation of NSAIDs in Promyelocytic Leukemia (HL-60) Cells for Potential Cytotoxic Selectivity]

2.1. ABSTRACT

Several lines of evidence have pointed towards the potential therapeutic benefit of NSAIDs in cancer therapy. In our studies, we have investigated the acute bio-activation of NSAIDs and their metabolites via myeloperoxidase (MPO), a highly-expressed peroxidase enzyme in acute myeloid leukemia. As bio-activation involves the formation of reactive metabolites, we hypothesized that NSAIDs which produced reactive metabolites would be correlated with leukemia cell toxicity. We tested the enzymatic peroxidation of three NSAIDs, namely diclofenac, indomethacin, and naproxen in comparison with their hepatic metabolites, 4'-hydroxydiclofenac (4'-OHD), 5-hydroxydiclofenac (5-OHD), O-desmethyl-N-deschlorobenzoylindomethacin (DMBI), O-desmethylindomethacin (DMI) and O-desmethylnaproxen (ODN). Firstly, we used purified peroxidases in kinetic UV-visible kinetic spectrophotometry, and electron paramagnetic resonance (EPR) experiments to determine oxidation of ascorbic acid and glutathione (GSH), respectively. We then used HL-60 cells, as a model of acute myelogenous leukemia to carry out trypan blue exclusion, cellular analysis, mitochondrial membrane potential (MMP) and cytofluorometric GSH assays. Our results present evidence that diclofenac, 4'-OHD, 5-OHD, DMBI and DMI demonstrated significant cytotoxic effect in the leukemic cells through oxidation by intracellular MPO. In the same vein, only diclofenac and its two metabolites caused a significant drop in the MMP and cellular ATP level; however, the cell death induced by indomethacin metabolites reflected a subtle effect on MMP or GSH content. Interestingly, only diclofenac and 4'-OHD (and not 5- OHD) caused a significant drop in HL-60 cells' GSH content. Among diclofenac compounds, only 4'-OHD also generated $GS^{\bullet}$ radicals and caused a significant increase in ascorbate co-oxidation rate.

Lastly, even though ODN also generated GS$^{\bullet}$ radicals and potently cooxidized ascorbate, it showed no significant cytotoxicity. These results provide evidence of a correlation between acute cytotoxicity and MPO-bioactivated NSAIDs, though this was not correlated for all compounds (e.g., ODN). Further studies are required to determine both the MPO-dependent and MPO-independent mechanisms of cytotoxicity.

Key words: NSAID, diclofenac, indomethacin, naproxen, oxidative stress, myeloperoxidase, free radicals, drug metabolism, leukemia

2.1. INTRODUCTION

Extensive data demonstrate the causal correlation between chronic inflammation, innate immunity and the development of different forms of cancer (e.g. colorectal cancer, pancreatic cancer, liver carcinoma, stomach cancer)[121]. Consequently, non-steroidal anti-inflammatory drugs (NSAIDs) have been widely investigated for their plausible benefit in cancer prevention and therapy. For instance, celecoxib, a known selective COX-2 inhibitor, and sulindac, a non-selective COX-1 and COX-2 inhibitor, have been particularly focused on. For example, the former is a currently approved adjuvant therapy in the treatment of familial adenomatous polyposis (FAP)[12]; although it is believed that NSAIDs have much promise against cancer, the limited data available regarding their mode of actions and safety present the major limitation to increase their clinical use in cancer therapy.

Acute myeloid leukemia (AML) is the most common type of acute leukemia that affects adults, accounting for 1.2% of cancer deaths in the United States[155]. It is generally characterized by rapid increase in the myeloid cells associated with an arrest in their

maturation. Earlier, AML diagnosis was based solely on the pathological and morphological examination of the bone marrow and the blood. However, with growing knowledge about the heterogeneity of AML, subcategorization into nine subtypes has been established by the French-American-British (FAB) group, depending on the particular myeloid lineage, morphologic appearance and the reactivity with three histochemical stains, including myeloperoxidase (MPO), Sudan black, and the nonspecific esterase α-naphthylacetate and naphthylbutyrate. Six (M1 to M4, M4EO and M6) out of the nine subtypes are MPO-positive[149].

MPO expression in leukemia cells is tightly controlled in a tissue-dependent manner; thus, it provides critical information about leukemia phenotype.

It has been well documented that most cancer cells display elevated reactive oxygen species (ROS) compared to their normal counterparts, and that is crucial for their proliferative advantage as it promotes malignant progression as the tumor develops[156,157]. However, ROS may cause cell damage and induce cell death if they accumulate. Therefore, an essential adaptive response for the tumor cells to survive is to upregulate vital antioxidant systems. For instance, GSH and manganese-dependent superoxide dismutase (Mn-SOD) concentrations in tumor cells are highly correlated to tumor cellular proliferation and metastasis[158,159,160,161,162,163]. Since many commonly used clinical chemotherapeutic agents rely on their potential to generate ROS in order to kill the tumor and to induce apoptosis,[164] redox adaptive responses in cancer cells can represent a significant therapeutic obstacle[129]. Moreover, one of the biggest challenges in AML treatment is the remission induction, and with these very quickly proliferating cells, using long chemotherapy cycles is a lifesaving intervention, despite the high toxicities and side effects associated with its use. Therefore,

the search for adjuvant therapies that could kill the leukemic cells efficiently might be of great value in terms of reducing the chemotherapy doses.

In addition to being a key marker of AML diagnosis, MPO has demonstrated its capacity to bio-activate a small number of chemotherapeutic agents (e.g. etoposide[129], mitoxantrone[126], ellipticine[130]) into reactive species/radicals as a postulated additional mode of action for these agents against acute myeloid leukemia. In the present work, we used the HL-60 (human promyelocytic leukemia) cell line to investigate the metabolism of three NSAIDs of widespread use that generally have good safety profiles (diclofenac, indomethacin, and naproxen) along with their known hydroxylated hepatic metabolites, 4'-OHD, 5- OHD, DMBI, DMI and ODN (Fig. 1). As MPO is abundant in these cells, we hypothesized that MPO oxidation of the NSAIDs' parents, and their metabolites, would result in pro-oxidant species that will cause oxidative damage and induce leukemic cell death.

2.2. MATERIALS AND METHODS

2.2.1. Chemicals and kits

All drug metabolites (4'-OHD, 5-OHD, ODN, DMI, DMBI, Fig. 1) were purchased from Toronto Research Chemicals, Inc. (Toronto, ON). Horseradish peroxidase (specific activity: 332.5 units/mg) was purchased from AMRESCO, LLC (Solon, OH), Human purified neutrophil myeloperoxidase (MPO, 180-220 units per mg lyophilized proteins) was acquired from Athens Research & Technology (Athens, GA). 5,5-Dimethyl-1-pyrroline-N-oxide (DMPO), manufactured by Dojindo Molecular Technologies, Inc., was purchased from Cedarlane Laboratories Ltd (Burlington, ON), and was stored under

nitrogen atmosphere at -80°C and used without further purification. 0.4% Trypan blue stain was obtained from Lonza (Anaheim, CA). Micro BCA™ protein assay kit and Halt ™ Protease inhibitor cocktail were purchased from Thermo Fischer Scientific (Burlington, ON). Phosphoric acid was purchased from EMD Millipore. 0.1 M Sodium phosphate buffer (pH 7.4) was prepared and chelated with Chelex® 100 resin (obtained from Bio-Rad Laboratories, Mississauga, ON) at 4°C overnight and treated with 100 μM of diethylenetriamine-penta acetic acid (DTPA) to further prevent metal-catalyzed auto-oxidation. RIPA buffer was prepared using 1% Triton X-100 (v/v), and 0.1% SDS (sodium dodecyl sulfate, w/v) in PBS (phosphate buffered saline), containing 0.01% (v/v) protease inhibitor cocktail, which was added immediately before use. CellTiter-Glo® luminescent cell viability assay kit was purchased from Promega (Madison, WI). Parent NSAIDs (naproxen sodium, diclofenac sodium and indomethacin at a purity of ≥99%, Fig. 1), glucose oxidase from Aspergillus niger (≥100,000 units/g), L-ascorbic acid, hydrogen peroxide (H_2O_2), reduced glutathione (GSH), taurine, DTPA, SDS, N-ethylmaleimide (NEM, ≥ 98%), o-phthaldehyde OPA, ≥98.5%), menadione, tetrachloro-1,4-benzoquinone (TC1,4-BQ), and all other chemicals (unless noted otherwise) were from Sigma-Aldrich Canada Co. (Oakville, ON).

2.2.2. Cell culture

HL-60 (human promyelocytic leukemia) cells were obtained from ATCC (Cat No. CCL-240, Manassas, VA), and grown in a medium consisting of RPMI-1640 medium with L-glutamine (Gibco® Reference No. 11875-093) with added 10% heat-inactivated fetal bovine serum (FBS, Gibco® Cat No. 12483) and 1% of antibiotic-antimycotic mixture

(Gibco®; Reference No. 15240-062, 10 000 units/mL of penicillin, 10 000 µg/mL of streptomycin, and 25 µg/mL of amphotericin B). Cells were maintained in a humidified atmosphere with 5% CO_2 at 37 °C and were allowed to grow with density, maintained at 0.5-1 x 10^6 cells/ml, and split every 2 days. Doubling time for HL-60 cells was reported to be 34 h[165]. Cells used did not exceed passage 30 and cell viability was greater than 90%.

2.2.3. Kinetic spectrophotometry (ascorbate co-oxidation rate)

To a cuvette containing 50 µM ascorbate in 0.1 M sodium phosphate buffer (pH = 7.4, supplemented with 100 µM DTPA and treated with Chelex® 100 resin to prevent metal catalyzed auto-oxidation), 1 µM, 5 µM or 10 µM of parent NSAID or metabolite. That was then mixed with 250 nM of peroxidase from horseradish (HRP), the reaction was triggered by adding 50 µM H_2O_2. Ascorbate co-oxidation is a two-step process. First, in presence of a reactive metabolite, it is converted to ascorbyl radical formation via one electron oxidation, which is followed by the formation of two electron oxidized product, dehydroascorbate. To monitor the ascorbate oxidation rate, kinetics scans were recorded every 30 s at the maximum ascorbate absorption wavelength (λ_{max} = 266 nm) to record the rate of oxidation, using Thermo Scientific NanoDrop 2000c dual-mode UV-Vis spectrophotometer (Wilmington, DE) connected to a desktop PC supplied with NanoDrop 2000c software for data acquisition. The rates were compared to the vehicle control. Each measurement was done at least in triplicate. Data were expressed as Δ Absorbance per min (mean ± SD).

2.2.4. Electron paramagnetic resonance (EPR)

In a flat cell, reactions (200 μL final volume) of 10 μM of drug or metabolite, 1 mM GSH and 50 nM of MPO, were carried out in 0.1 M phosphate buffer (pH 7.4, Chelex® 100 resin-treated with added 100 μM DTPA). As soon as the reactions were triggered with 100 μM H_2O_2 and mixed, the sample was transferred to a flat cell and placed in an Elexsys E500 EPR spectrometer cavity for analysis using the following instrumental settings; microwave frequency, 9.8 GHz; incident microwave power, 0.02 W; center field, 3485 G; scan range, 100.0 G; field modulation amplitude 1 G; receiver gain, 60.0 dB. All controls were run in parallel. Each individual reaction was run (one scan each) at least in duplicate on nonconsecutive days.

2.2.5. Trypan blue exclusion in vitro cytotoxicity assay

HL-60 cells were harvested, spun down at 120 g for 15 min and re-suspended in pre-warmed PBS to 37°C in 96-well microplate at 2×10^6 cells/mL (>90% viability) for treatment. For initial experiments, the cells were treated with increasing concentrations (from 0-2 mM) of each of the NSAID parent and metabolite to estimate the IC50 for each molecule (see Table 1). IC50 values were determined by interpolation using a 4-parameter sigmoidal regression function in GraphPad Prism V. 7.01 (GraphPad Software, Inc., La Jolla, CA) using at least 4 different concentrations of drug/metabolite (Fig. 5). However, we selected 600 μM of the NSAID parent/metabolite in order to determine if MPO metabolism would have an effect, which was below the relative IC50 for all compounds tested. To test our hypothesis regarding the effect of MPO oxidation of these drugs/metabolites, the reactions were incubated for 3 h at 37 °C, 5% CO_2 in a VWR

Signature™ incubating 3-D Rotator Waver. Then samples from the reaction were mixed (1:1) with 0.4% trypan blue reagent, and the cell viability was measured by using a TC-10 automated cell counter (Bio-Rad Laboratories). HL-60 cells were treated with 600 μM drug/metabolite ± 5 mM glucose & 20 mU/mL glucose oxidase (G/GOx); all other controls were done in parallel, and reactions were incubated for 3 h under the same conditions and viability was checked with trypan blue as mentioned earlier. Although this treatment time may appear short, the approach taken here was that of ACMS in order to determine relative reactivity and cytotoxicity for the compounds tested[166]. All reactions were run at least in triplicate on different days. Data were expressed as mean ± SD.

2.2.6. Relative cellular ATP analysis

Cellular ATP levels were determined by using CellTiter-Glo® luminescent viability assay kit (Promega, WI) as per the manufacturer's protocol. This assay determines the cell viability by quantifying the ATP present in the cell culture as an indicator of the metabolic activity. The kit acts by inducing cell lysis and extracting ATP, which acts as a co-factor helping the recombinant luciferase enzyme to act on luciferin in presence of Mg^{2+} to produce oxyluciferin while releasing a luminescent signal. The signal is, therefore, proportional to the amount of ATP present. . It is worth mentioning that we were not able to use viability assays like CCK-8 that measure the metabolic activity of the cells because of the interference between the kit and some metabolites. Unlike the trypan blue assay, we found that 600 μM of NSAID/metabolite resulted in a dramatic drop in ATP which prevented observing the effect of MPO metabolism. Therefore, we used 100 μM for this assay. In brief, the working reagent was prepared by thawing buffer solution and adding it

to the substrate. The reactions were performed by treating HL-60 cells (5×10^4 cells/well) with 100 µM drug/metabolite with or without 5 mM glucose & 20 mU/mL glucose oxidase (G/GOx) in a 96-well black plate (Corning Costar). All other controls were tested in parallel (the final concentration of DMSO in each well was 0.3%), and the plates were incubated for 3 h at 37°C, 5% CO_2 in a VWR Signature™ incubating 3-D Rotator Waver. Then, freshly prepared CellTiter-Glo® reagent was added in a 1:1 ratio to each well of the plate, which then was shaken for 2 min on a shaker. After 10 min of incubation at RT, luminescent signals were recorded using a SpectraMax® M5 Multi-Mode Microplate reader (Molecular Devices, Sunnyvale, CA). Each reaction was repeated at least 3 times on different days, and the results were expressed as mean ± SD.

2.2.7. Mitochondrial membrane potential change

This assay was performed using JC-1 reagent as described before[167]. Unlike cytotoxicity and GSH content screening, we found that 3 h incubation of cells with 600 µM of NSAID parent or metabolite alone (without G/GOx) resulted in a dramatic drop in MMP which prevented observing the effect of MPO metabolism. Therefore, we used 300 µM for 1 h. Briefly, after harvesting HL-60 cells and centrifugation at 150 g for 15 min., cells were re-suspended in PBS, pre-warmed to 37°C in a 96-well microplate at 2×10^6 cells/ml (>90% viability). Thereafter, the cells were treated with 5 mM taurine (to scavenge HOCl, produced from oxidation of Cl^- anions by MPO upon addition of G/GOx, and thus minimizing the resulting drop in mitochondrial membrane potential), and 300 µM drug/metabolite ± G/GOx. All controls were done in parallel. As a positive control, a known mitochondrial toxin, 50 µM CCCP (carbonyl cyanide *m*-chlorophenyl hydrazine), was used. Reactions were incubated for 1 h at 37 °C in 5% CO_2 atmosphere in a VWR

Signature™ incubating 3-D Rotator Waver. After completion, reactions were incubated for 30 min with 0.3 μM of JC-1, and then transferred into 1.5 mL micro test tubes, washed twice at 200 g for 5 min. to discard the unincorporated free dye. The cells were then resuspended and added to a black 96-well microplate; the fluorescence intensity was measured using SpectraMax® M5 Multi-Mode Microplate reader. For red aggregates, fluorescence was measured at excitation and emission of 490 nm and 595 nm, respectively, whereas for green monomers, the emission was changed to 535 nm, and then the ratio of red aggregates/green monomers was calculated. Each reaction was repeated at least 3 times on different days, and results were expressed as mean±SD.

2.2.8. GSH assay in 96-well plate

Total GSH content was measured using OPA, which forms an isoindole adduct based on a previously described method[168]. A calibration curve of known GSH concentrations (0 - 2.5 μM) was constructed showing a linear correlation (r^2=0.99). HL-60 cells were incubated for 3 h with 600 μM drugs/metabolites ± G/GOx (5 mM glucose and 20 mU/ml GOx) and known GSH depleting agents were used as a positive control (30 μM menadione and 20 μM TC1,4-BQ). The cells were harvested, washed and then pellets were suspended in cold PBS and lysed by mixing for 20 min at 7 °C with ice-cold RIPA buffer extraction solution (prepared as described in the materials section) + 10% *v/v* metaphosphoric acid, followed by three cycles of freezing and thawing and spinning down at 4000 g for 5 min at 4 °C. Samples were dissolved in 1 M NaOH for BCA assay, and supernatants were transferred into pre-chilled Eppendorf® tubes for GSH assay. 10μL of each sample was pipetted three times into an opaque (white) 96-well plate, and pH was adjusted using 0.25

M NaOH to a final pH between 7-8, then 10 mM of NEM (a non-selective thiol inhibitor) was mixed with duplicate samples for 15 min at room temperature to account for background fluorescence; then 70 µL of 0.1 M sodium phosphate buffer (pH 6.2) was added, and fluorescence was measured (λ_{ex}=340nm, λ_{em}=420nm) after 15 min of vortexing at 7 °C with 37.27 mM OPA at 500 rpm in darkness. Every reaction was repeated at least three independent times in three consecutive days. GSH concentrations were normalized by estimating total protein concentration using BCA assay (as per manufacturer's instructions) and expressed as mean ± SD of ng GSH/µg protein.

2.2.9. H_2O_2 flux by glucose/glucose oxidase (G/GOx)

The amount of H_2O_2 generated in cell culture by G/GOx was quantified using a colorimetric method, previously described[152]. In brief, 150 µM phenol red was allowed to be oxidized using 2 µM HRP and known concentrations of H_2O_2 (3, 6, 10, 20, 30, 40 and 60 µM) for 5 min in PBS, then pH 12.5 was reached by using 11.42 mM of NaOH, which produced a stable purple-mauve colored product, whose absorbance at 610nm was linearly correlated to H_2O_2 concentration (r^2=0.99). Afterwards, G/GOx was tested using the previous reaction to obtain the produced H_2O_2 over 1 h with readings at every 15 min to calculate the rate of H_2O_2 production over 1 h.

2.2.10. Statistical analysis

Data were expressed as mean ± standard deviation of independent experiments ($n \geq 3$) performed on separate days. Statistical significance ($p < 0.05$) was verified by running a one-way pairwise multiple comparison ANOVA followed by Student–Newman–Keuls post hoc using SigmaPlot 11.0 software.

2.3. RESULTS

2.3.1. Ascorbate co-oxidation

In this study, ascorbic acid oxidation rate was measured by recording the ascorbate absorbance at λ_{max} = 266 nm every 30 s (see Materials and Methods), immediately after triggering the reaction with H_2O_2 (added to HRP and drug/metabolite). Parent NSAIDs (diclofenac, indomethacin, and naproxen) showed no ascorbate oxidation (data not shown). However, three NSAIDs metabolites, namely DMBI, ODN and 4'-OHD showed a significant increase (∗ *P<0.05)* in ascorbate oxidation rate in a concentration-dependent manner (Fig. 2). 4'-OHD and ODN showed the highest oxidation rates, giving almost equal rates at 1 μM and 5 μM. However, at 10 μM, ascorbate oxidation rate with ODN (Δabs/min.=3.20±0.075) was significantly higher than that with 4'-OHD (Δabs/min. = 2.70±0.090).

2.3.2. Electron paramagnetic resonance (EPR)

In this study, we first tried EPR experiments using DMPO as a spin trap to trap and characterize free radical intermediates produced by NSAID/metabolite enzymatic

peroxidation with MPO/H_2O_2 in a biochemical system; however, we were not able to trap/detect the intermediates directly. Therefore, we utilized GSH as an intermediate to react with free radical metabolites. When GSH was added to the reactions (as described in Materials & Methods), a typical EPR spectrum characteristic of glutathionyl-DMPO was obtained exclusively with 4'-OHD and ODN (Fig. 4), while the rest of the compounds in Fig. 1 gave negative results; the signal intensity with 4'-OHD was approximately 4 times more intense than that of ODN based on peak height.

2.3.3. Cytotoxicity in HL-60 cells

Cells were treated with parent NSAIDs and their hepatic metabolites in the presence and absence of G/GOx (as described in Methods and Materials), which was added to provide continuous production of H_2O_2 in order to trigger the catalytic activity of intracellular MPO in HL60 cells. The rate of H_2O_2 flux was 2.93±0.072 μmol $U^{-1}ml^{-1}$ h^{-1}. After 3 h incubation, the trypan blue exclusion assay results (Fig. 5) showed that diclofenac as well as its two metabolites, 4'-OHD and 5-OHD, significantly decreased the cell viability in the presence of G/GOx compared to G/GOx or the drug/metabolite alone (ϕ $P<0.05$). Although indomethacin did not affect the viability significantly, both of its metabolites (DMI and DMBI) dropped the viability substantially in the presence of G/GOx compared to G/GOx or the metabolite alone ($*\phi$ $P<0.05$). Naproxen did not affect the viability significantly after G/GOx addition, and ODN + G/GOx showed only a significant decrease in viability when compared to ODN alone but not G/GOx alone.

2.3.4. Relative cellular ATP analysis

After incubating HL-60 cells with drugs/metabolites ± G/GOx, CellTiter-Glo® luminescent viability assay kit was used to investigate their effect on the cells' metabolic activity based on the amount of cellular ATP (as described in Materials and Methods). Diclofenac and its two metabolites, 4'-OHD and 5-OHD caused a significant drop in the relative ATP content (∗ϕ *P<0.05*, Fig. 6) when G/GOx was added compared to the drug/metabolite alone or G/GOx alone. DMBI, naproxen and ODN showed a significant decrease in ATP level upon addition of G/GOx, but the drop was not significant when compared to G/GOx alone.

2.3.5. Mitochondrial membrane potential analysis

Cells were incubated for 1 h with NSAIDs' parents and metabolites in presence and absence of G/GOx (5 mM glucose and 20 mU/mL glucose oxidase), and the JC-1 fluorescence assay was used to determine the effect on the mitochondrial membrane potential (as described in Materials and Methods). Only diclofenac and its two metabolites, 4'-OHD and 5-OHD caused a significant drop in the mitochondrial membrane potential (∗ϕ *P<0.05*, Fig. 7) when G/GOx was added compared to the drug/metabolite alone or G/GOx alone. No significant decline in mitochondrial membrane potential was observed in the case of naproxen, indomethacin or the related metabolites.

2.3.6. Effect on HL-60 cells' GSH content

After incubating HL-60 cells for 3 h with drugs/metabolites in the presence or absence of G/GOx, cells were lysed, and a fluorometric assay of GSH content using OPA was carried out. Results show GSH content standardized to the total protein content of each sample using BCA assay (as described in Materials and Methods). Under these conditions, we found that only diclofenac and 4'-OHD significantly depleted the cellular GSH content (*ϕ $P<0.05$) when compared to the treatment with the drug/metabolite alone or G/GOx alone (Fig. 8). A slight decrease was also found (not statistically significant) with the metabolites, 5-OHD, DMBI, DMI, and ODN, but no decrease with indomethacin and naproxen parent drugs.

2.4. DISCUSSION

In the present work, we studied the possibility of enzymatic bioactivation of three clinically relevant NSAIDs, diclofenac (an anthranilate), indomethacin (a benzoylated indole acetic acid) and naproxen (methoxy naphthyl propionic acid) by human neutrophil MPO, and we further examined such bioactivation in HL-60 leukemia cell line (rich in MPO) in order to further investigate the opportunity of such oxidation to form prooxidant metabolites that affect leukemic cells' viability and its oxidative status. We also included hydroxylated metabolites of these NSAIDs for their potential to be better MPO substrates.

The following evidence shows that there is a fundamental difference between different NSAIDs and between the parent drugs and their metabolites in their oxidation

capacity by MPO. For instance, indomethacin did not undergo peroxidase oxidation, giving negative results in all the performed biochemical and *in vitro* assays. In a previous study, indomethacin was also found not to be oxidized by MPO nor by activated neutrophils (as a source of MPO)[98]. Nevertheless, we observed that indomethacin depleted (by ~60%) the GSH content of HL-60 cells. This effect may have been responsible for its synergistic cytotoxicity in HL-60 cells and lung cancer cell lines when co-treated with different anthracycline chemotherapeutic agents[169]. Although indomethacin itself only slightly decreased the mitochondrial membrane potential and ATP level, but unexpectedly, in presence of G/GOx, it increased the apparent mitochondrial membrane potential significantly, which correlates with the trend observed with ATP level. Further investigation is required to explain this effect.

For indomethacin metabolites, the formation of a reactive iminoquinone electrophile was reported to be formed by MPO oxidation of DMBI, but not with DMI[98]. In this study, the *in vitro* reactivity of such bioactivation in HL-60 cells was investigated, where we found that both DMI and DMBI resulted in a significant cytotoxic effect in HL-60 cells after MPO oxidation (Fig. 5), as opposed to what was expected based on the previous findings that negated DMI being oxidized by MPO. However, neither DMI nor DMBI cytotoxicity (catalyzed by MPO) was found to involve the mitochondria or to be accompanied by a significant depletion of GSH (Fig. 7 and 8); further studies need to investigate the mechanism of cell death.

It was found that DMBI only, and not DMI, significantly increased the ascorbate oxidation rate as a result of peroxidase bioactivation. We concluded that the cytotoxicity

produced by DMI arose from intercellular hydrolysis of DMI into DMBI, which would be metabolized eventually, as explained earlier, into the reactive iminoquinone.

Surprisingly, DMBI and DMI, by themselves, without MPO oxidation, caused a significant drop in mitochondrial membrane potential. Indomethacin, however, did not demonstrate the same effect.

In this study, diclofenac was the only drug among the parent NSAIDs that was oxidized by MPO into reactive species that induced cell death in HL-60 cells. Moreover, diclofenac metabolites, 4'-OHD and 5-OHD also induced HL-60 cell death when oxidized by MPO (Fig. 5). Although all the three compounds shared a similar effect in depolarizing the mitochondrial membrane potential, depleting intracellular GSH and causing a significant drop in ATP level (Fig. 6, 7 and 8), 4'-OHD showed a distinct reactivity, as it exclusively caused a significant increase in the ascorbate oxidation rate when it was oxidized by peroxidase. It was previously reported that both diclofenac and 5-OHD are bioactivated by MPO resulting in the same reactive iminoquinone[125]. However, 4'-OHD was not included in that study.

Formation of glutathionyl radical (GS$^{\bullet}$) with 4'-OHD (Fig.3) suggests 4'-OHD oxidation led to a potent oxidizing phenoxy radical that abstracted an electron from GSH. The presence of two chlorines on the hydroxylated benzene ring in 4'-OHD leads to a potent oxidizing phenoxy radical by their electron withdrawing effect. Further studies are needed to investigate the ultimate cellular targets of the produced radicals. Indeed, similar findings with lumiracoxib, that has a fluorine replacing one of the chlorines, where the 4'-hydroxylumiracoxib was suggested to undergo one-electron oxidation by MPO to form a phenoxy radical as an intermediate for another electron loss to form a quinoneimine that

formed GSH adducts[170]. Further studies are needed to test the formation of an electrophile with 4'-OHD in the same manner as lumiracoxib.

Finally, naproxen did not undergo MPO oxidation as determined in all the endpoints we examined. However, the O-demethylated metabolite, ODN was oxidized by MPO and caused GS$^{\bullet}$ generation (Fig. 3) that suggests the oxidation of the metabolite into a phenoxy radical intermediate occurred, since the unmasked hydroxyl group is the only structural difference from the parent drug molecule. Although ODN-derived radical formation also caused a significant increase in the ascorbate oxidation rate (Fig. 2), it did not significantly affect the HL-60 cell viability, GSH, mitochondrial membrane potential or cellular ATP level under our experimental conditions. This could be explained by the observation that the amount of the formed radical was not abundant, as seen in the EPR experiment (Fig. 3), when compared to 4'-OHD, which made it easy to get neutralized by the cellular antioxidants and resulted in no oxidative damage. Further investigation might be needed to better understand the cellular mechanisms involved in preventing free radicals-induced oxidative damage and whether or not it is a cell line specific.

This study presents novel evidence that some clinically used NSAIDs and their normal human hepatic metabolites demonstrate a cytotoxic potential in leukemia cells due to their enzymatic bioactivation by MPO, highly expressed in these cells, into prooxidant species, causing deleterious effects (as summarized in Table 2), which can be an advantageous approach in the targeted killing of leukemic cells. Further studies are required to determine the mechanisms of cytotoxicity that are MPO-dependent, as well as for drugs/metabolites that showed MPO-independent cytotoxicity.

2.5. ACKNOWLEDGEMENT

This work was supported by the Natural Sciences and Engineering Research Council of Canada (NSERC) (RGPIN-2014-04878).

2.6. FIGURES

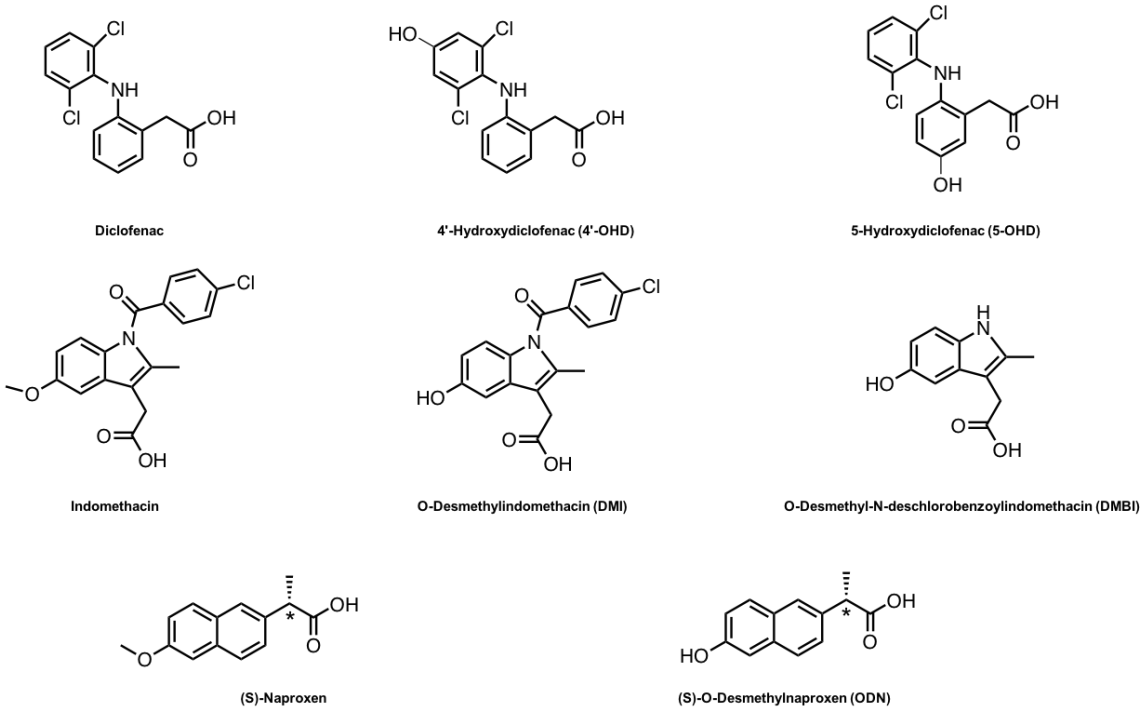

2.6.1. Figure 1. Molecular structures of NSAIDs' parent molecules and their hepatic metabolites involved in this study. * indicates a chiral center

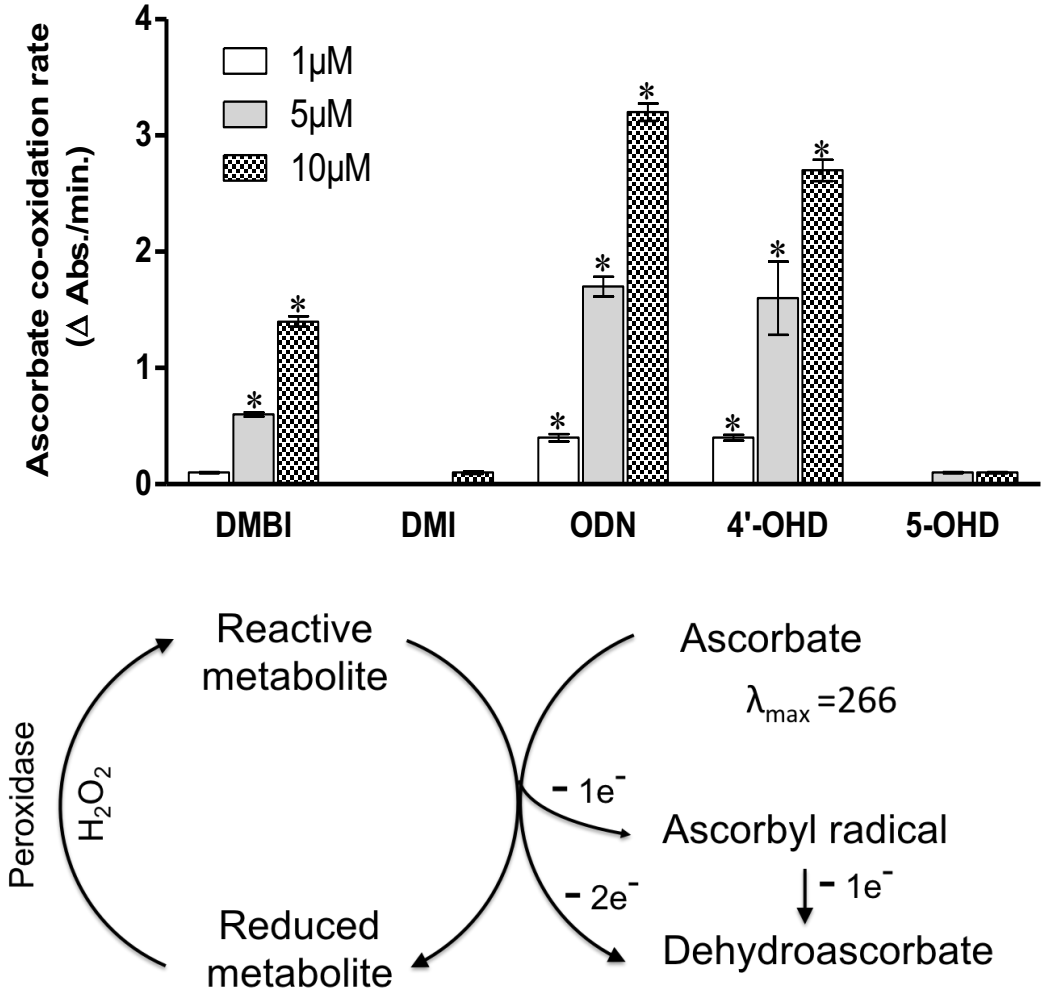

2.6.2. Figure 2. UV-Vis studies of ascorbate oxidation rate. Reactions were carried out in chelex-100- treated 0.1 M phosphate buffer (pH=7.4), containing 1, 5 and 10 μM of NSAID, and 250 nM of HRP and the reactions were triggered by addition of 50 μM of H_2O_2. Ascorbate co-oxidation rate (Δ Absorbance/min.) was calculated after recording ascorbate absorbance at λ_{max} = 266nm every 30 seconds. Each set of data represents three independents runs. * ($p<0.05$) compared with the vehicle control. One-way ANOVA & Student–Newman–Keuls post hoc were used. In presence of a reactive metabolite,

ascorbate first undergoes two-electron oxidation into dehydroascorbate, producing ascorbyl radical intermediate as shown in the diagram.

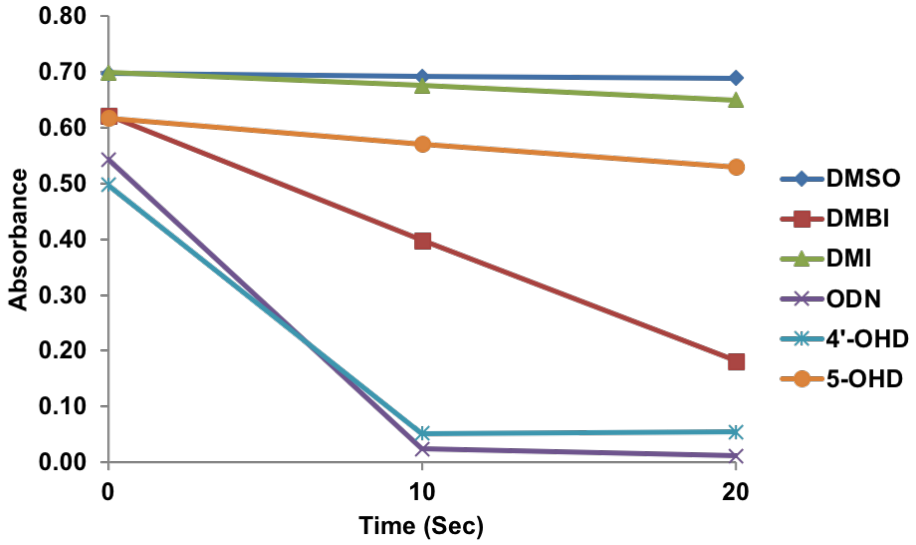

2.6.3. Figure 3. Ascorbate co-oxidation kinetics. Reactions were carried out in chelex-100- treated 0.1 M phosphate buffer (pH=7.4), containing 10 µM of NSAID/metabolite and 250 nM of HRP and the reactions were triggered by addition of 50 µM of H_2O_2. Absorbance at λ_{max} = 266nm was recoreded every 10 sec for 5 min. 4'-OH and ODN completely annihilated ascorbate absorbance at λ_{max} = 266nm after 20 sec.

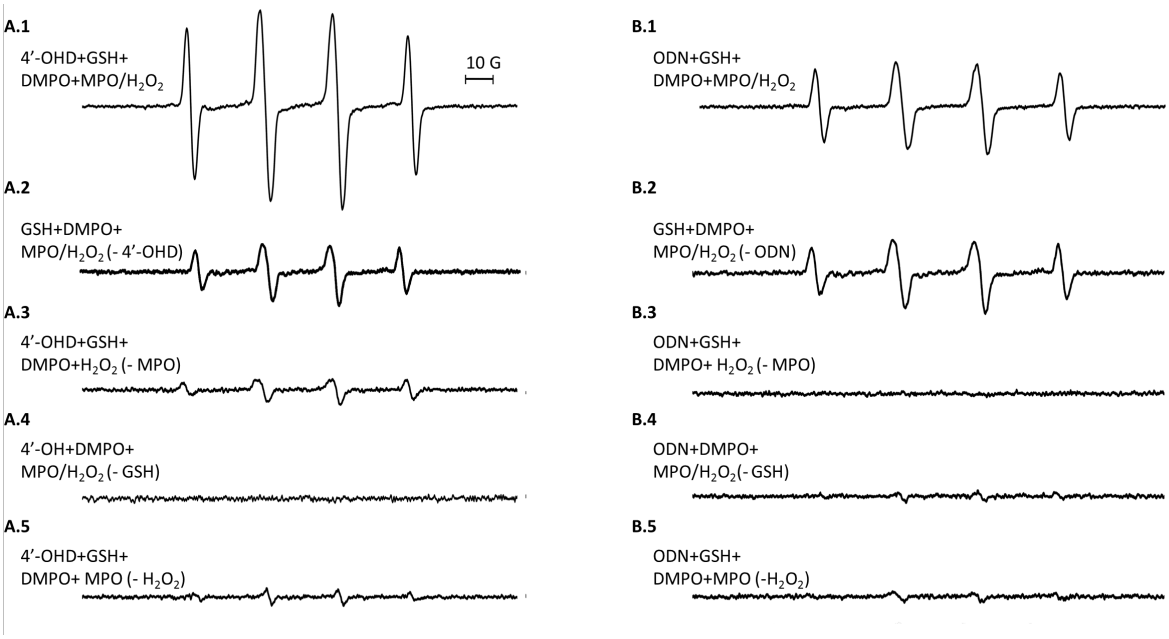

	Peak height		Peak height
A.1	0.4275 ± 0.0106	**B.1**	0.2345 ± 0.0077
A.2 (= B.2)**	0.129 ± 0.0036	**B.2**	0.129 ± 0.0036
A.3	0.085 ± 0.009	**B.3**	0.0275 ± 0.00494
A.4***	N/A	**B.4**	N/A
A.5	0.0605 ± 0.0007	**B.5**	0.0305

2.6.4. Figure 4. EPR spectra resulting from glutathionyl (GS•) radical formation. Reactions were carried out in Chelex-100- treated 0.1 M phosphate buffer (pH=7.4). The EPR spectra in A.1 contained 10 μM 4'-OHD, 1 mM GSH, 100 mM DMPO, 50 nM MPO, and was triggered with 100 μM H_2O_2. Other reactions in this series omitted 4'-OHD (A.2), MPO (A.3), GSH (A.4), or MPO & H_2O_2 (A.5). The same reactions were carried out in B.1 – B.5, except that ODN was used. Each reaction was repeated three times, and the average value of height peak for each reaction was calculated as shown in

the table. ** Both reactions A.2 and B.2 have the same peak heights as both 4'-OHD and ODN were dissolved in DMSO. *** Reactions A.4 and B.4 showed no distinct peaks.

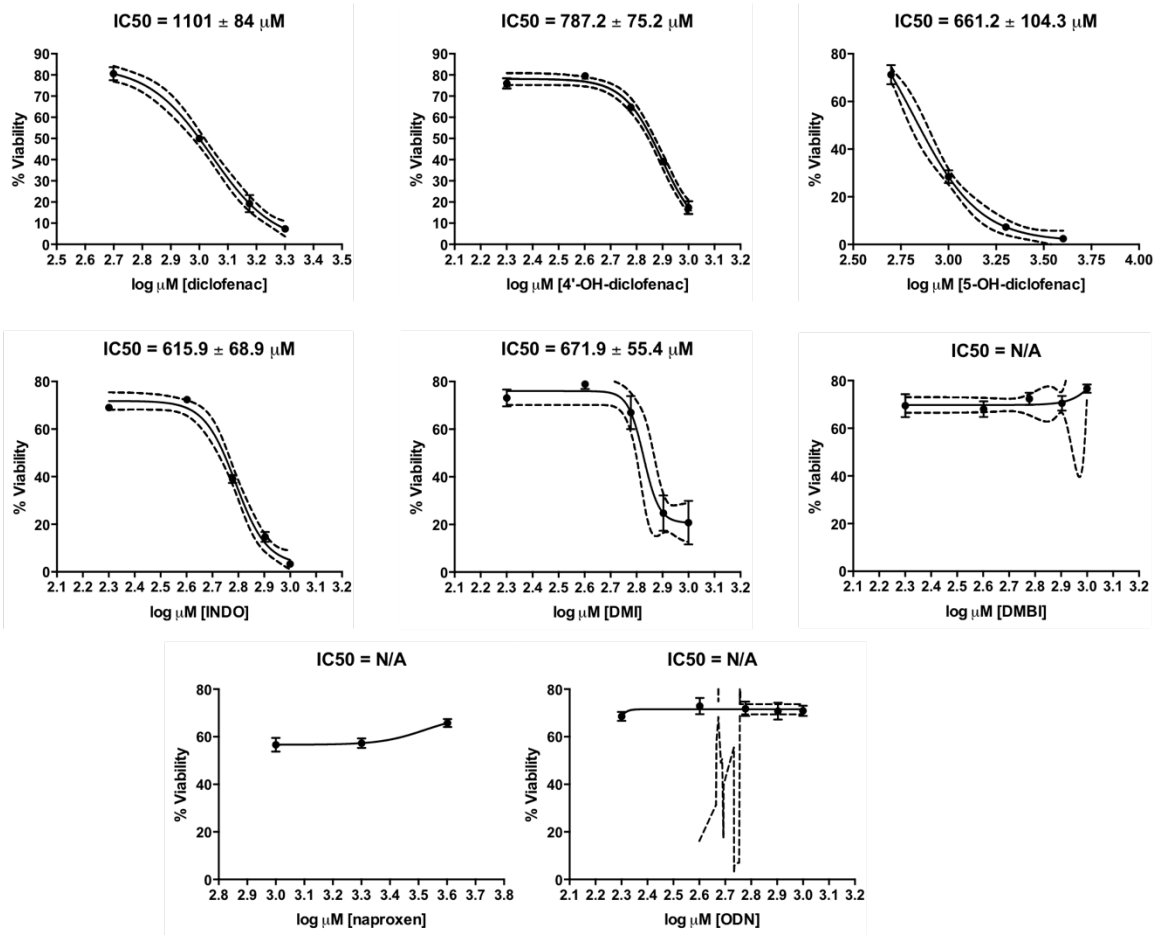

2.6.5. Figure 5. Determination of IC50 values for NSAIDs and their hepatic metabolites in HL-60 cells after 3 h incubation**.** Each compound was added to cells at increasing concentrations ranging from 0.1 up to 2 mM and incubated at 37°C an 5% CO_2 at 37 °C. Cell viability was measured afterwards using trypan blue exclusion assay. Concentration-toxicity curves were then plotted and IC_{50} values were estimated by interpolation using a 4-parameter sigmoidal regression function in GraphPad Prism V. 7.01. Dashed lines

represent 95% confidence interval. Naproxen did not demonstrate a typical concentration-toxicity curve.

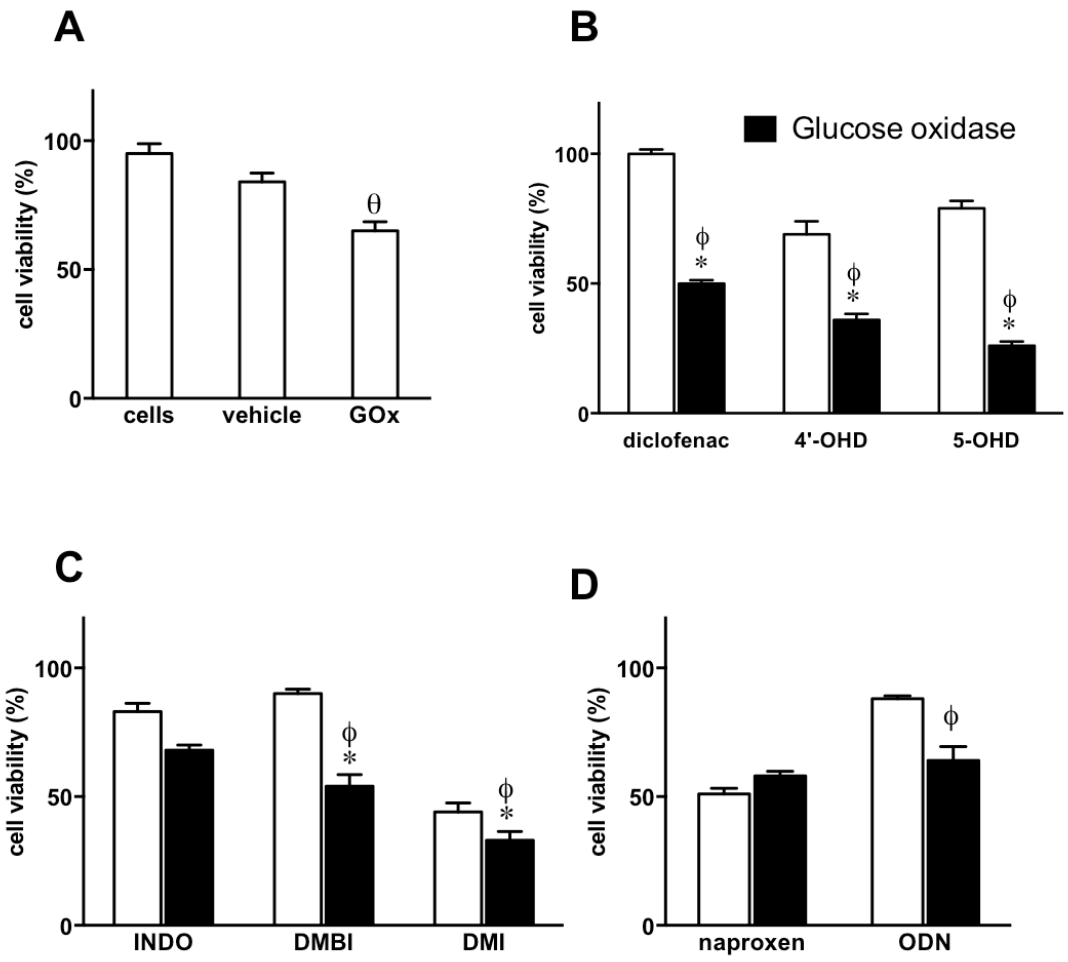

2.6.6. Figure 6. Trypan blue exclusion cell viability assay. Effect of NSAIDs/NSAID metabolites on HL-60 cell viability after 3 h incubation in absence and presence of GOx (5 mM glucose & 20 mU of glucose oxidase) as a source of H_2O_2 to trigger MPO catalytic cycle. (A) shows controls, (B) diclofenac & metabolites, (C) indomethacin & metabolites and (D) naproxen & metabolite. * ($p<0.05$) compared to the drug/metabolite alone (600 μM). $^{\phi}$ ($p<0.05$) compared with GOx alone shown in A. $^{\theta}$($p<0.05$) compared to untreated cells. Each set of data represents at least 3 independent experiments. One-way ANOVA & Student–Newman–Keuls post hoc were used.

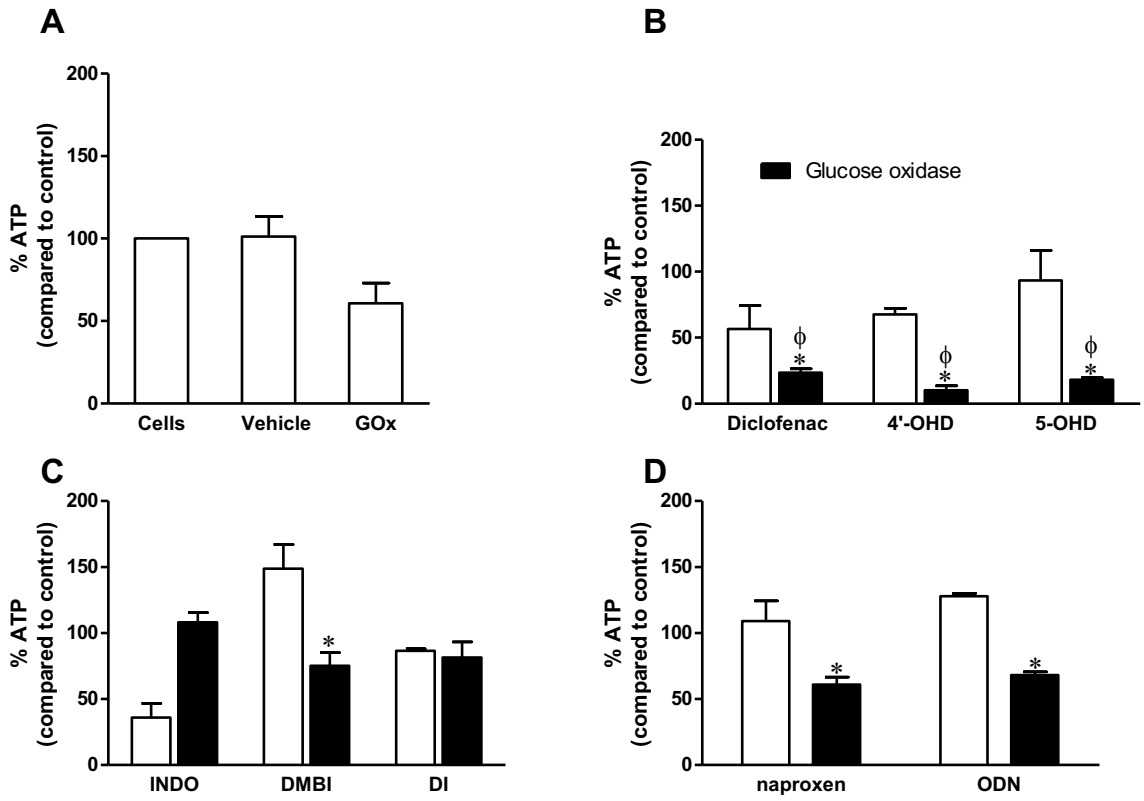

2.6.7. Figure 7. ATP-based cell viability assay. Effect of NSAIDs/NSAID metabolites on HL-60 relative ATP levels after 3 h incubation in absence and presence of GOx (5 mM glucose & 20 mU of glucose oxidase) as a source of H_2O_2 to trigger MPO catalytic cycle. (A) shows controls, (B) diclofenac & metabolites, (C) indomethacin & metabolites and (D) naproxen & metabolite. *($p < 0.05$) compared to the drug/metabolite alone (100 μM). Φ ($p < 0.05$) compared with GOx alone shown in A. Each set of data represents at least 3 independent experiments. Oneway ANOVA & Student–Newman–Keuls post hoc were used.

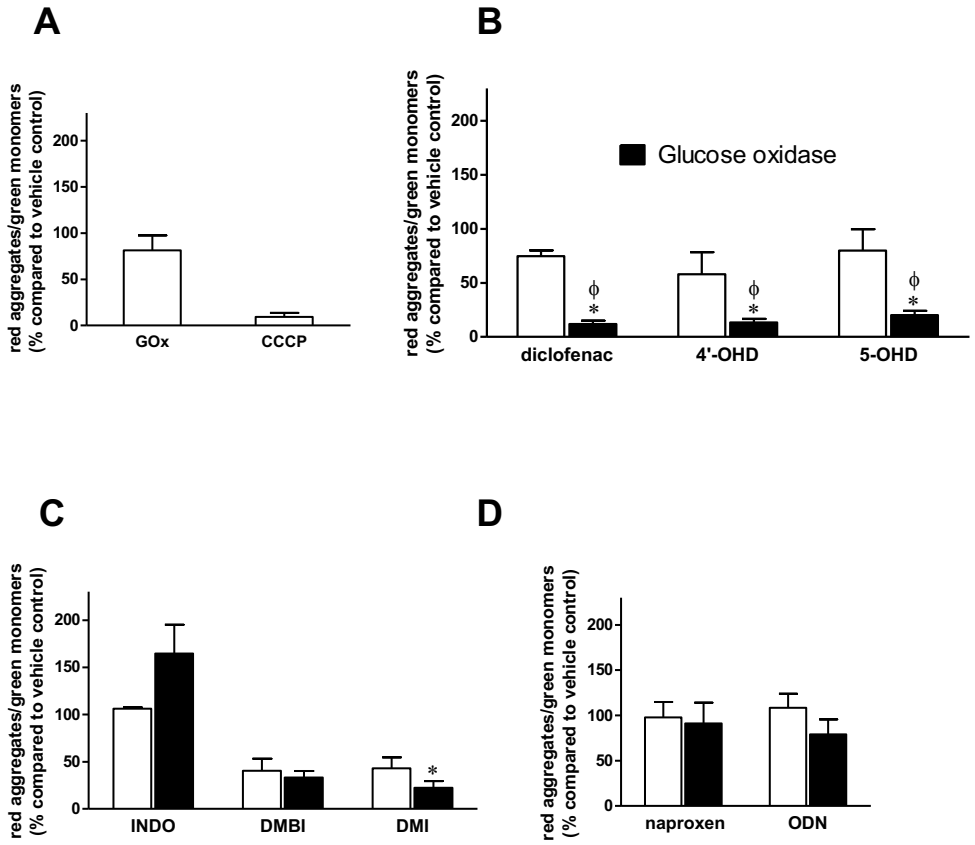

2.6.8. Figure 8. Mitochondrial membrane potential assay (MMP). Effect of NSAIDs/NSAID metabolites on MMP of HL-60 cells after 1 h incubation in absence and presence of GOx (5 mM glucose & 20 mU of glucose oxidase) as a source of H_2O_2 to activate the intracellular MPO. Red aggregates/green monomers ratio was expressed as % compared to vehicle control (DMSO); each value represents mean ±SD, n=3) Graph (A) shows the controls, (B) for diclofenac& metabolites, (C) for indomethacin& metabolites, (D) for naproxen& metabolite. * ($p<0.05$) when compared to drug/metabolite alone (100 μM). ϕ ($p<0.05$) compared to GOx alone. Each set of data represents at least 3 independent replicas. One-way ANOVA & Student–Newman–Keuls post hoc were used.

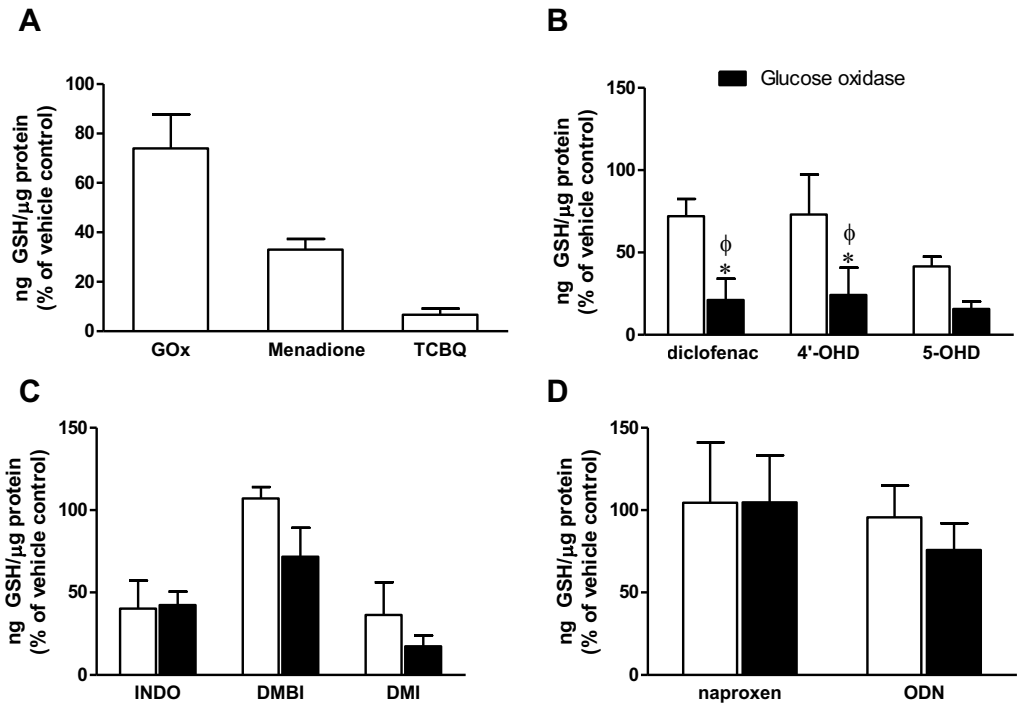

2.6.9. Figure 9. GSH assay. Effect of NSAID metabolism by cellular MPO on HL-60 cells' GSH content after 3 h incubation in absence and presence of GOx (5 mM glucose & 20 mU of glucose oxidase) as a source of H_2O_2. GSH content was quantified as ng GSH/µg protein and expressed as % of vehicle control (DMSO), and each value represents mean ±SD, n=3. Graph (A) shows the controls, (B) for diclofenac& metabolites, (C) for indomethacin& metabolites, (D) for naproxen& metabolite. *($p<0.05$) when compared to drug/metabolite alone. ϕ ($p<0.05$) compared to GOx alone. Each set of data represents at least 3 independent replicas. One-way ANOVA & Student–Newman–Keuls post hoc were used.

2.7. TABLES

Compound	**IC50 (μM)**
Diclofenac	1101 ± 84
4'-OHD	787 ± 75
5-OHD	661 ± 104
Indomethacin	616 ± 69
DMBI	> 2000
DMI	672 ± 55
Naproxen	~ 1000*
ODN	> 2000

2.7.1. Table 1. IC50 values (3 h) for NSAIDs and their hepatic metabolites in HL-60 cells. Each compound was added at different concentrations to cells and incubated as described in Materials and Methods. IC50 values were determined through interpolation.

* Naproxen did not demonstrate a typical concentration-toxicity curve.

End point	NSAIDs/Metabolites							
	Diclofenac	4'-OHD	5-OHD	INDO	DMBI	DMI	Naproxen	ODN
GSH depletion	+	+	-	-	-	-	-	-
Mitochondrial depolarization	+	+	+	-	-	-	-	-
Cell death	+	+	+	-	+	+	-	-
ATP depletion	+	+	+	-	-	-	-	-
Glutathionyl radical	-	+	-	-	-	-	-	+
Ascorbate co-oxidation	-	+	-	-	+	-	-	+

2.7.2. Table 2. Summary of results from peroxidase metabolism of NSAIDs and their metabolites. Positive (+) and negative (-) symbols were assigned from data shown in Figs. 2-7; a "+" indicates a statistically significant endpoint, and "-" indicates no significant effect.

CHAPTER 3

OXIDATION OF MEFENAMIC ACID AND ITS ANALOGUES BY PEROXIDASE ENZYMES INTO REACTIVE METABOLITES INDUCE LEUKEMIC CELL DEATH IN HL-60 CELLS

[Parts of the work in this chapter were carried out by Nadine Commandeur – MSc student and Harunur Rashid- PhD student]

3.1. ABSTRACT

In this study, we investigated the bio-activation of mefenamic acid (MFA) and its two chemical analogues, diphenylamine (DPA) and N-phenanthranilic acid (N-PA) via myeloperoxidase (MPO). The latter is a gold standard in the diagnosis of acute myeloid leukemia (AML) and is highly expressed in some AML phenotypes. As MPO is known to catalyze one-electron oxidation of chemically stable xenobiotics into reactive pro-oxidant species, we hypothesized that the enzymatic oxidation of MFA and its analogues by MPO will result in reactive metabolites that induce cell toxicity in leukemia cells. To test our hypothesis, we used both *in-vitro* and biochemical approaches. For biochemical studies, a purified MPO from human neutrophils was used for kinetic UV-vis spectrophotometry, electron paramagnetic resonance (EPR) and liquid chromatography–mass spectrometry (LC-MS) studies. UV-Vis spectrophotometry studies showed that both MPO and horseradish peroxidase (HRP) catalyzed oxidation of MFA. EPR spin trapping with 5,5-dimethyl-1-pyrroline-N-oxide (DMPO) revealed that DPA produced an apparent hydroxyl radical and carbon radical with HRP/H_2O_2. N-PA produced an intense stable radical when oxidized by horseradish peroxide HRP/H_2O_2, and MFA produced a similar spectrum albeit less intense, indicating peroxidase activity was needed for free radical metabolite formation. In addition, HRP/H_2O_2 oxidation of all analogues showed the formation of glutathionyl radical ($^{\bullet}$SG). To determine the cytotoxic potential of these radical metabolites, we used HL-60 promyelocytic leukemia cells which highly express MPO.

DPA and N-PA demonstrated MPO-catalyzed cytotoxicity in these cells, but not mefenamic acid (MFA). LC/MS analysis of the MFA oxidized product showed hydroxylated and quinoneimine species formation. The quinoneimine products reacted with GSH, forming GSH conjugates. Future studies are needed to determine the molecular mechanisms of the underlying MPO- dependent as well as MPO-independent cytotoxicity pathways.

3.2. INTRODUCTION

Because of the longstanding association between chronic inflammation and tumorigenesis, anti-inflammatory agents including non-steroidal anti-inflammatory drugs (NSAIDs) have been used in numerous studies to investigate their potential therapeutic benefit in cancer treatment or prevention. Some NSAIDs, particularly celecoxib and sulindac, have been proven to have anti-cancer activity against colon cancer[14,12]. Studies are still being carried out to delineate the underlying mechanism(s) of anti-cancer action, especially since it was shown that it is likely independent of COX-inhibition[35].

Acute myeloid leukemia (AML) is the most common type of leukemia in adults[155]. AML is a fast-growing cancer characterized by maturational arrest of progenitor cells resulting in the accumulation of immature, malfunctioning cells that replace normal blood cells in bone marrow and blood. Myeloperoxidase is an antibacterial heme protein that is most abundant in human neutrophils and plays a pivotal role in fighting infections. MPO is biosynthesized in the early stages of myeloid differentiation of progenitor stem cells, and because it is almost exclusively present in the myeloid lineage, it has been considered a gold standard to differentiate between AML and acute lymphoid leukemia (ALL). MPO

expression in AML was found to be correlated to a good prognosis and better patient response and benefit from different chemotherapy and stem cell treatments[,171,172]. In addition, MPO also has a strong oxidizing capacity as it has been implicated in the extrahepatic bio-activation of xenobiotics[98,173,174] through one-electron oxidation into toxic reactive metabolites. Interestingly, MPO was also found to bio-activate a number of chemotherapeutic agents and the resulting reactive species were shown to cause cellular oxidative damage[131,129]. In this study, we examine the bio-activation of mefenamic acid (MFA) and its two chemical analogues, diphenylamine (DPA) and N-phenanthranilic acid (N-PA) (Fig.1) by MPO. MFA was previously shown to be hydroxylated into 3'-hydroxymethyl-MFA, 4'-hydroxy-MFA or 5-hydroxy-MFA by various CYPs, which can be precursors to reactive metabolites[175]. To the best of our knowledge, the approach of targeting the MPO bio-activation pathway in the context of modulating leukemia cells' oxidative balance and to examine the differential reactivity between MFA and chemical analogues have not yet been studied. In this study, we used human promyelocytic leukemia cell line (HL-60) to investigate the metabolism of MFA and its compounds since MPO is highly expressed in this leukemic cell line.

3.3. METHODS AND MATERIALS

3.3.1. Chemicals and kits

MFA was purchased from EMD Millipore USA (Temecula, CA). Human purified MPO (180-220 units per mg protein after lyophilization) was purchased from Athens Research & Technology (Athens, GA). Sodium phosphate buffer (PB, 0.1M, pH 7.4) was treated with Chelex-100 resin purchased from Bio-Rad Laboratories (Mississauga, ON) at

4 °C overnight and treated with 100 μM of diethylenetriamine-penta acetic acid (DTPA) to further prevent metal-catalyzed auto-oxidation. 5,5-Dimethyl-1-pyrroline-*N*-oxide (DMPO), manufactured by Dojindo Molecular Technologies, Inc., Japan, was purchased from Cedarlane Laboratories (Burlington, ON). Human promyelocytic leukemia cells (HL-60 cells) were purchased from ATCC (Manassas, VA). 0.4% Trypan blue stain was obtained from Lonza (Anaheim, CA). All other chemicals (unless otherwise noted) were purchased from Sigma-Aldrich Canada (Oakville, ON) and were of the highest grade available.

3.3.2. UV-Vis analysis

Reactions (500 μL total volume) were carried out in Chelex-100 treated PB (0.1 M, pH 7.4), containing 100 μM of MFA or the analogue, 500 nM horseraish peroxidase (HRP) or 100 nM MPO. and when required 500 μM GSH. Reactions were initiated by the addition of 100 μM H_2O_2 and the absorbance was measured using a SpectraMax M5 spectrophotometer. Absorbance was measured within a range of 200-800 nm. Spectra were measured every 5 min. for 1 h, and results showed that the amount of product reached a stable level for all three compounds after 5 min. 500 μM glutathione (GSH) was added either prior to the addition of H_2O_2 or 30 min. after triggering the reactions by H_2O_2.

3.3.3. Electron paramagnetic resonance (EPR)

Reactions were prepared in chelex-100 treated PB (0.1 M, pH 7.4), containing either 2 mM of MFA/DPA/NPA, 200 mM DMPO, 20 μM HRP/50nM MPO. Reactions were initiated by the addition of 100 μM H_2O_2 and reactions were transferred into a flat cell and placed in an Elexsys E500 EPR spectrometer cavity for analysis using the following

settings: microwave frequency 9.8 GHz; incident microwave power, 20.0 mW; center field, 3496.95 G; scan range, 100.0 G; field modulation, 1.0 G; receiver gain, 60.0 dB; and time constant, 167.8 ms. Each individual reaction was run (one scan each) at least in duplicate on different days. Computer simulation was done using WinSim v1.0 software.

3.3.4. LC-MS analysis

Samples were prepared just as described in the spectrometry section, and samples were filtered accordingly. RP-HPLC-MS was performed using an Agilent 1200 SL HPLC System with a Kinetex EVO C18, 2.1 x 50 mm with guard (Phenomenex, Torrance, CA, USA), 3 μM particle size, thermostated at 40 °C, with a buffer gradient system composed of 0.1% formic acid in water as mobile phase A and 0.1% formic acid in acetonitrile (ACN) as mobile phase B. Samples were loaded onto the column at a flow rate of 0.5 $mLmin^{-1}$ and an initial buffer composition of 98% mobile phase A and 2% mobile phase B. After injection, the column was kept at the initial loading conditions for 1.0 minute followed by elution of the analytes by using a linear gradient from 2% to 98% mobile phase B over a period of 9 minutes, held at 98% mobile phase B for 4.0 minutes to remove all analytes from the column and back to 2% mobile phase B over 1 minute. UV absorbance was monitored at 254 nm. Mass spectra were acquired in positive mode of ionization using an Agilent 6220 Accurate-Mass TOF HPLC/MS system (Santa Clara, CA, USA) equipped with a dual sprayer electrospray ionization source with the second sprayer providing a reference mass solution. Mass spectrometric conditions were drying gas 9 L/min at 300°C, nebulizer 30 psi, mass range 100-1000 Da, acquisition rate of ~1.03 spectra/sec, fragmentor 150 V, skimmer 65 V, capillary 3200 V, instrument state 4 GHz High Resolution. Mass correction was performed for every individual spectrum

using peaks at m/z 121.050873 and 922.009798 from the reference solution. Data acquisition was performed using the Mass Hunter software package (ver. B.04.00.). Analysis of the HPLC-UV-MS data was done using the Agilent Mass Hunter Qualitative Analysis software (ver. B.07.00).

3.3.5. Trypan blue exclusion cell viability assay

Human promyelocytic leukemia cells (HL-60 cells) were cultured in Gibco™ RPMI-1640 medium containing 10% fetal bovine serum and 1% antibiotic-antimycotic and were maintained in a 37 ˚C, 5% CO_2 atmosphere. Change of media occurred every two days, and cells did not exceed a passage number of 35. Cells (2 x 10^6 cells/ml) were harvested and resuspended in warm PBS (while remaining at a temperature of 37 ˚C) after centrifugation for 5 min. at 150 g for 15 min. Cells were exposed to 100 μM and 300 μM of MFA, DPA or NPA for 3 h in presence and absence of 5 mM glucose and 10 mU glucose oxidase. The enzymatic system of glucose and glucose oxidase (GGOx) acts as a source of H_2O_2 to activate the intracellular MPO. To measure the cytotoxicity, Gibco™ 0.4% trypan blue reagent was added in a 1:1 ratio and mixed for 2 min. then viability was measured using a Bio-Rad TC-10 automatic cell counter. All treatments were run at least triplicate on three different days. Data were expressed as mean ± SD.

3.4. RESULTS

3.4.1. UV-Vis spectrophotometry

To study the metabolic activation of MFA, DPA and NPA, biochemical reactions of each compound were prepared using MPO and HRP with addition of GSH either before or after initiating the peroxidase reaction by H_2O_2 as described under Materials and Methods

(section 3.2.2). In the case of MFA, its peroxidation resulted in the formation of two new peaks at λmax = 249 nm and λmax = 384 nm, which were observed with both MPO (Fig.2A) and HRP (Fig.2B); a color change into light brown was also observed. The formation of the new peaks and the color change were completely inhibited in the presence of GSH (Fig.2C). After the addition of H_2O_2 to DPA and either MPO or HRP, two new peaks were observed at λmax = 265 and 451 nm (Fig.3A and Fig.3B) with the formation of a strong red color. Like MFA, GSH inhibited the formation of the new peaks resulting in no spectral change from the parent spectrum (Fig.3C) and no color change. N-PA showed formation of new peaks at λmax = 256 and 447 nm after addition of H_2O_2 (Fig.4A and 4B) with a light brown color formation. The presence of GSH inhibited the formation of new peaks and the color change. When GSH was added after the formation of peaks in each of MFA, DPA and N-PA, the peaks did not disappear, but a bathochromic shift at λmax ≈ 300 nm was observed (Fig.2D, 3D and 4D), indicating a possible interaction (conjugation) between GSH and the formed product(s). In all three compounds, spectral changes were the same in presence of MPO or HRP, with much higher rate of spectral changes in case of HRP.

3.4.2. EPR characterization of MFA/analogues oxidation paramagnetic intermediates

EPR studies were carried out after mixing 2 mM of MFA, DPA or N-PA with DMPO, as a spin trap, 20 μM HRP or 50 nM MPO and H_2O_2 was added last to start the reactions as described under Material and Methods (section 3.3.3). DPA showed the formation of two species of radicals as displayed in Fig. 5A. First, a C-centered radical (DMPO/$^{\bullet}CH_3$), indicated by a hyperfine splitting constant of a^N = 15.4 G and a^H = 22.6

G, represented by an EPR spectrum consisting of 6 peaks. In addition, DPA demonstrated the formation of hydroxyl-radical (DMPO/•OH) with a hyperfine splitting constant of $a^H = a^N = 14.8$ G. Unfortunately, we were not able to characterize radicals formed in the case of MFA (Fig. 5B), however, N-PA formed a stable radical in both H_2O_2/HRP and MPO/H_2O_2 systems with no need of DMPO spin trap (Fig.5C and 5D). In order to characterize the N-PA free radical, computer simulations were performed based on the assumption that the free radical is predominantly N-centered. As shown in Fig. 6, the computer simulation closely correlated with the experimental spectrum (r = 0.997). The parameters for the hyperfine splitting constants were $a^N = 6.19$ G, $a^H = 6.18$ G for two equivalent protons, and $a^H = 3.1$ G. This species corresponds to an N-centered radical that is interacting with two adjacent protons on the phenyl ring and the proximal proton (circled in Fig. 6 C). This species was sufficient for characterization, however, the simulation was improved when an additional species corresponding to a nitroxide (derived from N-oxidation) was included, though this was minor (Fig. 6D).

3.4.3. EPR detection of MFA- glutathionyl (GS•) radicals.

To study the pro-oxidant potential of the MPO-catalyzed MFA/MFA analogues' free radicals, glutathione was utilized as an intermediate to react with the free radicals, with the formation of glutathionyl (•SG) radical as a surrogate marker of the presence of a reactive paramagnetic species. DMPO spin trap was added for trapping glutathionyl radicals as described under Materials and Methods (section 3.3.3). When GSH was added a typical EPR spectrum characteristic of glutathionyl-DMPO adduct was obtained with

MFA, DPA and NPA (Fig.7) The signal was most intense with DPA, which indicates more abundant radical formation and it was least intense with MFA.

3.4.4. LC-MS analysis of stable MFA and DPA peroxidation metabolites

The product formation of MFA was analysed in more details by using liquid chromatography-mass spectrometry (LC/MS) as described under Materials and Methods (section 3.3.4). To analyse the MFA product formation, a reaction (500 μL total volume) was carried out in chelex-100 treated PB (0.1 M, pH 7.4), containing 100 μM of MFA, 500 nM HRP, and 100 μM H_2O_2 to trigger the reaction. To study the GSH-adduct formation, 500 μM of GSH was added to a reaction containing the same components. Here, GSH was added after initiating the oxidation by H_2O_2 (endorsed by the observation of color change). MS analysis of the MFA reaction (without GSH) showed the formation of a product eluting at 4.57 min with *m/z* 258.1 that was assigned to a hydroxylated product (Fig.8). A second peak was eluted at 4.28 min. to which a quinone-imine structure (m/z 256.15) was assigned (Fig.8), and MFA itself was eluted at 5.21 min. In addition, two MFA dimers were found eluting at 5.71 min and 5.78 min with *m/z* of 479.20 and *m/z* 481.15 (Fig.9). In the presence of GSH, LC/MS analysis showed the formation of three GSH-MFA adducts (Fig.10). The first GSH-adduct eluted at 3.58 min. (*m/z* 561.10); the second GSH-adduct eluted at 3.97 min (*m/z* 563.20), and the third adduct eluted at 4.93 min (*m/z* 786.10). These fragments correspond with MFA-dimer GSH-adducts with molecular masses of 560.16 g/mol, 562.17 g/mol, and 785.27 g/mol respectively. The first two adducts correlate to hydroxylated/oxidized MFA-GSH. The third GSH-adduct was assigned to a MFA dimer-GSH adduct; the latter GSH-adduct was shown to be the major product to be formed in this reaction.

3.4.5. Cytotoxicity in HL-60 cells

HL-60 cells were incubated with two different concentrations (100 μM and 300 μM) of MFA and its two analogues, DPA and NPA for 3 h in the presence and absence of G/GOx as described under Materials and Methods (section 3.3.6). After 3h, the cell viability, measured using trypan blue exclusion assay, showed that both concentrations of DPA caused a significant decrease in HL-60 cell viability in the presence of G/GOx compared to G/GOx or DPA alone *($p<0.05$) (Fig.11D). N-PA was found to cause significant cytotoxicity at 300 μM but the decrease in viability was not significant at the lower concentration. (Fig.11C). Decrease in cell viability in the case of MFA + G/GOx was not significant when compared to MFA alone and G/GOx. The cytotoxicity of MFA and its analogues were tested at 1 mM concentrations as well, but this concentration was too cytotoxic (data are not shown).

3.5. DISCUSSION

In a previous study, we showed that metabolic bio-activation of three NSAIDs, diclofenac, indomethacin and naproxen by MPO presents a cytotoxic potential to HL-60 leukemic cells[176]. In the present work, we studied the possibility of metabolic bio-activation of MFA, first by purified human neutrophil MPO and HRP which is known to have similar activity as MPO, and then we examined the effect of such bio-activation on the leukemic cell viability. We also included in the study closely related chemical analogues to MFA, DPA and NPA for comparing the differential reactivity. The study provided evidence that even though there are minor structural differences between MFA and its analogues, they demonstrated differences in their oxidation potential by MPO and in the reactivity of the

resulting compounds. In UV spectrophotometry studies, MFA and both DPA and N-PA were all shown to be oxidized in the peroxidase enzymatic system, which was indicated by the formation of new peaks in UV sepctra and with the quick change in color upon triggering the peroxidase cycle by H_2O_2. New peaks were at different wavelengths, which indicates different identities. DPA appeared to have the most intense visible spectral changes, and MFA demonstrated the least changes. In all three compounds, the observed color formation of the reactions along with the general increase in absorbance from the UV-Vis studies is suggesting the formation of metabolites.

Addition of GSH before starting the oxidation reaction resulted in no spectral change or formation of new peaks, and that could be because GSH prevented the formation of the initial free radical metabolites which would lead to products; later addition of GSH caused a peak bathochromic shift in all three compounds, indicating the formation of adducts with GSH when the oxidized products were allowed to form. This indicates that the products formed were electrophilic metabolites that formed GSH conjugates. EPR spin trapping was not able to elucidate the precise free radical metabolites of MFA/analogues, except for N-PA, which remarkably formed a stable free radical that did not require spin trapping. It is possible that MFA formed a similar species; however, the spectrum was too weak to allow for characterization (Fig.5B). The spectra resulting from DPA displayed the apparent formation of hydroxyl radical (DMPO/$^{\bullet}$OH) and/or alkyl (methyl) radicals. The carbon radical may be due to solvent (EtOH or DMSO), which can be oxidized by a free radical intermediate. The apparent hydroxyl radical formation suggests a relatively high oxidation potential of DPA, which was also evident as DPA was the most potent at GSH oxidation and glutathionyl radical formation (Fig.7). It is possible that this occurred due to

quinone/H_2O_2 interactions that have been noted to produce hydroxyl radical[177]. To investigate the oxidation products formed in these reactions more closely, LC/MS analysis was focused on the parent MFA. MFA appeared to be hydroxylated, and further oxidized to quinoneimine and dimers (Fig.8 and Fig.9), quinoneimine product in turn appeared react with GSH, forming a GSH conjugate. This is unusual because such two-electron oxidation is typical cytochrome P-450 bio-activation reaction[175]. In fact, a recent study performed by Venkataraman et al. investigated the oxidative bioactivation of MFA using recombinant human CYPs. By characterizing the structures of the reactive intermediates, it was demonstrated that besides being oxidized into the major 3'-OH-methyl-MFA, 4'-OH-MFA and 5-OH-MFA, reactive metabolites were formed by various CYPs through the oxidation of both MFA aromatic rings. In addition, a GSH-adduct was formed, resulting from GSH conjugation of the quinoneimines formed after further bio-activation of the found metabolites[175]. Our studies demonstrated a similar oxidation pattern of MFA by peroxidase-system. First, three products were formed after MFA oxidation in a HRP/H_2O_2-system. A hydroxylated MFA product was detected, and a dimer was found. MS analysis of the GSH-adduct formation showed the detection of two GSH-adducts. One GSH-adduct appeared to involve hydroxylation and subsequent oxidation of MFA to a quinoneimine electrophile. The other GSH-adduct was significantly larger and was assigned to a GSH-adduct of an electrophilic MFA-dimer indicating that the MFA dimer was hydroxylated prior to the formation of a GSH conjugate. It appeared that peroxidases produced similar metabolites as cytochrome P450s. Further studies can also be done to confirm the proposed structures by LC/MS analysis, by using proton nuclear magnetic resonance (H-NMR) or by LC-MS/MS fragmentation data analysis.ftitl

In summary, this study provides insight into the differential reactivity of MFA and fenamic acid analogues and the consequent effect on glutathione after oxidation by MPO or HRP. Including chemical analogues in the study also provided useful information about the relevance of structural residues of MFA. Masubuchi et al. previously suggested that the substituted group(s) on diphenylamine-structures are important for their cytotoxicity.[178] They demonstrated that the cytotoxicity caused by various NSAIDs relates to their differential structure. Our cytotoxicity studies support this statement. MFA and its analogues showed the formation of differentially reactive radicals, as shown by cytotoxicity in HL-60 cells to different extents. This study presents additional evidence that NSAIDs or their chemical derivative could have cytotoxic potential in leukemia cells that highly express MPO, which can be a novel approach of targeting leukemia cells based on MPO-dependent cytotoxicity. Further studies are required to investigate the molecular pathways involved and their application to targeting leukemia cells.

3.6. ACKNOWLEDGEMENT

This work was supported by the Natural Sciences and Engineering Research Council of Canada (NSERC) (RGPIN-2014-04878).

3.7. FIGURES

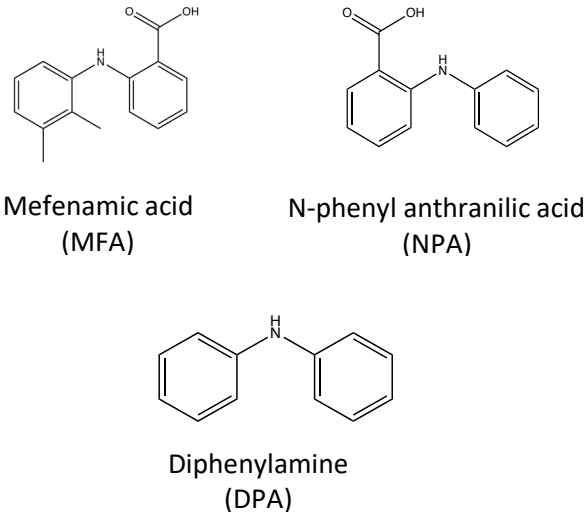

3.7.1. Figure 1. Molecular structures of mefenamic acid and its analogues used in this study.

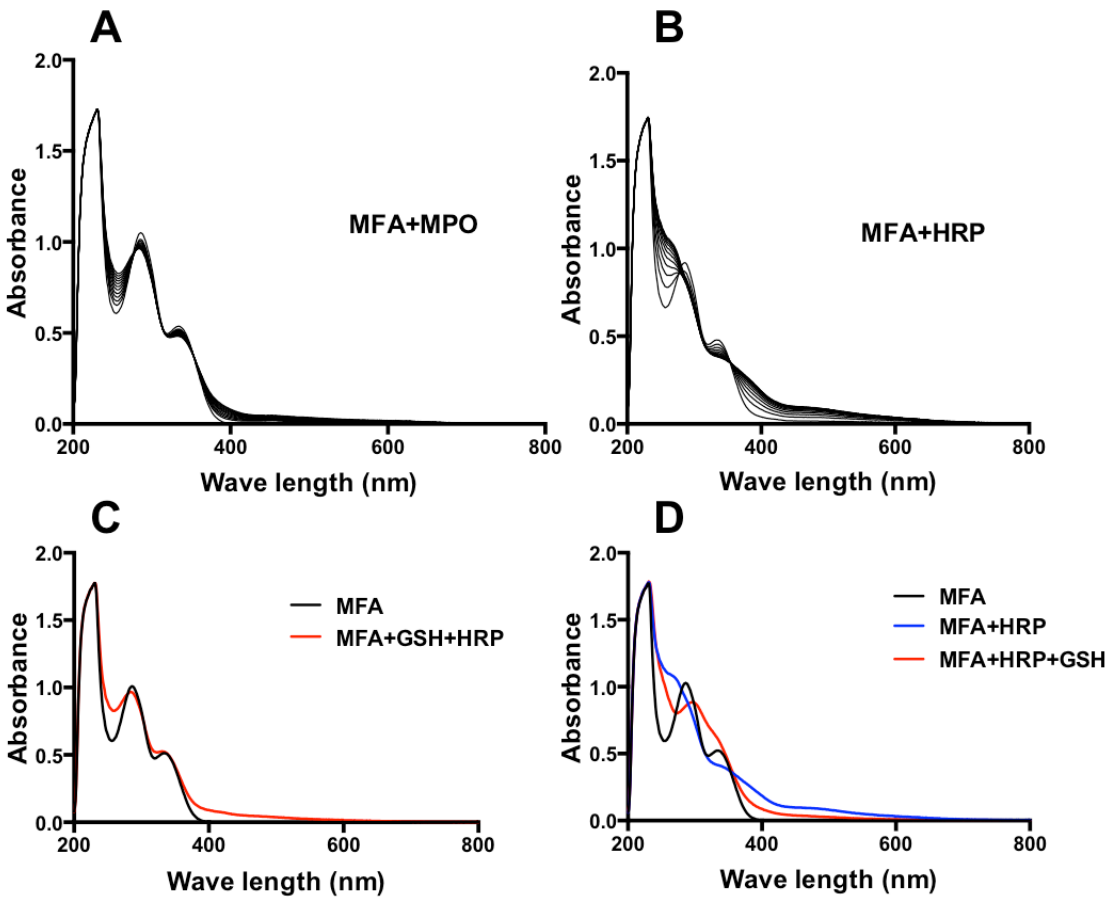

3.7.2. Figure 2. UV-Vis spectrophotometry studies on mefenamic acid (MFA) peroxidation. Reactions were prepared by mixing 100 µM MFA and 100 µM H_2O_2 in 500 µL 0.1M phosphate buffer (pH 7.4) containing 100 µM DTPA in presence of either 100 nM MPO (A) or 50 nM HRP (B). For (A) and (B), spectra were recorded every 5 min for a total of 60 min at $\lambda_{200\text{-}800}$. For (C), spectral scans were done for 100 µM MFA alone, and after 50 nM HRP was added to a reaction mixture of 100 µM MFA, 500 µM GSH, and 100 µM H_2O_2 (spectra did not change when recorded for 60 min). In (D), the same reaction as (B) containing MFA, HRP and H_2O_2 was run for 30 min (blue line) before the addition of 500 µM GSH (red line). Each reaction was repeated three times independently.

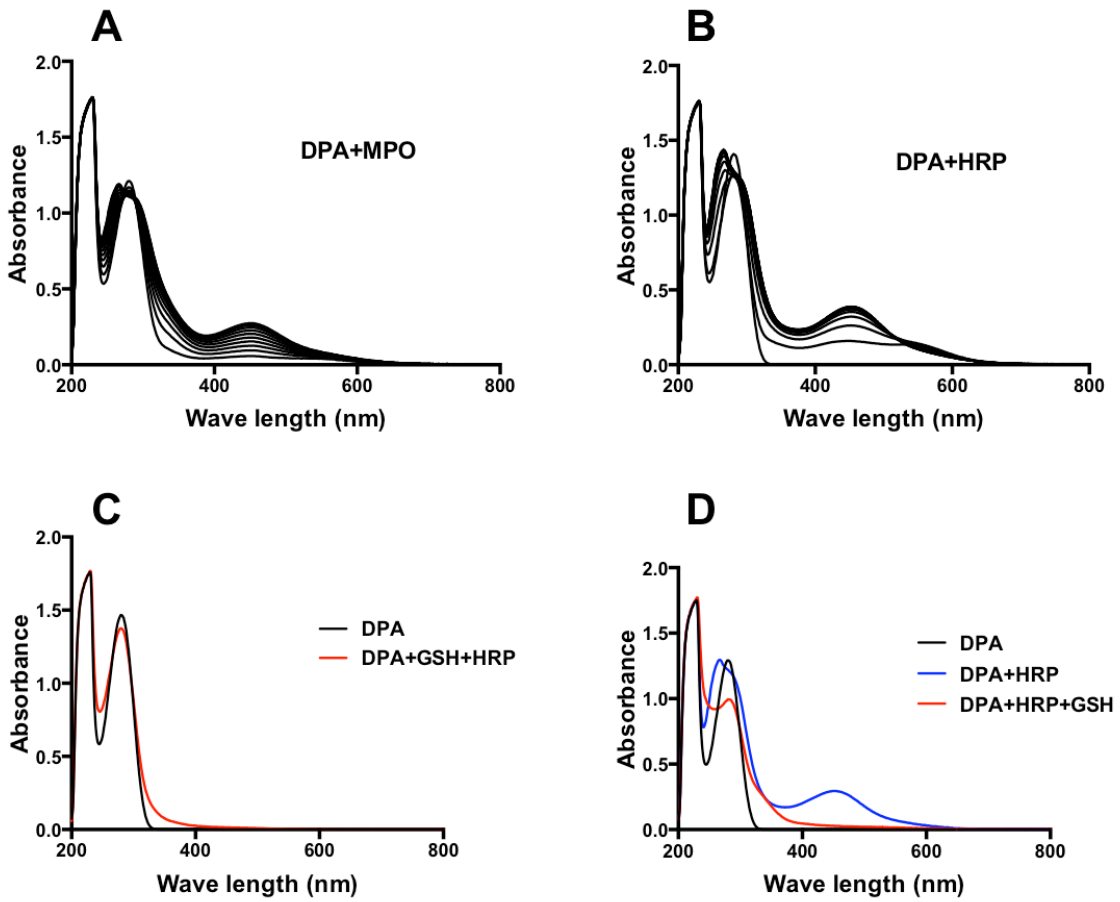

3.7.3. Figure 3. UV-Vis spectrophotometry studies on Diphenylamine (DPA) peroxidation. Reactions were prepared by mixing 100 µM DPA and 100 µM H_2O_2 in 500 µL 0.1M phosphate buffer (pH 7.4) containing 100 µM DTPA in presence of either 100 nM MPO (A) or 50 nM HRP (B). For (A) and (B), spectra were recorded every 5 min for a total of 60 min at $\lambda_{200\text{-}800}$. For (C), spectral scans were done for 100 µM DPA alone, and after 50 nM HRP was added to a reaction mixture of 100 µM DPA, 500 µM GSH, and 100 µM H_2O_2 (spectra did not change when recorded for 60 min). In (D), the same reaction as (B) containing DPA, HRP and H_2O_2 was run for 30 min (blue line) before the addition of 500 µM GSH (red line). Each reaction was repeated three times independently.

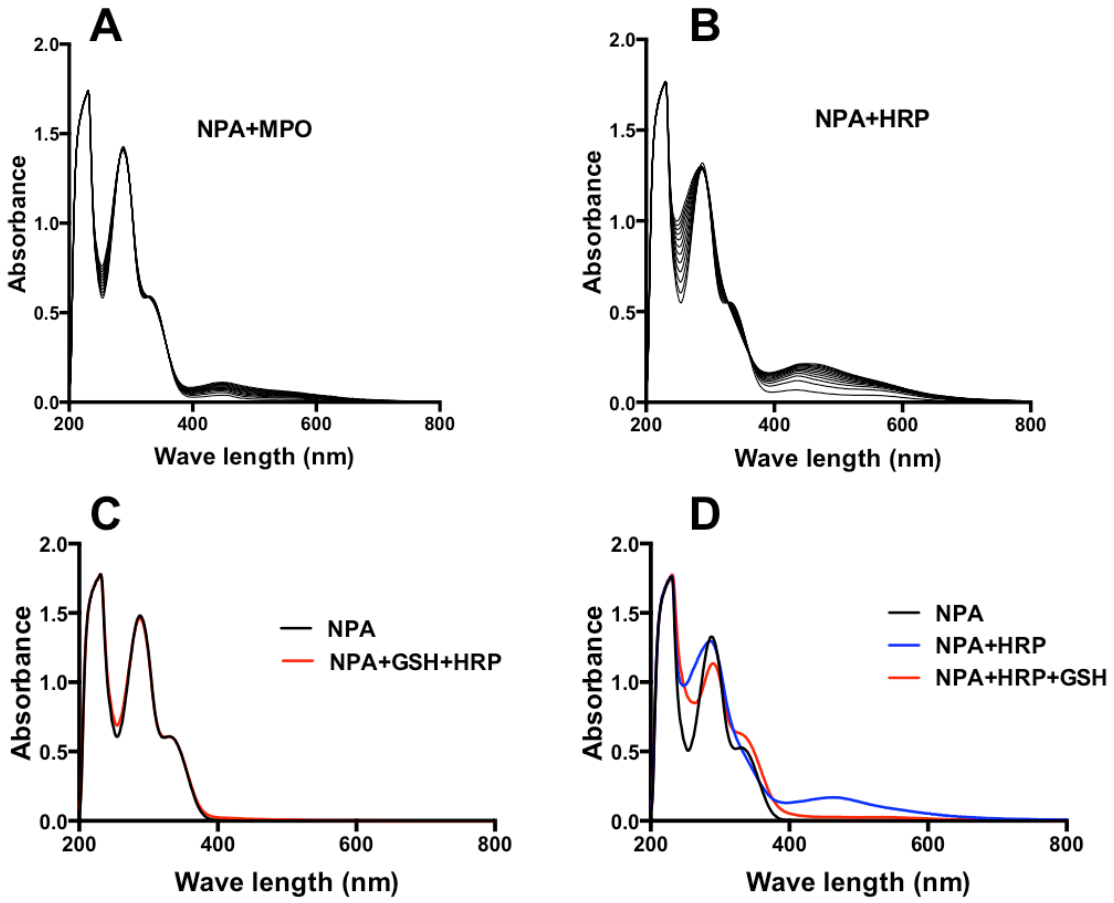

3.7.4. Figure 4. UV-Vis spectrophotometry studies on N-phenylanthranilic acid (NPA) peroxidation. Reactions were prepared by mixing 100 µM NPA and 100 µM H_2O_2 in 500 µL 0.1M phosphate buffer (pH 7.4) containing 100 µM DTPA in presence of either 100 nM MPO (A) or 50 nM HRP (B). For (A) and (B), spectra were recorded every 5 min for a total of 60 min at $\lambda_{200\text{-}800}$. For (C), spectral scans were done for 100 µM NPA alone, and after 50 nM HRP was added to a reaction mixture of 100 µM NPA, 500 µM GSH, and 100 µM H_2O_2 (spectra did not change when recorded for 60 min). In (D), the same reaction as (B) containing

NPA, HRP and H_2O_2 was run for 30 min (blue line) before the addition of 500 μM GSH (red line). Each reaction was repeated three times independently.

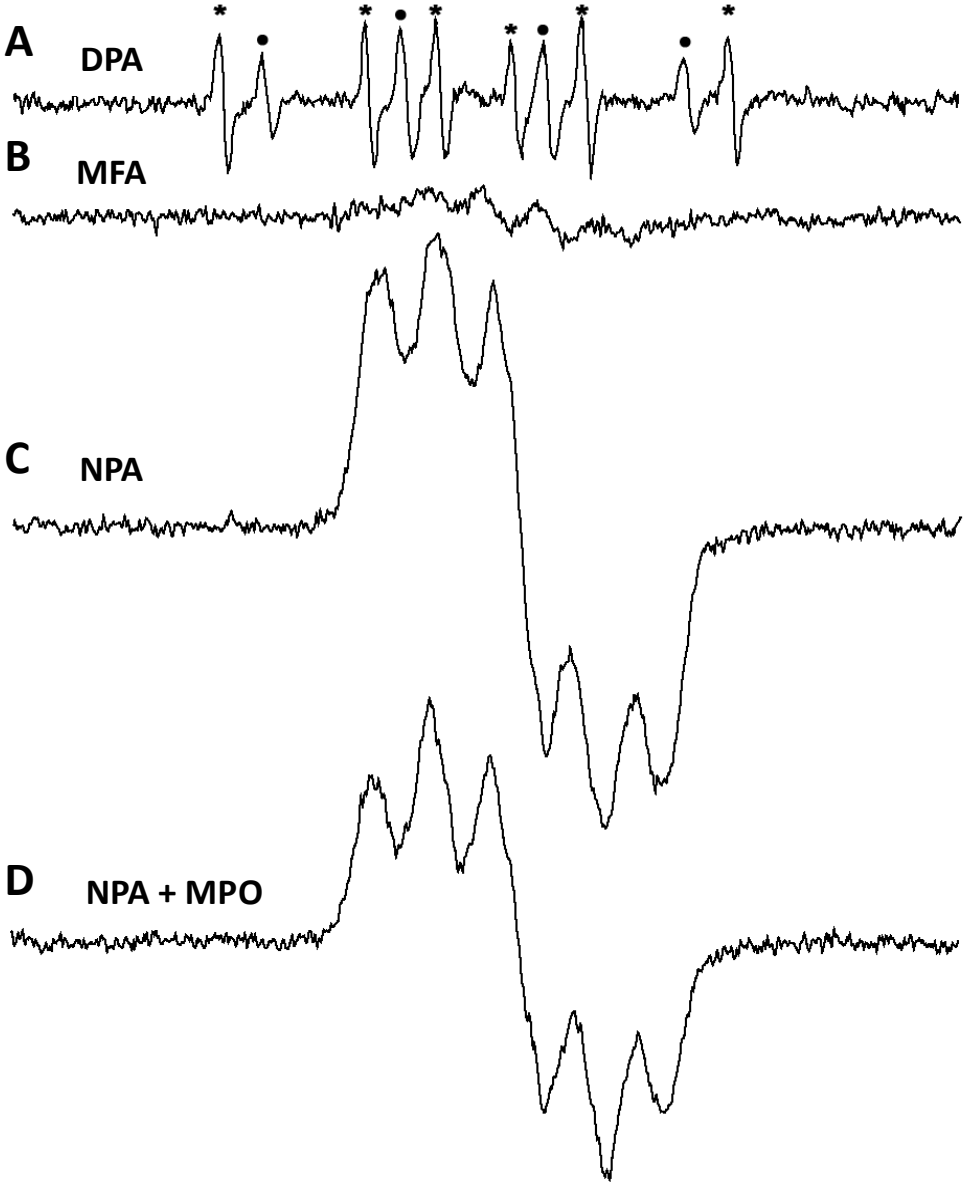

3.7.5. Figure 5. EPR spectra resulting from MFA/analogues peroxidation. Reactions were carried out in Chelex-100-treated 0.1 M phosphate buffer (pH 7.4). Reaction A contained 2 mM DPA, 200 mM DMPO and 20 μM HRP, and it was triggered by the addition of 400 μM H_2O_2. DPA was replaced by 2 mM MFA in B. In reactions C and D, spectra were obtained after mixing 2 mM NPA and 400 μM

H_2O_2 with HRP (C) or 50 nM MPO (D) in the absence of DMPO. DPA (A) showed the formation of both DMPO/•C with hyperfine splitting constants of a^N = 15.4 G and a^H = 22.6 G (due to DMSO, *) and DMPO/•OH (•). MFA free radical could not be characterized (B); NPA showed the formation of the same stable radicals without DMPO using HRP (C) and MPO (D).

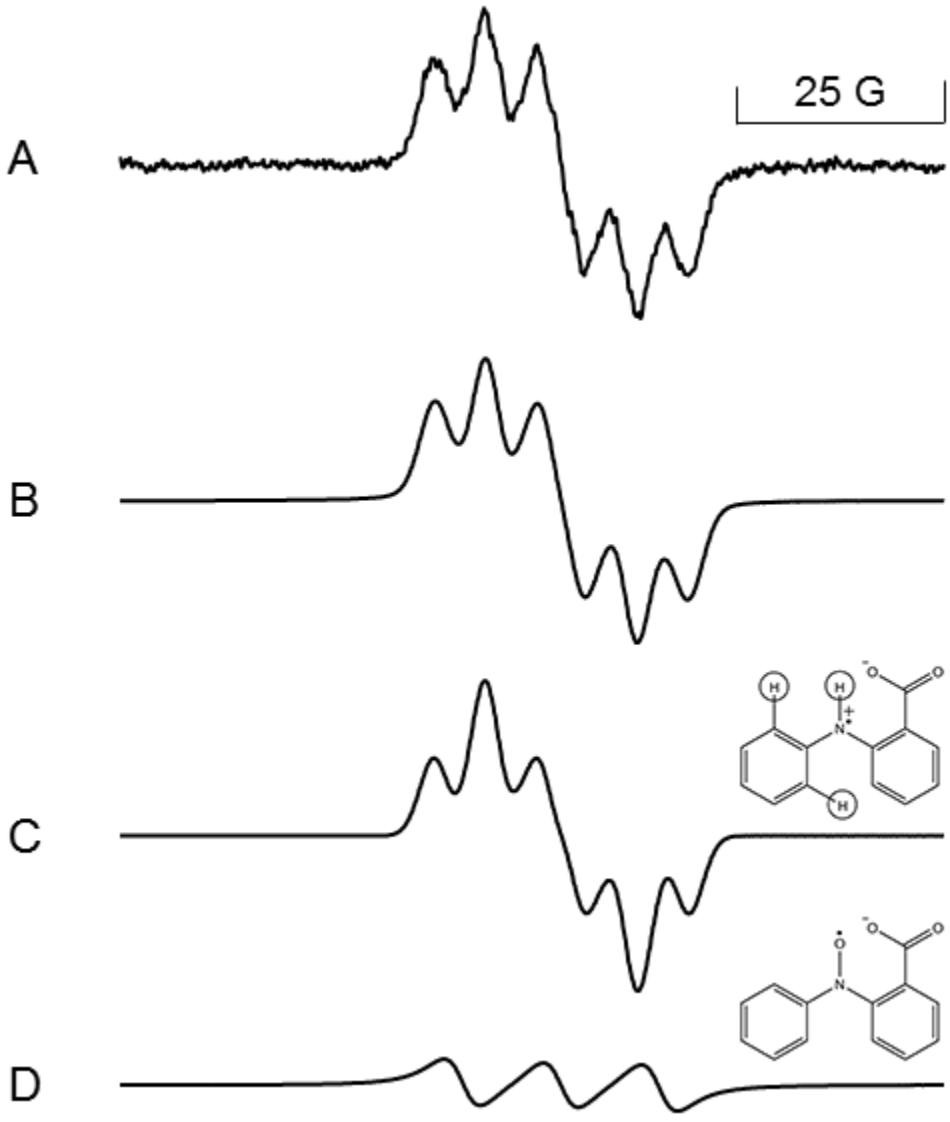

3.7.6. Figure 6. Simulation of the stable free radical resulting from NPA oxidation. In A, the experimental spectrum is shown for comparison to the simulation. The computer simulation of the experimental spectrum (B) involves the fitting of two species which produced a significant correlation (r = 0.997). The major free radical species (84.1%) contains an N-centered free radical (a^N = 6.19 G) and splitting occurred from two equivalent protons (a^H = 6.18 G) and a single proton (a^H = 3.1 G) from the phenyl rings (C). A minor free radical species (15.9%) was simulated (D) that is proposed to be a nitroxide radical (a^N = 11.9 G), presumably arising from N-oxidation.

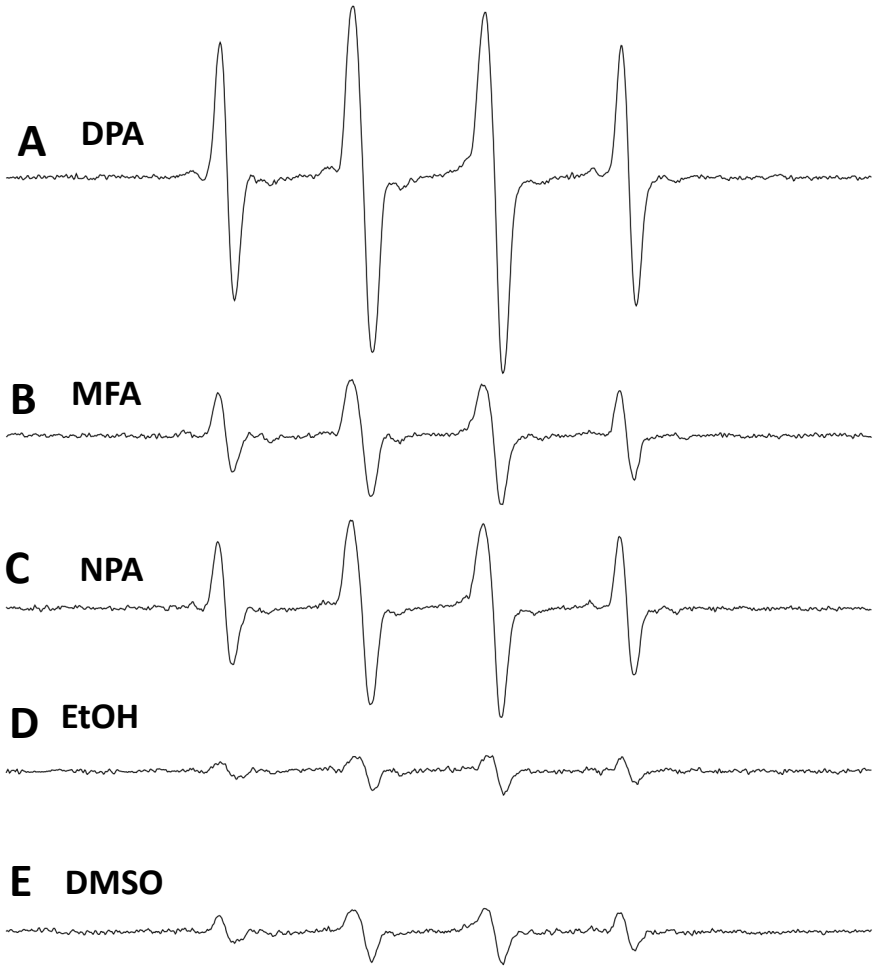

3.7.7. Figure 7. EPR spectra resulting from glutathionyl (GS•) radical formation. Reactions were carried out in Chelex-100-treated 0.1 M phosphate buffer, pH 7.4. reactions were carried out by adding 1 mM GSH, 100 mM DMPO, 50 nM MPO and 100

μM H_2O_2 to 20 μM of either DPA (A), MFA (B) or NPA in C. Vehicle controls (EtOH, DMSO) were done in D and E by omitting MFA or the analogue. MFA and its analogues showed MPO-catalyzed formation of glutathionyl radicals.

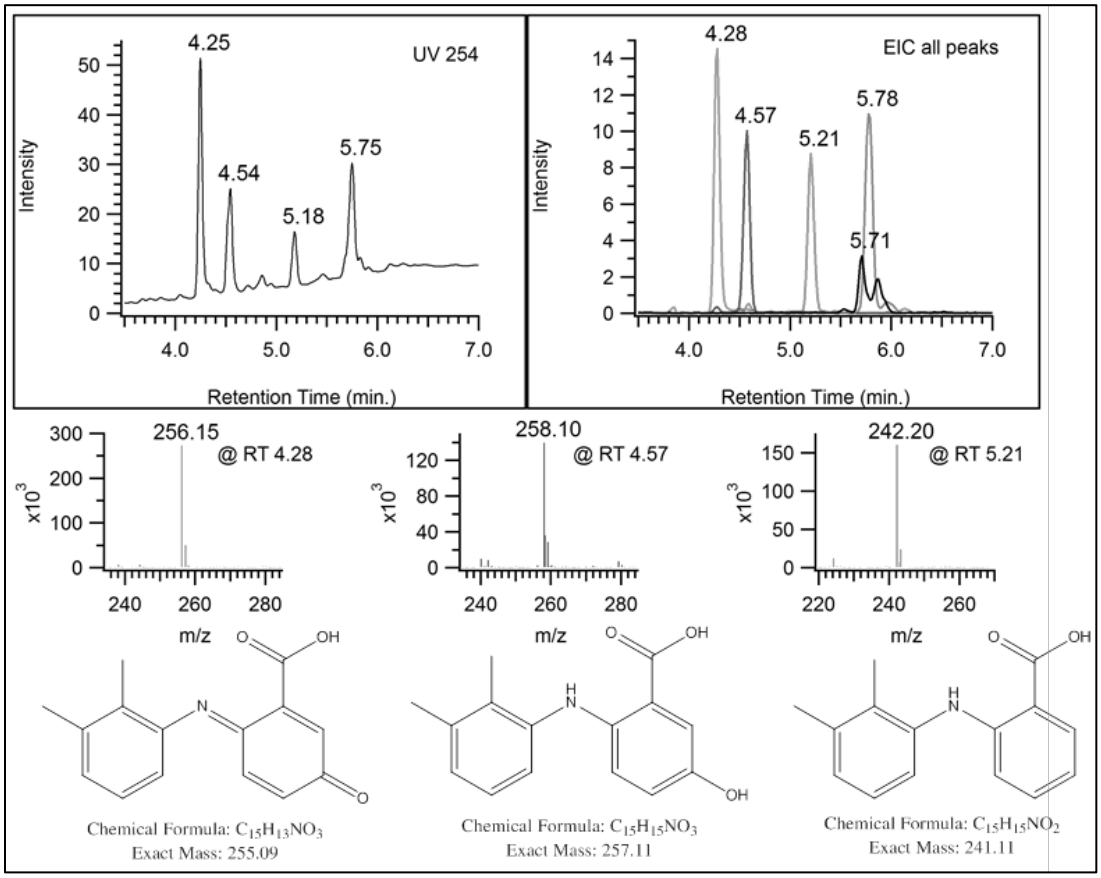

3.7.8. Figure 8. LC-MS of MFA-quinoneimine and hydroxy-MFA. Upper chromatogram depicts the elution of fragments with a m/z of 256.15, 258.10, and 242.20 at 4.28, 4.57 and 5.21 min respectively. These fragments correspond to a quinone-imine MFA, hydroxy-MFA and MFA (in order of elution time). The formulae were proposed by high-resolution MS analysis.

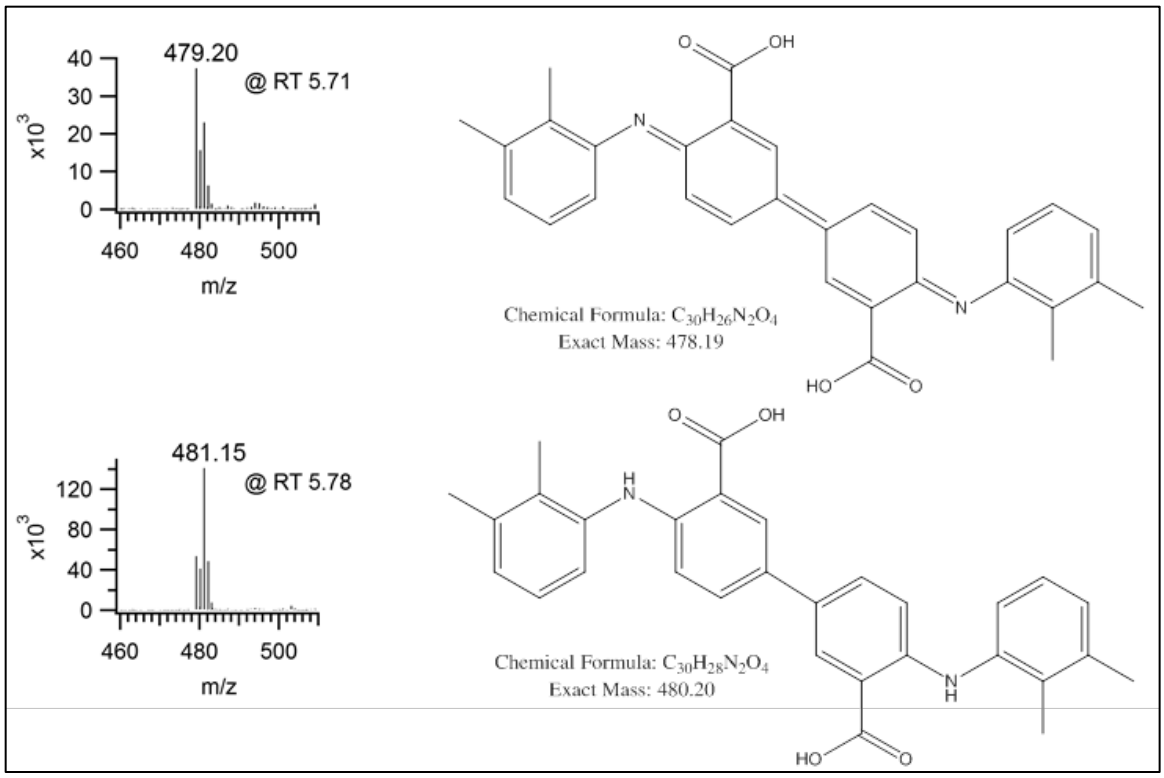

3.7.9. Figure 9. LC-MS of MFA dimerization products. The upper spectra depict the elution of a fragment with *m/z* 479.20 at 5.71 min. This fragment corresponds to a quinone-imine MFA-dimer with a molecular mass of 478.19 g/mol. Bottom spectra depicts the elution of a fragment with *m/z* 481.15 at 5.78 min. This fragment corresponds to a MFA-dimer. The formulae were proposed by using high-resolution MS analysis.

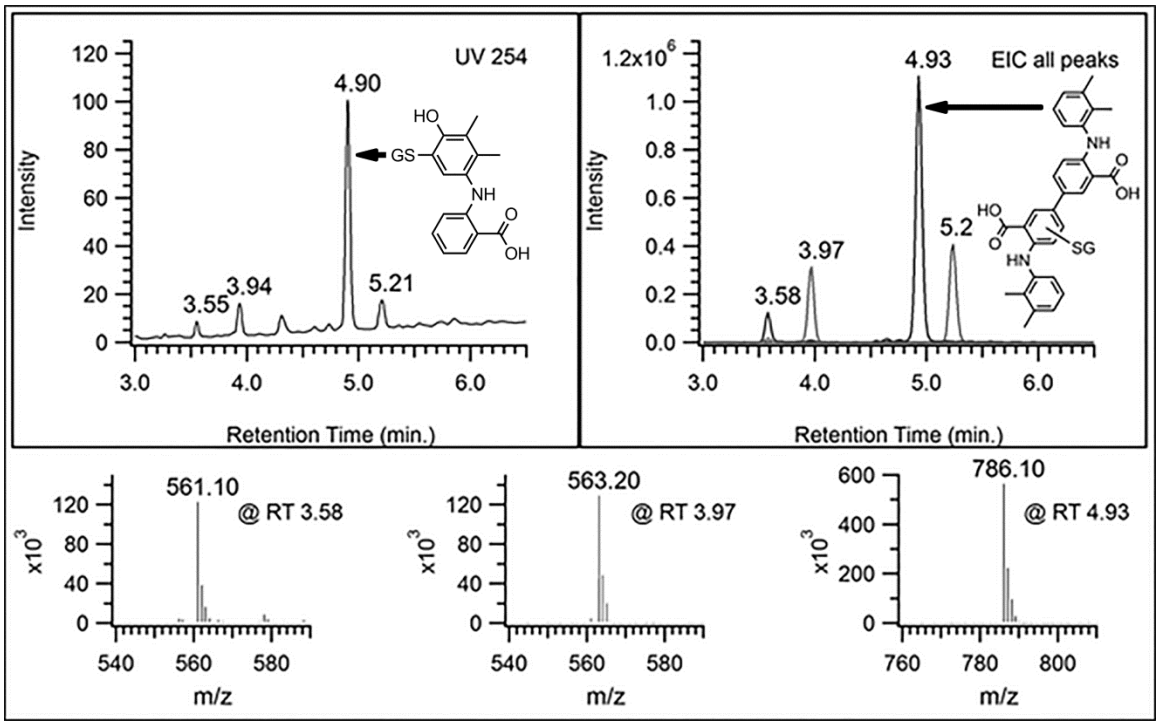

3.7.10. Figure 10. LC-MS of GSH-MFA adducts. Upper chromatograms depict the elution of a fragment at 3.58 min with a m/z of 561.10, a fragment eluting at 3.97 min with a m/z of 563.20 and a fragment at 4.93 min with a m/z of 786.10. These fragments correspond with MFA-dimer GSH-adducts with molecular masses of 560.16 g/mol, 562.17 g/mol, and 785.27 g/mol respectively. Bottom spectra depict the various mass spectra corresponding with upper chromatogram. The formulae for each eluted peak were proposed by high-resolution MS analysis.

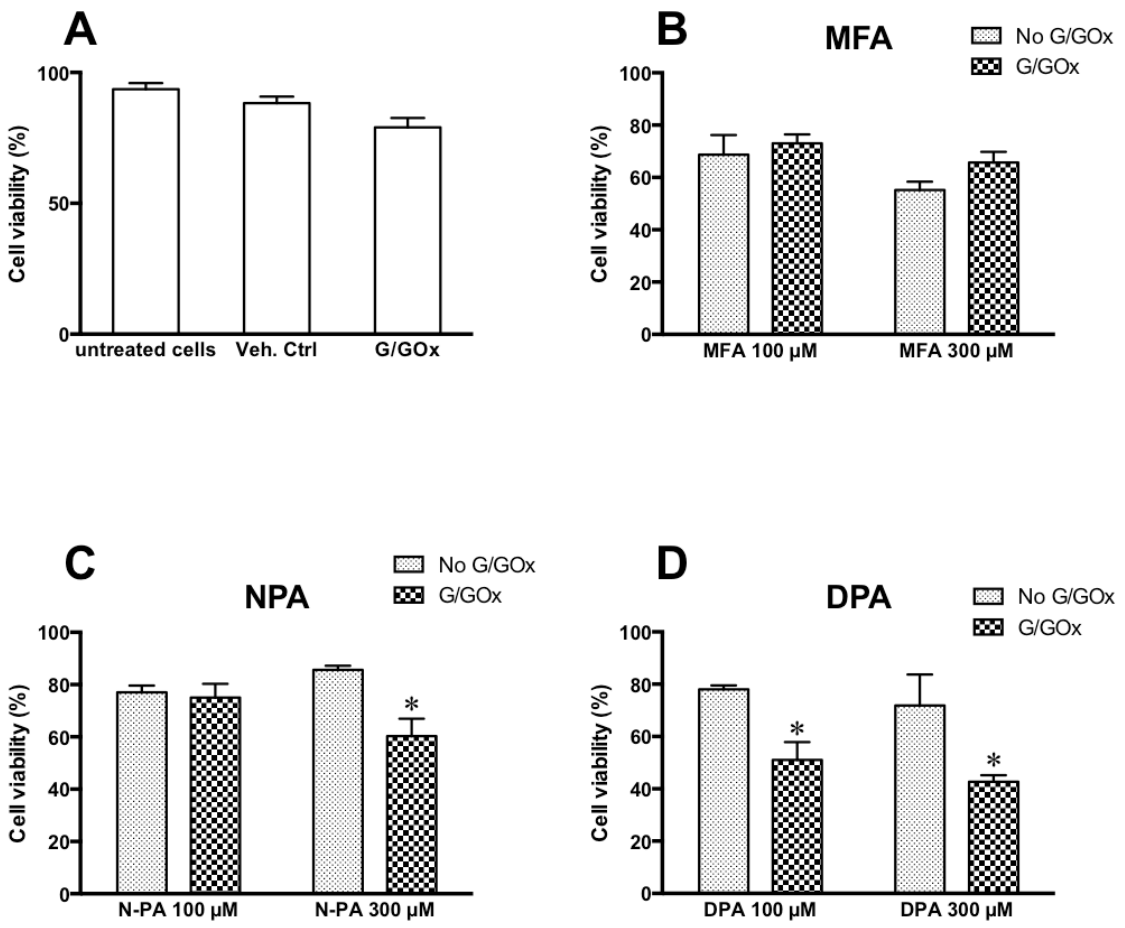

3.7.11. Figure 11. Trypan blue exclusion cell viability assay. Effect of MFA/analogues metabolism by intracellular MPO after 3h incubation of HL-60 cells with 100 µM and 300 µM of each compound in presence and absence of GGOx (5 mM glucose and 10 mU/mL of glucose oxidase) as a source of H_2O_2 to activate MPO catalytic cycle. (A) shows controls, (B) MFA, (C) NPA and (D) shows DPA. *(p <0.05) compared to both drug/metabolite alone and GGOx control. Each set of data represents at least 3 independent experimental runs. One-way ANOVA statistical analysis was used.

CHAPTER 4

CAUTION FOR THE ROUTINE USE OF PHENOL RED – IT IS MORE THAN JUST A PH INDICATOR

[A version of this work has already been published as Morgan, A., D. Babu, B. Reiz, R. Whittal, L. Y. K. Suh, and A. G. Siraki. 2019. Caution for the Routine use of Phenol Red – it is More than just a pH Indicator." Chemico-Biological Interactions 310. doi: 10.1016/j.cbi.2019.108739].

4.1. ABSTRACT

Phenol red (PR) is the standard pH indicator in various cell and tissue culture media, as it provides a quick check for the health of the culture. PR has also been used in multiple protocols to detect cellular hydrogen peroxide as well as peroxidase activity from human peroxidase enzymes. The majority of promyelocytic leukemia cell lines (e.g. HL-60 cells) express myeloperoxidase (MPO), which may react with PR, especially as the latter is present in cell culture media at sufficient concentrations (~15 μM) to partake in redox reactions. Moreover, phenolic molecules are often efficient donor substrates for peroxidase enzymes. In this study, we hypothesized that MPO metabolism of PR via MPO-expressing HL-60 cells could result in PR metabolite(s) that could modulate cell viability. We used purified human MPO for UV-visible spectrophotometry, electron paramagnetic resonance (EPR) and LC-MS analyses to investigate PR peroxidation. 2-chloro-5,5-dimethyl-1,3-cyclohexanedione (monochloro-dimedone, MCD) was used to assess the effect of PR on MPO-catalyzed chlorination activity, and we assessed PR uptake by HL-60 cells using LC-MS analysis. Lastly, we investigated the impact of PR metabolism by intracellular MPO on cell viability (ATP, using CellTiter-Glo™), and on reduced and oxidized glutathione (using GSH/GSSG-Glo™). Our results demonstrate that PR undergoes oxidative halogenation via MPO, resulting in its UV-vis spectral changes due to the formation of mono- and di-halogenated products. Moreover, a significant increase in MPO-catalyzed chlorination of MCD and an increase in glutathionyl radical detection (using EPR) were observed in the presence of PR. Our *in-vitro* studies revealed that PR is readily taken up

by HL-60 cells and its metabolism by intracellular MPO leads to a significant decrease in cellular glutathione as well as a significant increase in glutathione disulphide formation. In spite of the latter, PR had no significant effect on HL-60 cell viability. These results provide evidence that while no overt decrease in cell viability may be observed, PR does impart redox activity, which investigators should be wary of in experimental protocols.

4.2. INTRODUCTION

In-vitro oxidative stress studies often assume that cells in culture, in the absence of exogenous substances, are in the perfect oxidant-free environment; and that reactive oxygen species (ROS) would exclusively be generated intracellularly from well-defined sources[179]. However, several lines of evidence suggest that cells are exposed to ROS during *in-vitro* culture conditions. For instance, fibroblasts' cell culture showed only slightly higher free radicals being generated when compared to the cell-free culture medium. Moreover, ROS was photo-generated as a result of incubating different types of cell-free media, including RPMI and DMEM under daylight[151]. In attempts to detect the source(s) of ROS production, riboflavin was identified as the primary source of ROS produced by cell culture media. Although in the same study, the absence and presence of phenol red (PR) in the medium did not impact the quantity of ROS produced from the cell-free medium, interestingly, adding horseradish peroxidase (HRP) to both RPMI 1640 and DMEM media significantly increased ROS production.

Phenol red, as a source of ROS production in cell culture, has not been thoroughly investigated. PR is widely used in cell culture to observe pH changes, where it would have a yellow colour at a pH of 6.4 or below, that changes into red at pH of 8.2 and above. PR has also been used in various protocols to detect hydrogen peroxide (H_2O_2). For instance,

PR was used to quantify superoxide and H_2O_2, produced by macrophages and neutrophils upon the respiratory burst (initiated by phorbol ester)[180]. This method was based on HRP-mediated oxidation of PR by H_2O_2. The same HRP-mediated oxidation of PR was used to detect H_2O_2 for screening redox-cycling compounds[181,182]. PR also was used in protocols to assess peroxidase activities, such as vanadium bromoperoxidase[183,184]and eosinophil peroxidase[154]. PR has also been used as a key probe to detect halogens as it was found to be brominated and iodinated by hypohalous acids like hypobromous acid (HOBr) and hypoiodous acid (HOI)[153,185].

PR is used in cell culture media at 13-15 μM, which is sufficient to partake in redox reactions. The majority of leukemia cells express myeloperoxidase (MPO), which is capable of peroxidation and chlorination reactions[144,186]. We hypothesized that PR would undergo oxidation and halogenation by MPO, which would cause detrimental effects in cells. To test this hypothesis, both purified MPO and the HL-60 (human promyelocytic leukemia) cell line (which is abundant in MPO) was used to study the metabolism of PR and its cellular uptake and consequent effects.

4.3. MATERIALS AND METHODS

4.3.1. Chemicals and kits

Human purified neutrophil myeloperoxidase (MPO, 180-220 units per mg lyophilized proteins) was purchased from Athens Research & Technology (Athens, GA). 0.1 M sodium phosphate buffer was prepared and treated with 100 μM of diethylenetriamine-pentaacetic acid (DTPA) to prevent metal-catalyzed auto-oxidation. Sodium chloride (Cat.# BDH0286) was obtained from VWR™ chemicals. Methionine was

obtained from K & K Laboratories, Plainview, NY (Cat.# 13899). 2-chloro-5,5-dimethyl-1,3-cyclohexanedione (monochloro-dimedone, MCD) was purchased from Alfa Aesar (Cat.# H51035-03). 5,5-dimethyl-1-pyrroline-N-oxide (DMPO), manufactured by Dojindo Molecular Technologies, Inc., was purchased from Cedarlane Laboratories Ltd (Burlington, ON), and was stored under nitrogen atmosphere at -80°C and used without further purification. CellTiter-Glo™ cell viability (Cat.# G7570) and GSH/GSSG-Glo™ (Cat.# V6611) assay kits were purchased from Promega Co. (Maidson, WI). Glucose oxidase (GOx) from *Aspergillus niger* (≥100,000 units/g), phenol red sodium salt (PR), taurine (T0625-100G), DTPA, reduced glutathione (GSH), H_2O_2, and all other chemicals (unless stated otherwise) were purchased from Sigma-Aldrich Canada Co. (Oakville, ON).

4.3.2. Cell culture

HL-60 (human promyelocytic leukemia) cells were obtained from ATCC (Cat.# CCL-240, Manassas, VA). The cell culture medium consists of RPMI 1640 with L-glutamine, without PR and sodium bicarbonate (Sigma-Aldrich Canada, Cat.# R8755) with 10% fetal bovine serum (FBS, Gibco® Cat.# 12483) and 1% of antibiotic-antimycotic mixture (Gibco®; Reference No. 15240-062, 10,000 units/mL of penicillin, 10,000 µg/mL of streptomycin, and 25 µg/mL of amphotericin B). RPMI powder was reconstituted as per the manufacturer's protocol, and then filter-sterilized using Corning® bottle-top vacuum filter system (Sigma-Aldrich, Cat.# CLS431097). Cells were incubated in a humidified atmosphere with 5% CO_2 at 37°C and were allowed to grow with a density of 0.5-1 x 10^6 cells/mL, and subcultured every two days. All the experiments were performed in FBS-free, PR-free medium after re-suspending the cells from the continuous culture. All the

cells used for the experiments did not exceed passage 30, and cell viability was greater than 90%.

4.3.3. UV-vis spectrophotometry

In Eppendorf tubes, 500 μL reactions were prepared by adding 50 nM MPO into 0.1 M sodium phosphate buffer (supplemented with 100 μM DTPA as described under Chemicals and kits), containing 10 μM PR in the absence and presence of 500 mM sodium chloride (NaCl) or 200 mM NaCl with or without 5 mM GSH or 5 mM taurine. All the reactions were triggered by transferring them to a UV quartz cuvette that has H_2O_2 (to make final H_2O_2 concentration of 200 μM), and then, UV-vis spectra ($\lambda_{200\text{-}800}$) were immediately recorded using a Thermo Scientific NanoDrop 2000c dual-mode UV-vis spectrophotometer (Wilmington, DE), connected to a desktop PC supplied with NanoDrop 2000c software for data acquisition.

4.3.4. LC-MS analysis of PR metabolites

To further analyze the products of MPO-catalyzed PR oxidation, 1 mL reactions of 10 μM PR, 100 mM NaCl, 50 nM MPO and 200 μM H_2O_2 were prepared in 100 μM DTPA containing 0.1 M sodium phosphate buffer in the absence and presence of 1 mM methionine (hypohalous acids scavenger) and 2.5 mM taurine (hypochlorous acid (HOCl) scavenger). The reactions were left at RT for 30 min, then the reactions' contents were passed through an Oasis® HLB 1cc extraction cartridge, and the final eluent was extracted using acetonitrile (ACN). HPLC-MS was performed using an Agilent 1200 SL HPLC System with a Luna Omega 1.6 μm C18 Polar reverse-phase analytical column (2.1 x 50 mm) with guard (Phenomenex, Torrance, CA, USA), thermostated at 50°C followed UV

and mass spectrometric detection. An aliquot of 5 μL was loaded onto the column at a flow rate of 0.50 mL/min and an initial buffer composition of 98% of 0.1% formic acid as mobile phase A and 2% of 0.1% ACN as mobile phase B. Elution of the analytes was achieved by using a linear gradient from 2% to 60% mobile phase B over a period of 5 min, 60% to 95% mobile phase B over a period of 0.5 min, held at 95% mobile phase B for 2 min to remove all analytes from the column and 95% to 2% mobile phase B over a period of 0.5 min. UV absorbance was monitored at 410 nm.

Mass spectra were acquired in negative mode ionization using an Agilent 6220 Accurate-Mass TOF HPLC-MS system (Santa Clara, CA, USA) equipped with a dual sprayer electrospray ionization source with the second sprayer providing a reference mass solution. Mass spectrometric conditions were drying gas 9 L/min at 325°C, nebulizer 20 psi, mass range 100-1100 Da, acquisition rate of ~1.03 spectra/sec, fragmentor 150V, skimmer 65V, capillary 3500V, instrument state 4 GHz High Resolution. A mass correction was performed for every individual spectrum using peaks at m/z 112.98558 and 1033.98811 from the reference solution. Data acquisition was performed using the Mass Hunter software package (ver. B.04.00). Analysis of the HPLC-UV-MS data was done using the Agilent Mass Hunter Qualitative Analysis software (ver. B.07.00).

4.3.5. MPO chlorination activity assay

To study the effect of PR on MPO chlorination activity, MCD was used as a substrate, as previously described in the literature[187]. MPO-catalyzed MCD chlorination to dichlorodimedon results in a decrease in the absorbance at $\lambda = 291$ nm. To a UV quartz cuvette, 40 μM MCD was added to 0.1 M sodium phosphate buffer (supplemented with

100 μM DTPA) and mixed with 200 mM NaCl, 50 nM MPO and 100 μM H_2O_2 in the absence and presence of PR with concentrations ranging from 0.5 to 15 μM. The reactions were carried out at a pH of 7.4 at 21°C. A control reaction was included to study the kinetics of MCD chlorination without PR. Kinetic scans at λ_{291} were recorded every 20 s using Thermo Scientific NanoDrop 2000c dual-mode UV-vis spectrophotometer.

4.3.6. Electron paramagnetic resonance (EPR) spectroscopy

For EPR studies, free radical species resulting from MPO oxidation of PR were probed for by spin trapping, where a nitrone spin trap (DMPO) was used to form a relatively stable paramagnetic adduct when reacting with free radicals. Both human purified MPO and HL-60 cells were used in our study. For the biochemical system, reactions of 200 μM PR, 100 mM DMPO, 1 mM GSH, 50 nM MPO were carried out in 0.1 M sodium phosphate buffer (pH 7.4), containing 100 μM DTPA;, as soon as the reactions were triggered with 100 μM H_2O_2 and mixed, the sample was transferred to a Suprasil quartz EPR flat cell (Bruker Canada, Milton, ON) and placed in an EleXsys E500 EPR spectrometer cavity for analysis using the following instrumental settings: microwave frequency, 9.8 Hz; incident microwave power, 0.02 W; center field, 3485 G; scan range, 100.0 G; field modulation amplitude 1 G; receiver gain, 60.0 dB. Controls in the absence of MPO and the presence of 100 mM NaCl were also carried out. For the cellular system, HL-60 cells, cultured in PR-free RPMI medium (as described under Section 2.2), were harvested and spun down for 15 min at 300 x g and then suspended in phosphate buffer to have 2 x 10^6 cells per reaction. To cells, 100 mM DMPO, 1 mM GSH and 15 μM PR were added, then the reaction was either triggered right away by H_2O_2 or triggered after

incubating PR with cells at 37°C for 1 h and 2 h. The reactions with DMSO instead of PR, 100 μM PR and 200 μM PR were also carried out. Each reaction was carried out separately (one scan each) at least in duplicate on nonconsecutive days.

4.3.7. Phenol red uptake by HL-60 cells

PR uptake by HL-60 cells was investigated using LC-MS analysis. Firstly, 10 x 10^6 HL-60 cells, cultured in PR-free RPMI medium (as described under Section 2.2), were harvested and resuspended in PR-free RPMI medium, and immediately after addition of 15 μM PR to the cells, cells were spun down at 150 g for 5 min, and supernatant was separated from the cell pellets. For determining how much PR was taken up by the cells, PR was extracted by vortexing equal weights of the cell pellets and the supernatant for 2 min with 100 μl of ACN solution of 2 μM internal standard (IS, tolbutamide). After letting them settle down for 5 min, the ACN layers, of both cell pellet and supernatant, were analyzed with HPLC-MS. The same procedure was repeated after more prolonged incubation of HL-60 cells with PR for 10 and 60 min. HPLC-MS was performed using an Agilent 1260 Infinity HPLC System with a Kinetex C8 reverse-phase analytical column (2.1x50 mm) (Phenomenex, Torrance, CA, USA), thermostated at 50°C followed by UV and mass spectrometric detection using an Agilent 6130 MSD. The buffer gradient system was composed of 0.1% formic acid in water as mobile phase A and 0.1% formic acid in ACN as mobile phase B. Elution of the analytes was achieved by using a linear gradient from 2% to 95% mobile phase B over a period of 5 min and held at 95% mobile phase B for 3 min to remove all analytes from the column.

Mass spectra were acquired in positive mode of ionization using an Agilent 6130 LC-MSD (Santa Clara, CA, USA). Mass spectrometric conditions were drying gas 13 L/min at 325°C, nebulizer 30 psi, fragmentor 150 V, capillary 4000 V. Mass spectrometric signal was monitored in single ion monitoring (SIM) mode. The SIM signals were acquired at m/z 271.1 Da for the internal standard (tolbutamide) and m/z 355.1 Da for PR (Table 2). Data acquisition was performed using the OpenLAB software package (Rev. C 01.07). Analysis of the HPLC-UV-MS data was done using the Agilent Mass Hunter Qualitative Analysis software (ver. B.07.00) (data summarized in Table 2).

4.3.8. Cell viability and cytotoxicity assay

Cell viability was assessed by using CellTiter-Glo® Luminescent Cell Viability Assay kit (Promega, Madison, WI, USA) according to the manufacturer's protocol. This assay determines the number of viable cells in culture based on quantitation of ATP present, an indicator of metabolically active cells. Briefly, CellTiter-Glo® reagent was prepared by mixing the luminescent substrate and lysis buffer (which was thawed by storing at room temperature for 24 h) from the assay kit. All the reactions were performed in PBS. HL-60 cells were plated into opaque-walled 96-well plate at a density of 5 x 10^4 cells per well (50 µl) and treated with different concentrations of PR (15-200 µM) in the absence and presence of 5 mM glucose and 25 mU/ml GOx for 1 and 3 h at 37°C and 5% CO_2. Controls groups of DMSO and PR alone were included. At the end of the incubation period (1 and 3 h), an equal volume of freshly prepared CellTiter-Glo® reagent was added to each well, and the plate was shaken for 15 min at RT, and luminescent signals were recorded using a plate reader (SpectraMax M5). The index of cellular viability was

calculated as the percentage of luminescence with respect to untreated control cells. Data were expressed as means ± SD.

For cytotoxicity, we used the trypan blue exclusion assay to determine membrane intactness for each treatment in HL-60 cells. We carried out the same experiment as described above with the exception that it was performed at 3 h, and cells were incubated in 96-well plates at a density of $4x10^5$ cells/200 μL. Cells were removed (50 μL) from each well and mixed in a 1:1 ratio with 0.4% trypan blue solution (Lonza, Anaheim, CA). Cells were counted using a hemocytometer, using light microscopy.

4.3.9. Glutathione assay

In order to assess the effect of PR oxidation via intracellular MPO, GSH and glutathione disulphide (GSSG) in HL-60 cells were quantified using bioluminescent GSH/GSSG-Glo® kit (Promega, Madison, WI, USA), as per the protocol provided by the manufacturer. The assay uses a GSH probe that undergoes conjugation with GSH in the presence of glutathione S-transferase, while releasing luciferin. The later would proportionally give rise to a luminescent signal in the presence of a luciferase. Therefore, the resulting signal correlates to the amount of luciferin, which is dependent on the amount of GSH. . In brief, the cells were harvested, washed and then the pellets were suspended in 25 μl Hank's balanced salt solution (HBSS) and aliquoted into 96-well plates (white, opaque) at a density 1 x 10^4 cells per well. Cells were then incubated with 15 μM PR ± 5 mM glucose and 5 mU/ml GOx for 3 h. Also, 100 μM menadione (a known GSH depleting agent) was used as a positive control. After incubation, cells were lysed by being shaken with an equal volume of either total or oxidized glutathione reagent and shaking for 5 min, then incubated

for 30 min with 50 µl of luciferin generation reagent. After addition of 100 µl of luciferin detection reagent, plates were left to equilibrate for 15 min at RT before luminescence was measured using a plate reader (SpectraMax M5). Each reaction was repeated for at least three independent times, and the results were expressed as mean ± SD (Fig. 6).

4.3.10. Statistical analysis

Data were expressed as the mean ± standard deviation of independent experiments ($n \geq 3$) performed on separate days. Statistical significance ($p < 0.05$) was verified by running a one-way pairwise multiple comparisons ANOVA using GraphPad Prism 6 software.

4.4. RESULTS

4.4.1. UV-vis spectrophotometry analysis of PR oxidation by MPO

In this study, PR oxidation by MPO was examined by recording UV-vis spectra immediately after triggering the reactions by H_2O_2 (see Materials and Methods). No change was observed in the UV-vis spectra when H_2O_2 was added to MPO and PR (represented by the dotted line in Fig. 1, A.1). However, in the presence of 200 mM NaCl, increase and bathochromic shift were observed in the peak at 560 nm, a change that increased with increasing NaCl concentration to 500 mM (represented by solid lines in Fig. 1, A.1and A.2). Surprisingly, the spectral change was no longer observed when either GSH or taurine was added to the reactions with 200 mM NaCl (Fig. 1, B).

4.4.2. Characterization of the products of MPO metabolism of PR by LC-MS

LC-MS was carried out after the reactions (in 0.1 M phosphate buffer, pH 7.4) containing 10 μM PR, 50 nM MPO and 200 μM H_2O_2 in the presence of 100 mM or 200 mM NaCl with and without 1 mM methionine and 2.5 mM taurine were incubated for 30 min at room temperature (sample preparation was described under Section 2.4). The HPLC chromatogram revealed three main peaks (λ=410) at retention times 2.99, 3.35 and 3.43 min (Fig. 2.A). However, both peaks at retention times 3.35 and 3.43 min vanished in the presence of 1 mM methionine (Fig. 2.B) and only the peak at 3.35 min disappeared in the presence of 2.5 mM taurine (Fig. 2.C). In the presence of 200 mM NaCl, three more peaks appeared at retention times 3.72, 3.81 and 3.88 min (Fig. 2.D). A summary of m/z of the peaks is shown in Table 1, which were acquired using extracted ion chromatogram (EIC) for the particular species, which indicated the formation of halogenated phenol red products LC-MS chromatograms are provided in the Supplementary data (Fig. S.1).

4.4.3. Effect of PR on MPO-catalyzed chlorination activity

MPO-catalyzed chlorination of MCD to dichlorodimedon in the presence of NaCl leads to a decrease in absorbance of MCD at λ_{291}. The rate of decrease at MCD A_{291} is used as a function to measure MPO chlorination activity (see Materials and Methods). MPO chlorination activity was observed to increase in the presence of PR. Moreover, increasing PR concentrations from 0.5 - 15 μM resulted in a proportional increase in MPO chlorination of MCD, and hence ΔA_{291} (Fig. 3).

4.4.4. Detection of glutathionyl radical induced by PR using electron paramagnetic resonance (EPR) spectroscopy

Studies were first carried out using a commercially purchased MPO. We first tried to use DMPO to directly spin trap and characterize any free radical as a result of PR enzymatic peroxidation by MPO/H_2O_2, but we were not successful. Therefore, we used glutathione (GSH) as an intermediate co-oxidation target for free radical species. By adding GSH to biochemical reactions with PR/MPO/H_2O_2 (as described in Materials and Methods), a typical glutathionyl-DMPO EPR spectrum of four lines was obtained (Fig. 4, A.3). Interestingly, no change in the signal intensity was found when NaCl was added (Fig. 4, A.4). The signal was abolished when MPO or PR were not added to the reaction (Fig. 4, A.1&A.2). Moreover, using HL-60 cells produced a similar spectrum when 1 mM GSH was added in the presence of PR/HL-60 cells/H_2O_2 (Fig. 4, B.2). Also, incubating 15 μM PR with HL-60 cells for 1 and 2 h intensified the resulting glutathionyl radical detection (Fig. 4 B.3 and B.4, respectively). Increasing the PR concentrations (to 100 and 200 μM) resulted in increasing glutathionyl radical detection at 0 h (Fig. 4 B.5 and B.6, respectively). Experiments were carried out to detect glutathionyl radicals in cells without the addition of external GSH but were not successful, which could be due to the limitations with the sensitivity of the method (data not shown).

4.4.5. PR uptake by HL-60 cells

After collecting HL-60 cells following their incubation with 15 μM PR for 0, 10 and 60 min (as described under Section 2.7), ACN extracts of cell pellets and supernatant of each time point was analyzed by LC-MS to assess the PR uptake by the cells. Peak areas

of PR (m/z = 355.1) and tolbutamide (m/z = 271.1), from pellets and supernatants, were obtained by EIC (as summarized in Table 2), and the percentages of intracellular PR at 0, 10 and 60 min were estimated to be 45.16%, 42.70% and 52.29%, respectively.

4.4.6. Cell viability and cytotoxicity of HL-60 cells treated with PR and G/GOx

In order to evaluate the effect of PR and its metabolites on the cell viability, HL-60 cells were treated with 5 mM glucose and 25 mU/mL GOx (G/GOx) as a source of H_2O_2 in the absence and presence of PR (described under Section 2.8). H_2O_2 generated in this manner has demonstrated cytotoxicity of HL-60 cells, in part, due to the formation of HOCl by intracellular MPO activity. The H_2O_2 produced could activate MPO to oxidize other xenobiotics[122]. After incubation of the cells at 37ºC and 5% CO_2 for 1 and 3 h with G/GOx, the cell viability of the G/GOx-treated cells significantly decreased at 3 h (65.2 ± 9.7; P<0.01) as compared to the DMSO-treated control group, without any change at 1 h (Fig. 5A). However, co-incubation of different concentrations of PR (15-200 μM) with G/GOx did not show any significant difference in viability between the cells treated with G/GOx only and cells treated with G/GOx in the presence of PR both at 1 and 3 h (Fig. 5B). Moreover, the same studies were performed independently using trypan blue exclusion to determine membrane leakage or intactness. We performed the studies only at 3 h since metabolic effects are usually observed prior to cell membrane rupture (cytotoxicity). We observed that at the concentrations of G/GOx and PR, no cytotoxicity occurred (Fig. 6).

4.4.7. Reduced and oxidized glutathione assay of HL-60 cells treated with PR and G/GOx

After incubating HL-60 cells with 15 μM PR ± 5 mM glucose and 5 mU/mL GOx (G/GOx) for 3 h at 37ºC and 5% CO_2, GSH and GSSG cellular contents were measured using bioluminescent GSH/GSSG-Glo® kit (as described under Section 2.9). We used a lower concentration of GOx, to decrease the extent of GSSG formation in order to determine the effect of PR in this scenario. Under these conditions, there was no significant difference in GSH or GSSG contents between the DMSO group and either 15 μM PR or G/GOx groups. When the cells were co-treated with both 15 μM PR and G/GOx, a significant drop in HL-60 cellular GSH of that treatment group, accompanied with a significant increase in GSSG, were observed when compared to the cells treated with either DMSO or G/GOx alone (Fig. 7).

4.5. DISCUSSION

In this study, we have demonstrated that PR was halogenated (chlorination and bromination were detected) in the presence of analytical grade NaCl, MPO and H_2O_2. These reactions were attenuated in the presence of GSH (antioxidant mechanisms) or taurine (through HOCl scavenging) and methionine (both HOBr and HOCl scavenging). More in-depth LC-MS studies revealed that the initial observations were for mono-halogenated PR metabolites, for which the yield and di-halogenation could be increased with increasing NaCl. This finding was initially puzzling, as the formation of HOCl is believed to be the "physiological" oxidant produced by MPO in the presence of chloride and H_2O_2[188]. To our knowledge, commercially available, analytical grade NaCl contains a

certain degree of bromide as a contaminant. We calculated this to be 5.64 μM based on the preparation of a 0.1 M NaCl reaction medium. We were unable to acquire a bromide-free source of NaCl; however, we did observe chlorination solely if the source of chloride was from hydrochloric acid (data not shown). The findings of both chlorination and bromination reactions are consistent with previous reports in activated neutrophils[189]. Also, bromination appears to be a relevant marker for MPO activity based on 3-bromotyrosine analysis[190]. Interestingly, LC-MS studies indicated that the presence of a halogen was necessary to detect the changes in the PR spectrum. This observation is peculiar considering that phenol oxidation by peroxidases initially leads to phenoxyl radicals, dimers or quinones[191]. We have proposed a mechanism based on our findings in Scheme 1, in which the PR phenoxyl radicals formed are proposed to disproportionate, leading to PR and a putative PR quinone; the latter at pH 7.4 will equilibrate with PR, effectively showing no difference during MPO oxidation. Interestingly, phenolphthalein, which has a similar structure and was used for pH measurements, was proposed to form a quinone methide that could be involved in its mutagenicity and is classified as 2B by International Agency for Research on Cancer (IARC)[192,193]. There is no report of PR as mutagenic, and it is not classified by IARC; its quinone methide, thus, may not be reactive.

At cell culture media concentration of PR (~15 μM), MPO halogenation activity was accelerated. The latter also implicates PR as a substrate for MPO and that PR is redox active. This finding is in line with studies using spinach chloroplasts, where PR was demonstrated as an electron acceptor for photophosphorylation[194]. This observation led us to consider the possible involvement of phenoxyl radicals produced from PR during the peroxidase cycle of MPO. As phenoxyl radicals are difficult to detect (unless sterically

hindered), we utilized a well-established surrogate, that is, glutathionyl radical spin-trapping using EPR[195,196,197]. We observed a proportional PR concentration dependency for the formation of glutathionyl radicals (determined by the glutathionyl-DMPO adduct intensity), but most importantly, we observed a significant formation of the latter using the concentration of PR in cell culture media. An important caveat, however, is the observation that HL-60 cell cultures have a certain amount of MPO released extracellularly, which may have been the reason for the efficient oxidation of GSH that was added to cells[198]. Nevertheless, this led us to determine if such a reaction could take place intracellularly. The experiments with EPR were not successful, perhaps due to the limited sensitivity in detecting intracellular glutathionyl-DMPO. As such, we used a commercial luminescent-based detection assay for total and oxidized glutathione (glutathione disulphide; GSSG). As glutathionyl radical will ultimately form GSSG, we found this assay to be appropriate. We observed that when a combination of PR with an H_2O_2 source (G/GOx in this case) was used, a statistically significant increase in GSSG was found. This finding corroborates the EPR studies, and together with the data demonstrating rapid PR uptake into cells suggests that glutathione oxidation can occur more efficiently in the presence of PR in cells. With respect to PR cellular uptake, we could not find a specific mechanism/study for the transport of PR into HL-60 cells, although lipophilicity is a primary factor for uptake of phenols in murine leukemia cells[199]. Also, PR has a logP of 3.02 (https://comptox.epa.gov/dashboard/), making it significantly lipophilic, which would facilitate passive diffusion into cells. To our surprise, however, PR intracellular oxidation did not induce a significant change in cell viability (as assessed by ATP levels). There are known GSH-depleting compounds, such as diethyl maleate (conjugates GSH),

bromoheptane (GSH in rat hepatocytes), or buthionine sulfoximine, which do not cause overt cytotoxicity[200,201]. It is possible that GSH oxidation by PR also falls into this category of non-toxic GSH oxidizers. However, it is likely that the cells would be sensitized towards other toxicants.

In our studies, it was likely that MPO contributed to the observed biochemical changes; however, peroxidase activity from cyclooxygenase-2 is present in HL-60 cells and other tumour cell lines that may contribute to PR oxidation[202]. We propose that PR undergoes metabolism by MPO to generate a phenoxyl radical, which undergoes disproportionation to the starting compound (PR) and a nonreactive quinone methide (Scheme 1). In summary, care should be exercised when carrying out studies using PR, mainly if xenobiotic co-exposure takes place.

4.6. ACKNOWLEDGEMENT

This work was supported by the Natural Sciences and Engineering Research Council of Canada (NSERC) (RGPIN-2014-04878) as well as Alberta Innovates Graduate Student Scholarships (GSS) program for AM.

4.7. FIGURES

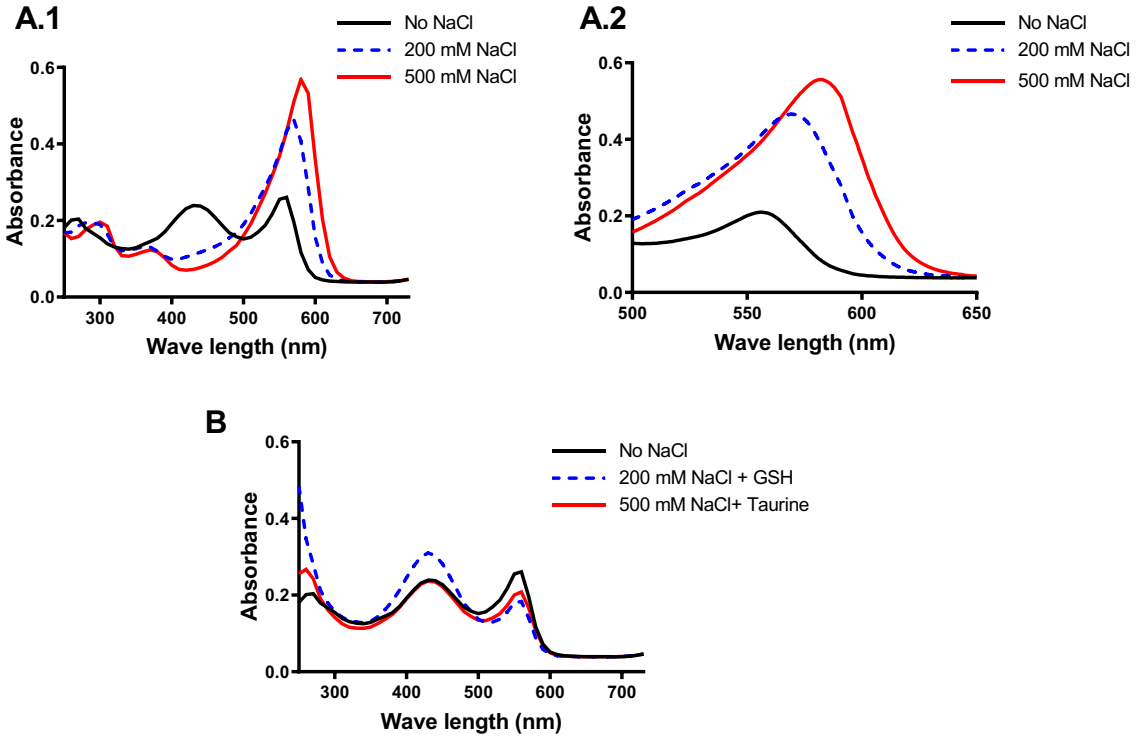

4.7.1. Figure 1: Phenol red (PR) UV spectral change due to its oxidation by MPO. The reactions were carried out by adding 50 nM MPO and 200 μM H_2O_2 to 0.1 M sodium phosphate buffer (pH=7.4) containing 10 μM PR in the absence and presence of 200 or 500 mM NaCl (spectra are shown in A.1 and zoomed in A.2). Either 5 mM reduced glutathione (GSH), or 5 mM taurine was also added to the reactions with 0.2 M NaCl (B). Spectra were recorded at $\lambda_{200\text{-}800}$. Each reaction was repeated three times independently.

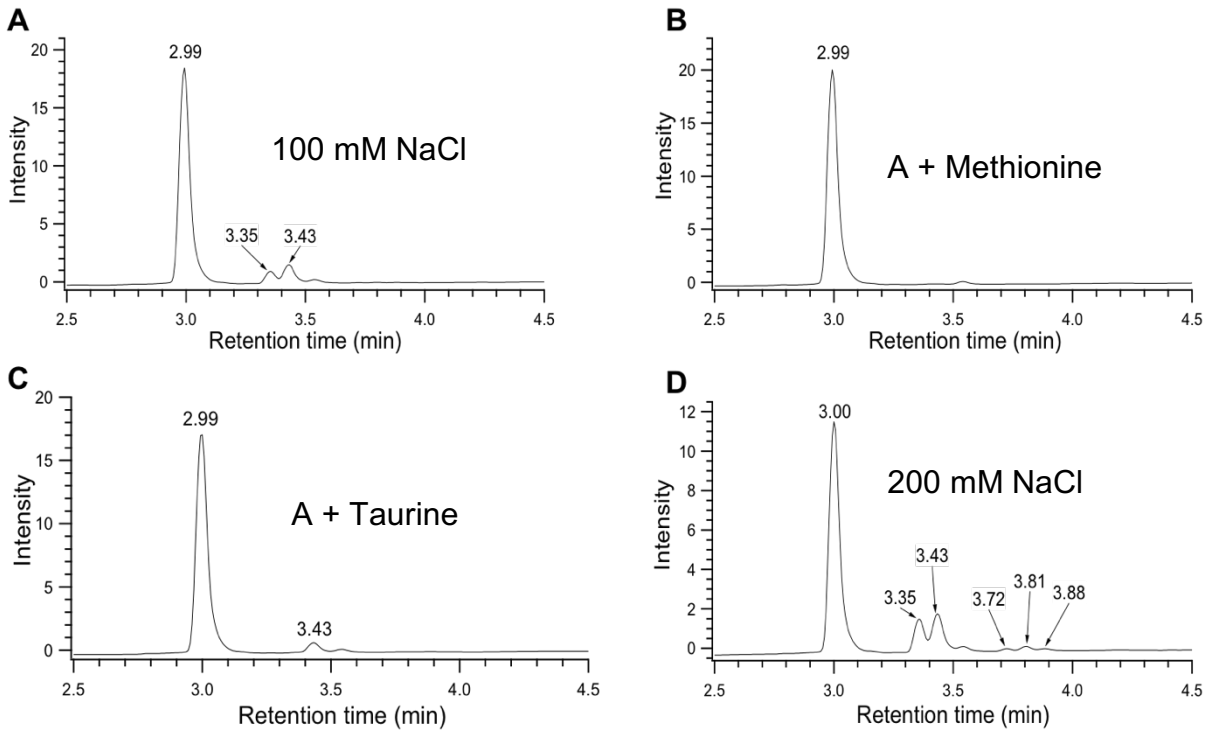

4.7.2. Figure 2: LC-MS study of phenol red (PR) metabolism by MPO.

Samples were prepared by mixing 10 μM PR, 100 mM NaCl, 50 nM MPO and 200 μM H_2O_2 in 100 μM DTPA containing 0.1 M sodium phosphate buffer (pH=7.4) (as described under Section 2.4). Three major peaks were found at λ = 410 nm in LC chromatogram at retention times 2.99 (PR), 3.35 and 3.43 min (PR metabolites, A). Methionine inhibited the formation of peaks at 3.35 min and 3.43 (B). Taurine selectively inhibited the formation of the peak at 3.35 min (C). Three more peaks appeared at 3.72, 3.81 and 3.88 min when NaCl was increased to 200 mM (D).

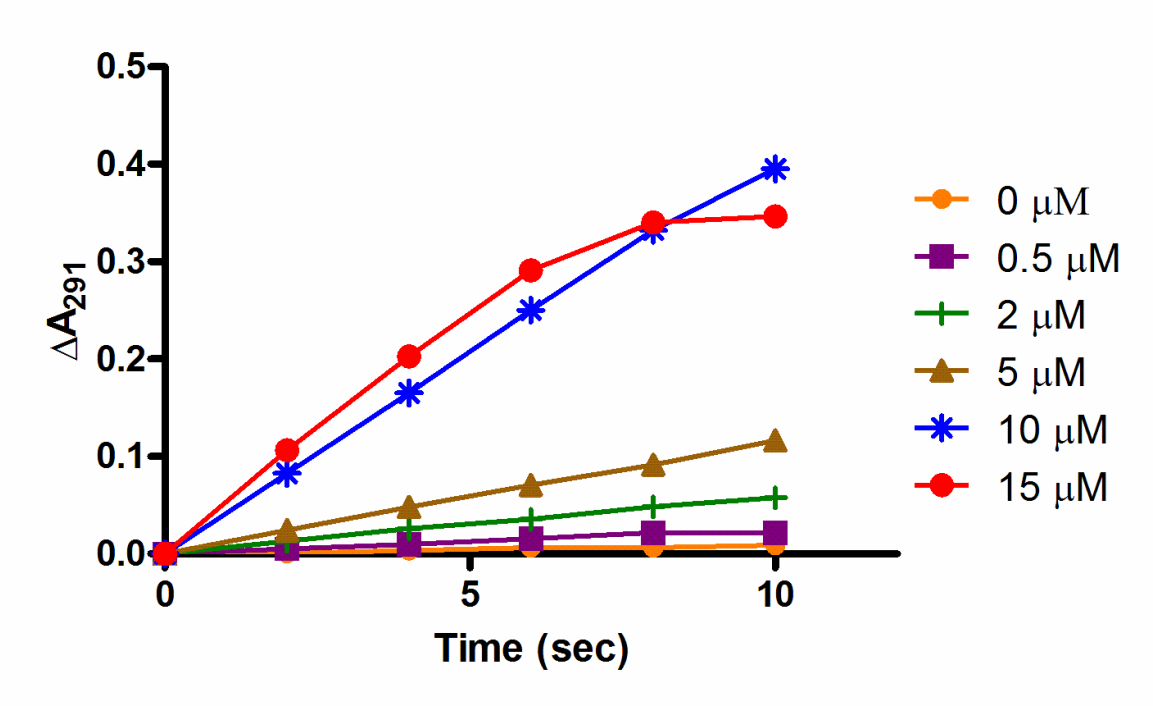

4.7.3. Figure 3: Effect of phenol red (PR) on MPO-catalyzed chlorination of MCD. The reactions were carried out in 0.1 M sodium phosphate buffer (pH=7.4), containing 40 μM MCD, 200 mM NaCl and 50 nM MPO in the absence (•) and presence of 0.5 μM (□), 2 μM (+), 5 μM (Δ), 10 μM (∗), or 15 μM (o) PR. The reactions were triggered by addition of 100 μM H_2O_2, and the decrease in A_{291} was followed immediately.

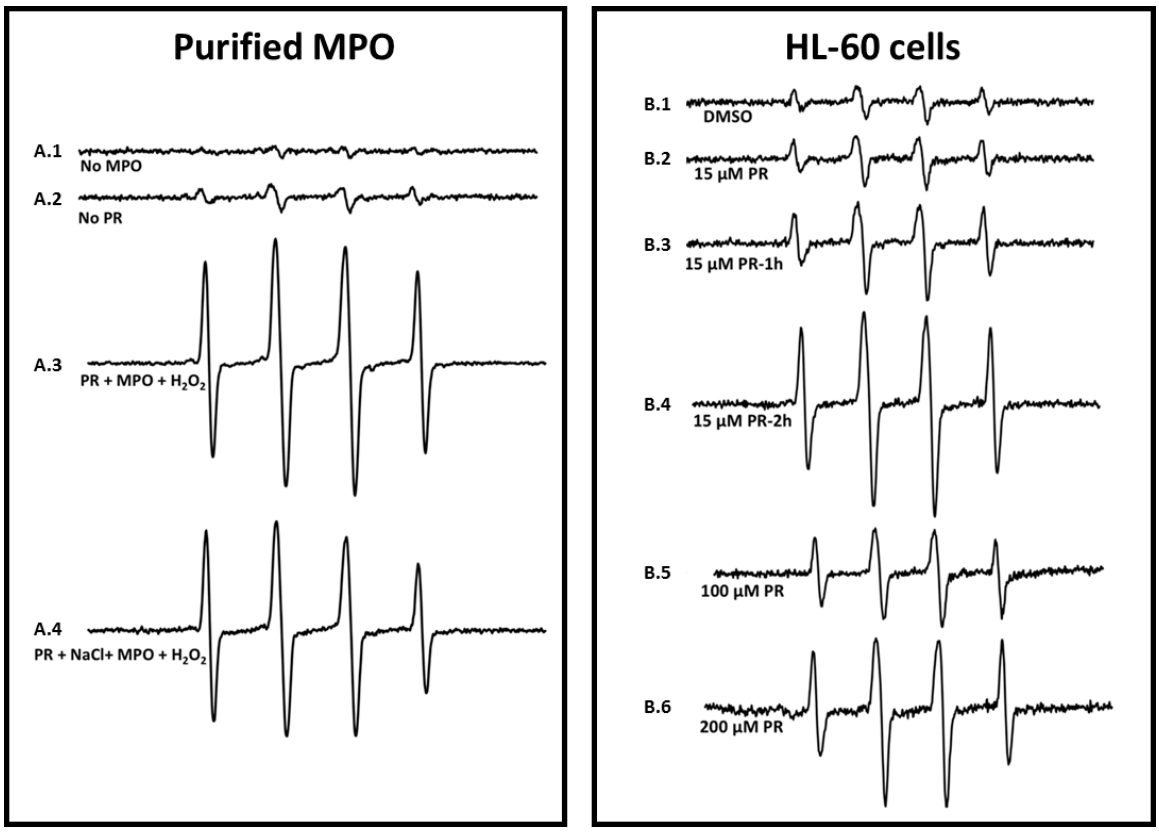

4.7.4. Figure 4. EPR spectra resulting from glutathionyl radical (GS•) formation by MPO metabolism of phenol red (PR). Studies were carried out using both purified MPO (A) and HL-60 cells (B). The reactions were carried out in 0.1 M sodium phosphate buffer (pH = 7.4) containing 100 µM DTPA. EPR spectra in **A** contained 100 mM DMPO, 1 mM GSH, 200 µM PR, 50 nM MPO and 100 µM H_2O_2 in the absence (A.3) and presence (A.4) of 100 mM NaCl. Control reactions were carried out in the absence of MPO (A.1) or in the absence of PR (A.2). The EPR spectra in **B** contained 2 x 10^6 HL-60 cells, 100 mM DMPO, 1 mM GSH and 15 µM (B.2, B.3 and B.4), 100 µM (B.5) or 200 µM (B.6) PR with 100 µM H_2O_2. A control reaction was carried using DMSO instead of PR (B.1). Spectra were acquired after co-incubating 100 µM H_2O_2 at 37ºC for 0 h (B.2), 1 h (B.3) and 2 h (B.4).

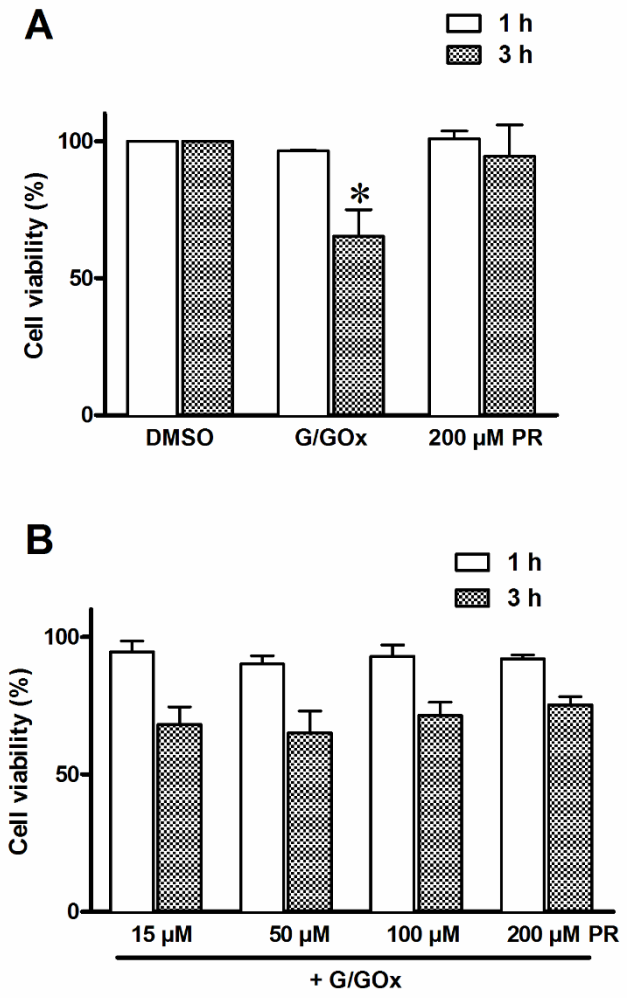

4.7.5. Figure 5: Effect of phenol red (PR) on the viability of HL-60 cells. Experiments were performed for 1 and 3 h in the absence (A) and presence (B) of 5 mM glucose and 25 mU/ml glucose oxidase (G/GOx). Controls of each of DMSO, PR or G/GOx are shown in (A). Data were expressed as the mean ± standard deviation of independent experiments ($n \geq 3$) . *($P<0.01$) when compared to DMSO group. One-way ANOVA statistical analysis was used to test for significance between PR-

treated groups in B and G/GOx control groups in A for corresponding 1 and 3 h treatment periods; no significant difference was found.

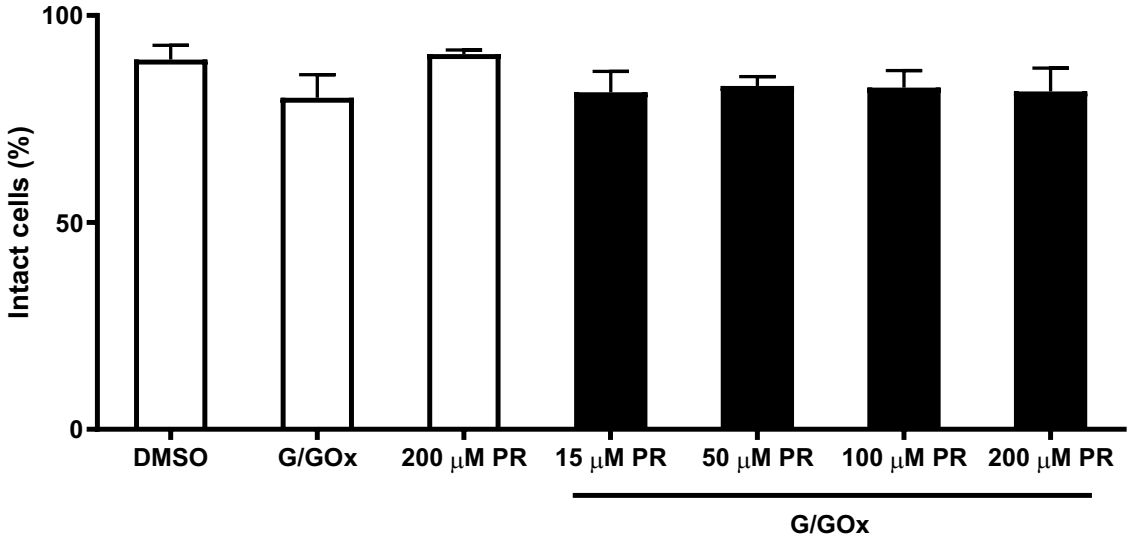

4.7.6. Figure 6. Effect of phenol red (PR) on the cytotoxicity of HL-60 cells. Experiments were performed for 3 h with the conditions indicated above. The amount of glucose and glucose oxidase (G/GOx) was the same as in Figure 5. Controls for DMSO, 200 μM PR, and G/GOx are shown (clear bars), followed by cotreatment of G/GOx with PR (black bars). Each bar represents n = 3 data points, performed on two different days. No significant difference was found.

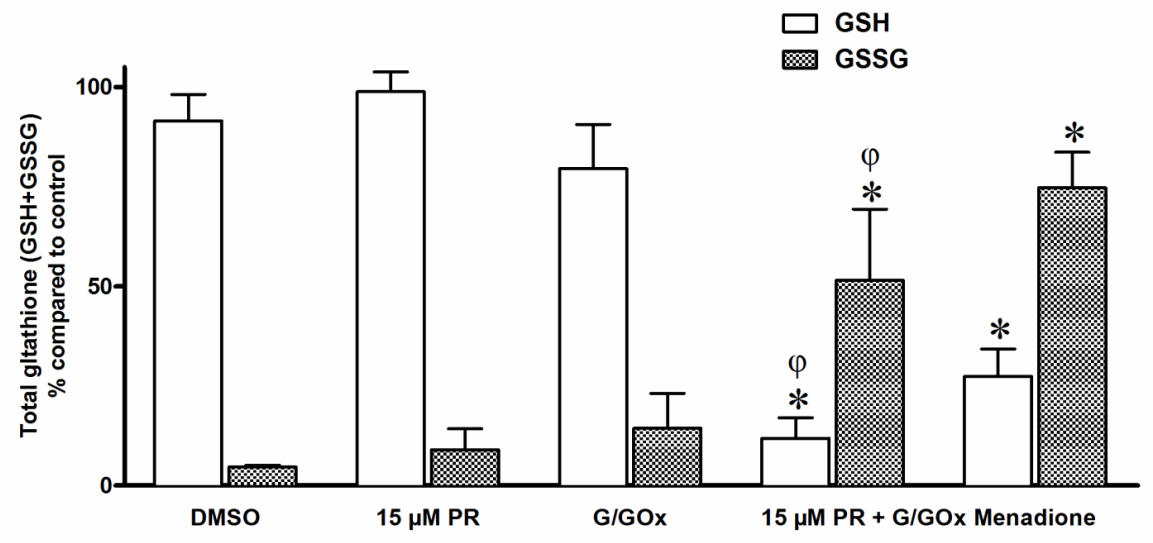

4.7.7. Figure 7: Effect of phenol red (PR) metabolism by cellular MPO on GSH and GSSG levels in HL-60 cells. Experiments were performed for 3 h in the absence and presence of 5 mM glucose and 25 mU/ml glucose oxidase (G/GOx) as a source of H_2O_2. GSH and GSSG contents were expressed as percentages compared to total glutathione (GSH+GSSG) in the DMSO group. *(P<0.01) when compared to DMSO group. $^{\varphi}$(P<0.01) when compared to G/GOx. Each set of data represents at least three independent replicas. One-way ANOVA statistical analysis was used to test for significance between treatment groups.

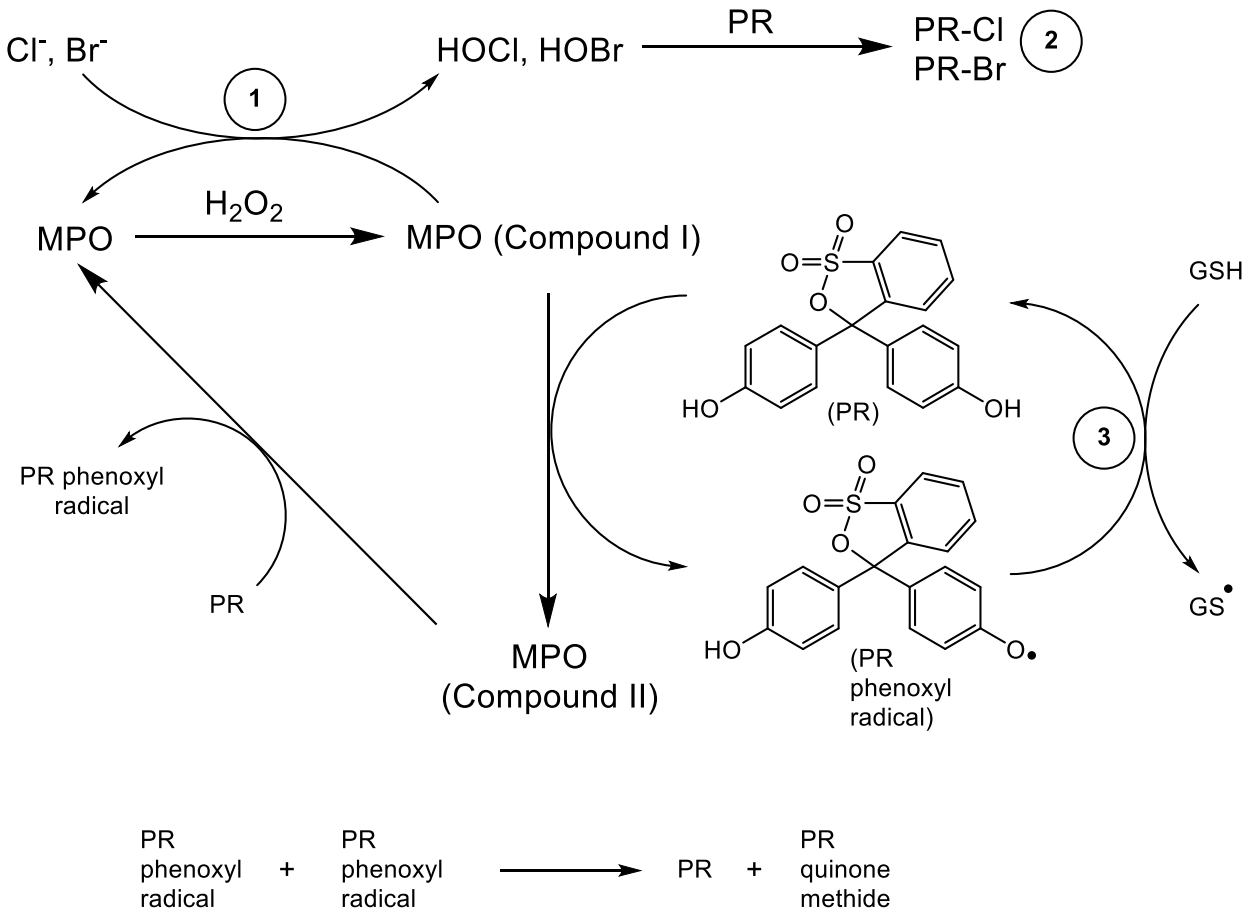

4.7.8. Scheme 1. Proposed mechanism for phenol red (PR) metabolism reactions. MPO is activated by H_2O_2 to Compound I (1), which can produce hypohalous acids (HOCl, HOBr) that oxidize PR (2). On the other hand, PR appeared to catalyze glutathionyl radical ($GS^{\bullet}$) formation, which likely involved an MPO-catalyzed PR phenoxyl radical (3). The latter is proposed to undergo a disproportionation reaction (meaning that two PR phenoxyl radicals react with each other) that yields oxidized PR (PR quinone) and the starting PR molecule.

4.8. TABLES

Analyte	RT (min)	Formula	m/z	Calc m/z	Δppm
Phenol Red	2.99	$C_{19}H_{14}O_5S$	353.0483	353.0490	1.77
Monochloro-phenol Red	3.35	$C_{19}H_{13}ClO_5S$	387.0100	387.0100	-0.13
Monobromo-phenol Red	3.43	$C_{19}H_{13}BrO_5S$	430.9594	430.9590	0.05
Dichloro-phenol Red	3.72	$C_{19}H13Cl_2O_5S$	420.9703	420.9710	1.55
Monochloro-monobromo-phenol Red	3.81	$C_{19}H_{13}ClBrO_5S$	464.9496	464.9210	1.79
Dibromo-phenol Red	3.88	$C_{19}H_{13}Br_2O_5S$	508.8699	508.8700	0.03

4.8.1. Table 1: Phenol red metabolism by MPO produces halogenated phenol red metabolites. Summary of resulting HPLC-UV chromatograms and the corresponding proposed analytes' chemical formulas based on both m/z ratios obtained from extracted ion chromatogram (EIC) for the particular species and calculated m/z (LC-MS chromatograms are provided in Supplementary data, 5.8.S.1).

Incubation time (min)	Phenol red		IS (Tolbutamide)		Phenol red/IS		% Phenol red intra-cellular	% Phenol red extra-cellular
	Cell pellets	Supernatant	Cell pellets	Supernatant	Cell pellets	Supernatant		
0*	352747	506450	358427	422208	0.98	1.19	**45.16**	**54.84**
10	466265	636311	420108	424995	1.11	1.49	**42.70**	**57.30**
60	522039	388564	456631	372965	1.14	1.04	**52.29**	**47.70**

4.8.2. Table 2. LC-MS analysis for phenol red (PR) uptake by HL-60 cells. After Incubation of 15 μM PR with 10×10^6 HL-60 cells for 0, 10 and 60 min (as described under Methods), cells were centrifuged, and both the pellets and supernatant samples were vortexed with ACN solution of internal standard (IS, tolbutamide), and the ACN extracts were then analyzed using LC-MS. Shown in the Table are peak areas of PR m/z 355.1 and tolbutamide m/z 271.1, obtained by extracted ion chromatograms (EIC) used to estimate PR uptaken by HL-60 cells. *Please refer to the Materials and Methods, Section 5.2.7, for additional information regarding processing step times.

4.9. SUPPLEMENTARY DATA

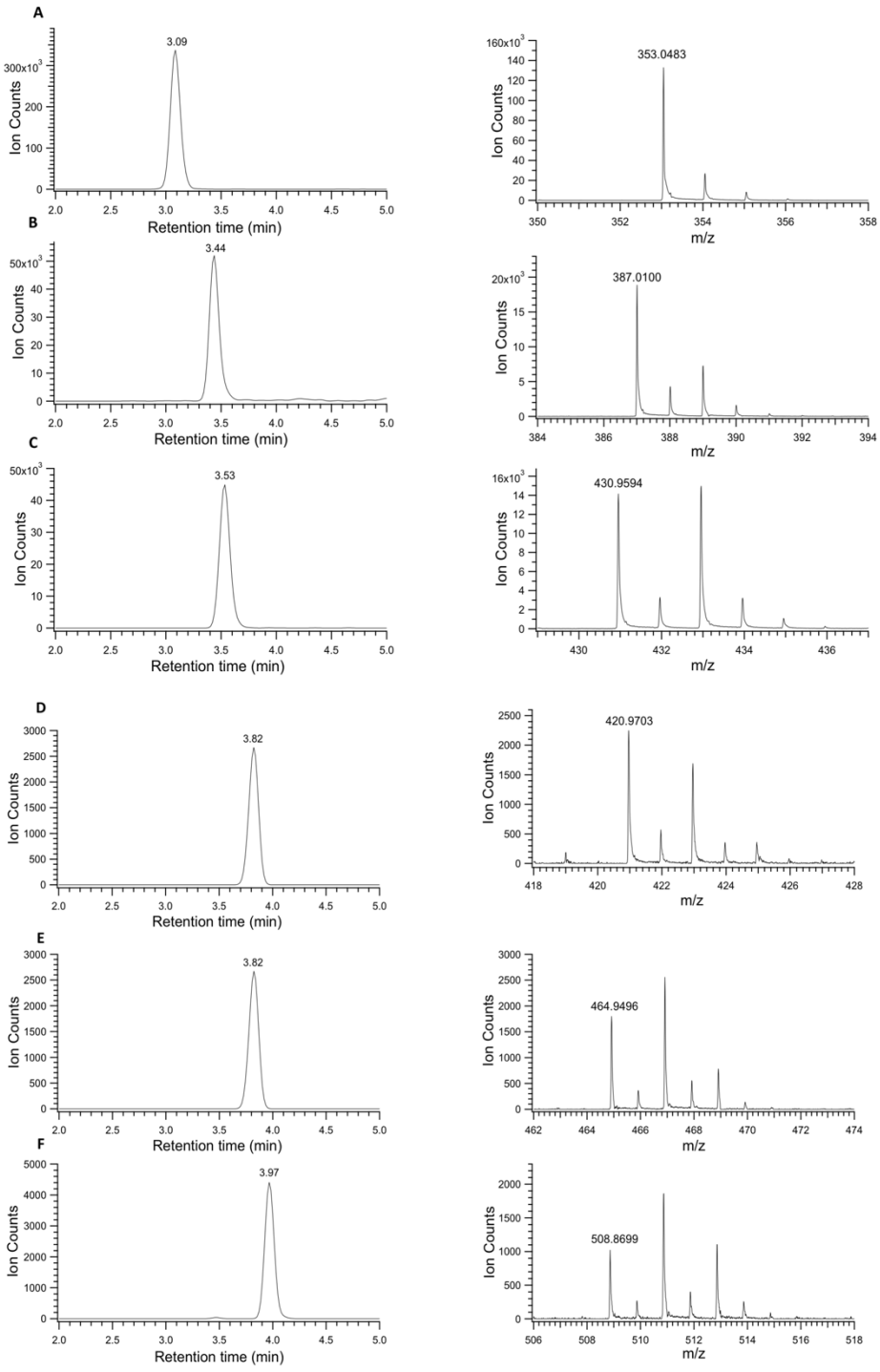

4.9.1. Figure S.1. LC-MS chromatograms for the analysis of halogenated phenol red metabolites. resolution LC-MS was performed for reactions containing 10 μM PR, 50 nM MPO and 200 μM H2O2 in 0.1 M phosphate buffer, pH 7.4 containing 200 mM NaCl. For clarity in presentation, the chromatograms have been separate to highlight the peaks identified using EIC. These chromatograms are best followed using Table 1. The retention times are indicated for MS analysis, which is 0.8-1 second later than UV retention times (shown in Table 1). (A) PR red, (B) monochloro-PR, (C) monobromo-PR, (D) dichloro-PR, (E) monochloro,monobromo-PR, and (F) dibromo-PR.

CHAPTER 5
DISCUSSION

5.1. CONCLUDING REMARKS

Our studies focused on MPO-catalyzed metabolic activation of aromatic chemical entities, including different NSAIDs, one of the most commonly used classes of medications used world-wide. As many NSAID liver metabolites are hydroxylated, it was important to consider the consequent reactivity that would occur. The importance of the hydroxylated or phenolic moiety was explicitly studied in chapter 4, which focused on phenol red, the universal pH indicator used in cell culture media. We presented a classic systematic approach of studying the bioactivation in a biochemical system using purified peroxidase enzymes followed by testing the implications of such bio-activation in leukemic cell culture. In addition, we studied the effect of alterations in the chemical substructures for the bioactivation as well as the differential reactivity of the oxidized products. Chapter 2 and Chapter 3 focused on NSAIDs metabolism by MPO and the possible cytotoxicity of the resulting products in the AML cell line HL-60. Chapter 4 examined the effect of a phenol red peroxidation on the cell viability and the resulting oxidants/antioxidant balance of the cultured HL-60 cells. Some of studied parent NSAIDs were shown, in one way or another, to be MPO substrates of a classic one-electron oxidation by MPO or surprisingly apparent two-electron oxidation in the case of diclofenac and mefenamic acid. We have used EPR spectroscopy as a novel tool to demonstrate the reactive nature of the species that resulted from MPO-catalyzed one-electron oxidation of NSAIDs as well as their hepatic metabolites. Our results showed that robust oxidizing free radical species were produced after MPO oxidation of the diclofenac metabolite, 4'-OHD, the naproxen metabolite, ODN, and also with PR. The latter was achieved by using the DMPO spin trap to detect the formation of GS-DMPO nitrone adducts in presence of GSH. In the case of mefenamic acid and its chemical analogues, direct detection of free radicals species was possible, which is likely the result of the relatively longer half-life of

the free radical products. Differential reactivity was also demonstrated through the ability of the oxidized products to oxidize physiologically relevant cellular anti-oxidants like GSH, ascorbate. Throughout our studies, it was quite evident that even small changes in the chemical structure of NSAIDs, either by having different substituents or exposing toxicophores had a dramatic impact on the oxidizing potential of the resulted metabolites as well as their effect on the viability of the leukemic cells that highly express MPO. It is particularly interesting that diclofenac and its two metabolites 4'-OHD and 5-OHD (chapter 2) significantly dropped the mitochondrial membrane potential after being metabolized by MPO. According to the chemiosmotic hypothesis, mitochondrial membrane potential, generated by proton pumps in the electron transport chain, is directly linked to ATP synthesis in oxidative phosphorylation. Even though it is widely accepted that cancer cells produce most of their energy through glycolysis in the absence of oxygen and rely minimally on oxidative phosphorylation (Warburg effect), one study has shown that blocking oxidative phosphorylation is an efficient way of causing leukemic cell death and decreasing the therapy-resistance in chronic myeloid leukemia[203]. In fact, it was found recently that AML cells are able to take up mitochondria from stromal cells in bone marrow[204], which was found to not only help cancer cells to survive and increase therapy resistance and their ability to relapse after treatment. So, it is believed that causing mitochondrial injury or targeting the mitochondrial transfer could be a novel target to increase the efficacy of the currently used chemotherapy.

Our *in-vitro* model aimed to provide a proof of principle for the tested hypotheses by assessing the acute response of cells after only 3 h of incubation. As such, we used a glucose/glucose oxidase enzymatic system as a source of H_2O_2 influx to trigger the catalytic cycle of the intracellular MPO to help answer our question in the given experimental time.

Glucose oxidase is naturally produced by fungi and has as antibacterial activity since it catalyzes the oxidation of glucose into gluconolactone and hydrogen peroxide. This enzyme is widely used in glucometers test strips used for a quick measure of glucose levels in blood[205], and due to its antibacterial activity, it is utilized in oral care products, but it is not naturally present in AML cells. It was used in this thesis as a source of a gradual influx of H_2O_2 with a certain rate over time for *in vitro* studies instead of adding a high concentration of H_2O_2 all at once. In AML, it is well known that there is a higher steady-state level of intracellular $O_2^{\cdot -}$ and H_2O_2 in cancer cells compared to normal cells[206,207]. This characteristic is believed to play a critical role in cancer cells' growth, proliferation and survival through activation of different signalling pathways[208,209,210]. Intracellular H_2O_2 comes from multiple sources, prominently from superoxide ($O_2^{\cdot -}$) dismutation, produced by the mitochondria electron transport chain, after being reduced by superoxide dismutase (SOD). Numerous mutations have been identified in cancer cells' mitochondrial DNA and it has been hypothesized that such alterations could lead to defects in the electron transport channel, causing the observed increase of ROS levels, but the direct evidence of that link is not convincing. Over-expression of a specific water channel aquaporin 8 (AQP8) was found to facilitate the permeability to H_2O_2 produced by NADPH oxidases. One of the most frequently occurring mutations in AML is in FMS-like tyrosine kinase 3 (FLT3). These mutations were found to occur in approximately 30% of all AML patients and it is associated with poor prognosis. Such mutation has been implicated with increased ROS production in AML via STAT5 signaling pathway, and that increases the aggressiveness of leukemia by increasing DNA doublestrand breaks[211].

Another limitation in our *in-vitro* studies was the concentrations of NSAIDs or their derivatives, which are higher than the plasma concentrations after using the current clinically

used doses as anti-inflammatory agents. In fact, after the oral administration of NSAIDs, the volume of distribution for these drugs is restricted because of the high plasma protein binding, which makes it even harder to reach to the bone marrow and other body tissues.

One more limitation is the use of HL-60 cells only which was derived from the peripheral blood of a female. Differences between both genders in the expression of MPO within the same subtype of AML has not been investigated. Another limitation is that HL-60 cells that it might have some metabolic capacity, other than MPO. After incubating the studied drugs with HL-60 cells, the cells could be lysed and analytical techniques like LC/MS could be used to further investigate this effect.

In summary, we provided evidence for a potential novel approach of compromising the leukemia cells oxidative balance and viability by taking an advantage of the high expression of MPO and its oxidizing capacity. The Canadian Cancer Society statistics show that leukemias are the most commonly diagnosed cancers in children, and it represents the second leading cause of cancer death among children in Canada. We hope that this thesis can provide a rationale for repositioning of existing therapeutic classes of medications as a pathway in the relentless battle against leukemia. From the aspect of basic laboratory science, we also demonstrated that using phenol red-containing cell culture media in *in-vitro* studies should be carefully considered in order to avoid misinterpretation of the results.

5.2. FUTURE DIRECTIONS

In the current studies, we only used one AML subtype, which is an acute promyelocytic leukemia cell model that highly express MPO. As described in the introductory chapter, there are currently 9 AML subtypes as defined by the FAB classification, and not all AML subtypes

express MPO as high as M3. We would like to investigate the different responses exhibited by different leukemic cell lines with different levels of MPO expression, which will give more insight into evaluating the degree of involvement of the metabolic activation by MPO. In addition, acute leukemias are characterized by the fast course of disease progress which might sometimes require the need to use extensive rounds to chemotherapy to decrease or suppress the number of leukemia cells, especially in the induction phase of treatments. For that, combinations of two or more chemotherapeutic medications are often used. We would like to investigate the effect of combining the clinically used chemotherapy agents with NSAIDs on the potency of the former in eradicating leukemia cells. We here propose a future study to use two or more different AML cell lines with different levels of MPO expression. Based on our findings in chapter 2, we decided to test the effect of combining diclofenac or lumiracoxib with the anthracycline chemotherapy (doxorubicin) in two different AML cell lines representing two different subclasses of AML. Lumiracoxib has high selectivity towards COX-2 inhibition but has a different structure from the standard COX-2 inhibitors (e.g. Celecoxib). It more closely resembles the structure of diclofenac (one chlorine in diclofenac is substituted with fluorine). Besides HL-60 cells, we also used THP-1which is a monocytic leukemia cell line (M5) that has no MPO expression[144]. Our preliminary results using CelltitreGlo® ATP cell viability assay showed that HL-60 cells are more sensitive compared to THP-1 to each of diclofenac, doxorubicin or lumiracoxib alone (5.3.1. Fig.1). When we co-treated THP-1 cells with either diclofenac and doxorubicin (5.3.2. Fig.2) or lumiracoxib and doxorubicin (5.3.4. Fig.4), we found no statistically significant differences between the co-treatment groups and either drug alone. On the other hand, HL-60 cell viability did not change as a result of diclofenac and doxorubicin combination (5.3.3. Fig.3), but interestingly, co-treating HL-60 cells with

doxorubicin and lumiracoxib significantly dropped the cell viability compared to either drug alone (5.3.5. Fig.5). These preliminary data suggest a potential additive or synergistic cytotoxic activity as a result of combining NSAIDs and chemotherapy, perhaps due to different modes of action involved. At the same time, it posed more essential research questions that we would like to address in our future studies. One clear direction is to investigate both the molecular mechanisms that had led to the observed effect and to further evaluate the role of MPO expression levels in leukemia cells' response to NSAIDs and the correlation between the degree of the selectivity of NSAIDs in their COX inhibition and their activity in affecting leukemia cells' viability.

5.3. MATERIALS AND METHODS

Both THP-1 cell and HL-60 cell lines were obtained from ATCC (Manassas, VA). Both cell lines are suspension cell lines. Cells were grown in a medium consisting of RPMI-1640 medium with L-glutamine (Gibco® Reference No. 11875-093) with added 10% heat-inactivated fetal bovine serum (FBS, Gibco® Cat No. 12483) and 1% of antibiotic-antimycotic mixture (Gibco®; Reference No. 15240-062, 10 000 units/mL of penicillin, 10 000 μg/mL of streptomycin, and 25 μg/mL of amphotericin B). Cells were maintained in a humidified atmosphere with 5% CO_2 at 37 °C and were allowed to grow with density, maintained at 0.5-1 x 10^6 cells/ml, and split every 2 days as recommended by the supplier. Lumiracoxib was purchased from abcam (product code ab142908) and diclofenac sodium was obtained from Sigma-Aldrich Canada Co. (Oakville, ON). Doxorubicin was purchased from Toronto Reseach Chemicals (Toronto, ON). CellTiter-Glo® luminescent cell viability assay kit was purchased from Promega (Madison, WI).

First, HL-60 cells and THP-1 were harvested and spun down at 120 g for 15 min and re-suspended in pre-warmed FBS-free RPM in a 96-well black plate (Corning Costar) at 5×10^4 cells (>90% viability) for treatment. Each cell line was incubated for 24 h with increasing concentration of doxorubicin (0.5 μM- 5 μM) (Fig. 1 A), lumiracoxib (5 μM-160 μM) (Fig. 1B) or diclofenac (3 μM-160μM) (Fig. 1C). Then, viability of both HL-60 and THP-1 cells were determined by measuring cellular ATP levels using CellTiter-Glo® luminescent viability assay kit (Promega, WI) as per the manufacturer' protocol. Briefly, the working reagent was prepared by thawing buffer solution and adding it to the substrate. Then, the freshly prepared CellTiter-Glo® reagent was added in a 1:1 ratio to each well of the plate (total volume is 100 μM), which then was shaken for 2 min on a shaker. After 10 min of incubation at RT, luminescent signals were recorded using a SpectraMax® M5 Multi-Mode Microplate reader (Molecular Devices, Sunnyvale, CA). Same protocol was also used to assess the effect on cell viability after treating HL-60 cells and THP-1 with a combination of either diclofenac (Fig. 2 and 3) or diclofenac (Fig. 4 and 5) and 0.5 μM doxorubicin. Each reaction was repeated 3 times on different days, and the results were expressed as mean ± SD.

5.4. FIGURES

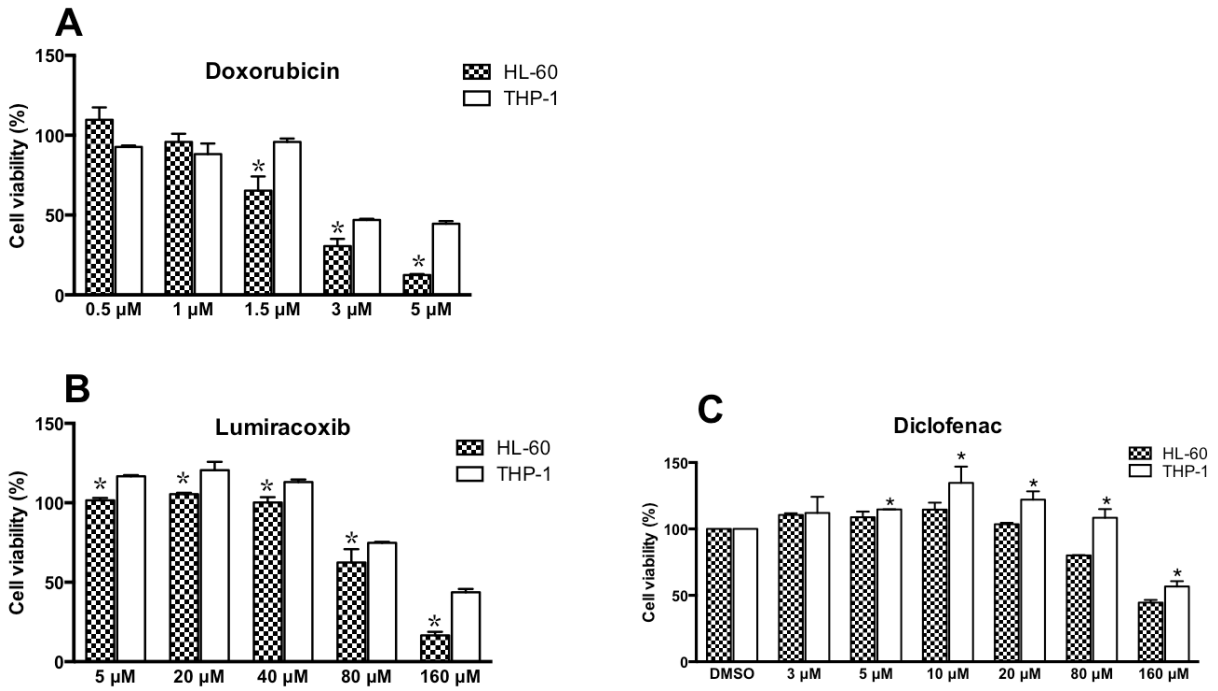

5.4.1. Figure 1: Effect of lumiracoxib, diclofenac or doxorubicin treatments on HL-60 and THP-1 cell viability. Cells were incubated with different concentrations of doxorubicin (A), lumiracoxib (B) or diclofenac (C) for 24 h. Each set of data represents at least three independent experiments. *(P<0.01) comparing HL-60 cell viability to THP-1 cell viability after the same treatment. One-way ANOVA statistical analysis was used to test for significance; statistical significance was found between HL-60 and THP-1 cell viability in the three drugs.

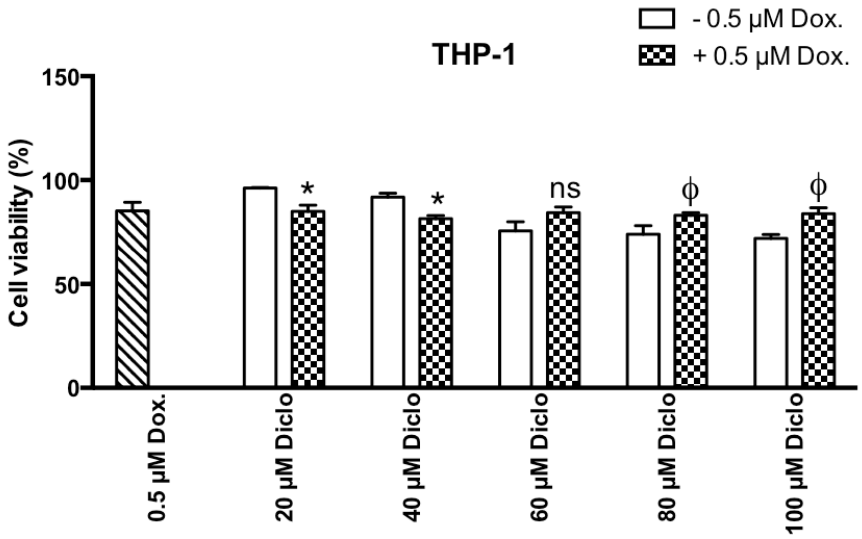

5.4.2. Figure 2: The effect of THP-1 cells co-treatment with diclofenac and doxorubicin on cell viability. Cells were incubated with 0.5 µM doxorubicin and increasing concentrations of diclofenac or 24 h. Each set of data represents at least three independent experiments. *(*P*<0.01) compared to treatment with doxorubicin alone. ϕ (P<0.01*)* compared to the treatment with the same concentration of diclofenac alone. One-way ANOVA statistical analysis was used to test for significance; no statistical significance was found between the co-treatment compared to each individual treatment.

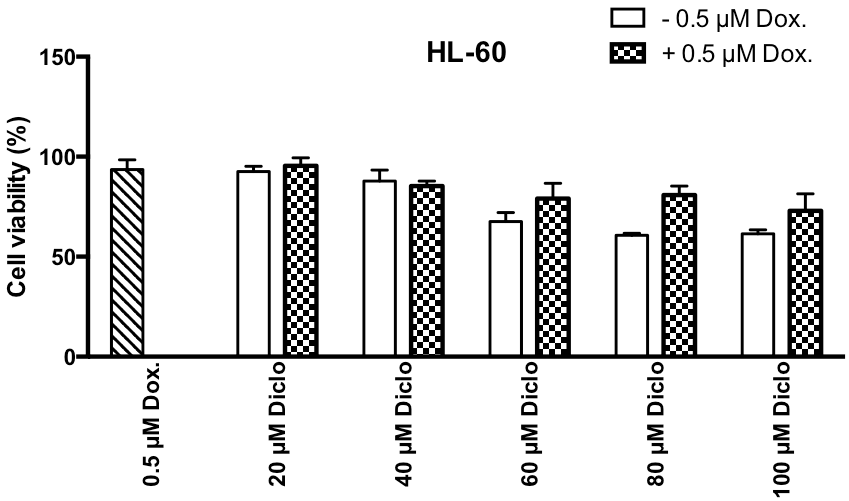

5.4.3. Figure 3: The effect of HL-60 cells co-treatment with diclofenac and doxorubicin on cell viability. Cells were incubated with 0.5 µM doxorubicin and increasing concentrations of diclofenac or 24 h. Each set of data represents at least three independent experiments. One-way ANOVA statistical analysis was used to test for significance; no statistical significance was found between the co-treatment compared to each individual treatment alone.

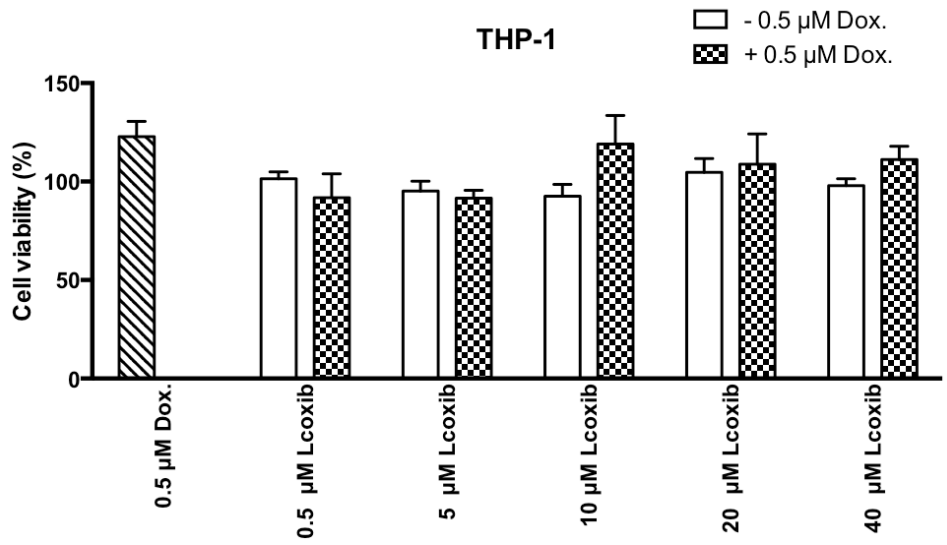

5.4.4. Figure 4: The effect of THP-1 cells co-treatment with lumiracoxib and doxorubicin on cell viability. Cells were incubated with 0.5 µM doxorubicin and increasing concentrations of lumiracoxib or 24 h. Each set of data represents at least three independent experiments. One-way ANOVA statistical analysis was used to test for significance; no statistical significance was found between the co-treatment compared to each individual treatment alone.

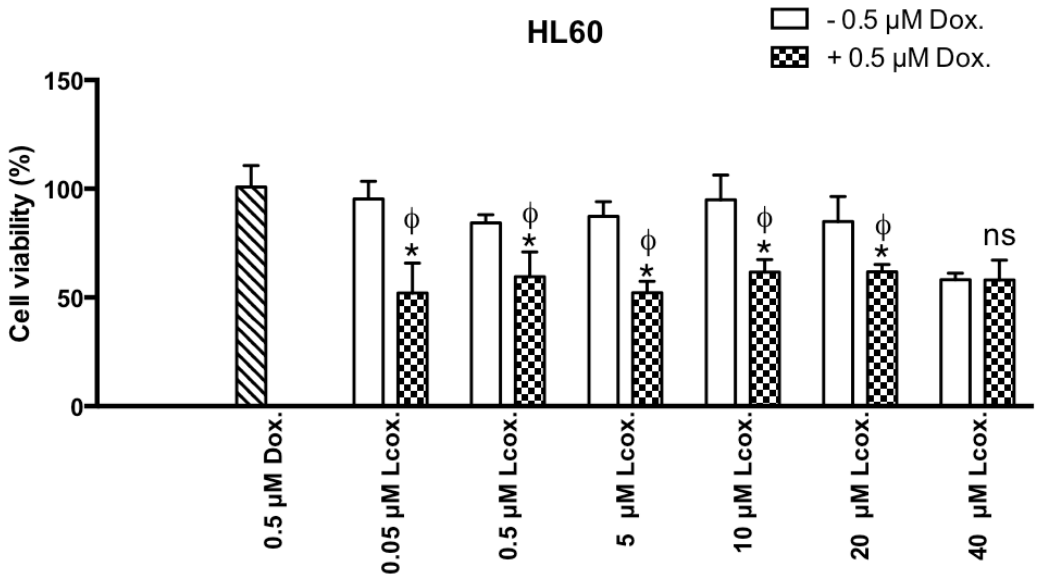

5.4.5. Figure 5: Effect of HL-60 cells co-treatment with lumiracoxib and doxorubicin on cells' viability. Cells were incubated with 0.5µM doxorubicin and increasing concentrations of lumiracoxib or 24h. Each set of data represents at least three independent experiments. One-way ANOVA statistical analysis was used to test for significance; $^{*}(P<0.01)$ compared to treatment with doxorubicin alone ϕ ($P<0.01$) compared to the treatment with the same concentration of lumiracoxib alone. Statistical significance was found between the co-treatments and either drug alone.

REFERENCES

1. Rayburn, E. Anti-Inflammatory Agents for Cancer Therapy. *Mol. Cell. Pharmacol.* (2009). doi:10.4255/mcpharmacol.09.05
2. Balkwill, F. & Mantovani, A. Inflammation and cancer: Back to Virchow? *Lancet* **357**, 539–545 (2001).
3. Coussens, L. M. & Werb, Z. Inflammatory Cells and Cancer. *J. Exp. Med.* **193**, F23 LP-F26 (2001).
4. Wu, Y. & Zhou, B. P. Inflammation: A driving force speeds cancer metastasis. *Cell Cycle* **8**, 3267–3273 (2009).
5. Hussain, S. P. & Harris, C. C. Inflammation and cancer: An ancient link with novel potentials. *Int. J. Cancer* **121**, 2373–2380 (2007).
6. Yan, X.-J. *et al.* Identification of outcome-correlated cytokine clusters in chronic lymphocytic leukemia. *Blood* **118**, 5201–5210 (2011).
7. Fayad, L. *et al.* Interleukin-6 and interleukin-10 levels in chronic lymphocytic leukemia: Correlation with phenotypic characteristics and outcome. *Blood* **97**, 256–263 (2001).
8. Yoon, J.-Y. *et al.* Association of interleukin-6 and interleukin-8 with poor prognosis in elderly patients with chronic lymphocytic leukemia. *Leuk. Lymphoma*

53, 1735–1742 (2012).

9. ten Hacken, E. & Burger, J. A. Microenvironment interactions and B-cell receptor signaling in Chronic Lymphocytic Leukemia: Implications for disease pathogenesis and treatment. *Biochim. Biophys. Acta - Mol. Cell Res.* **1863**, 401–413 (2016).
10. Rozovski, U., Keating, M. J. & Estrov, Z. Targeting inflammatory pathways in chronic lymphocytic leukemia. *Crit. Rev. Oncol. Hematol.* **88**, 655–666 (2013).
11. Carey, A. *et al.* Identification of Interleukin-1 by Functional Screening as a Key Mediator of Cellular Expansion and Disease Progression in Acute Myeloid Leukemia. *Cell Rep.* **18**, 3204–3218 (2017).
12. Thun, M. J., Jane Henley, S. & Patrono, C. Nonsteroidal anti-inflammatory drugs as anticancer agents: Mechanistic, pharmacologic, and clinical issues. *Journal of the National Cancer Institute* (2002). doi:10.1093/jnci/94.4.252
13. Bennett, A. & Del Tacca, M. Prostaglandins in human colonic carcinoma. *Gut* **16**, 409 (1975).
14. Steinbach, G. *et al.* The effect of celecoxib, a cyclooxygenase-2 inhibitor, in familial adenomatous polyposis. *N. Engl. J. Med.* **342**, 1946–1952 (2000).
15. Lynch, P. M. *et al.* The safety and efficacy of celecoxib in children with familial adenomatous polyposis. *Am. J. Gastroenterol.* **105**, 1437–1443 (2010).
16. Sgambati, S. A. Cardiovascular risk associated with celecoxib in a clinical trial for colorectal adenoma prevention: Commentary. *Dis. Colon Rectum* **48**, 1331 (2005).
17. CruzCorrea, M., Hylind, L. M., Romans, K. E., Booker, S. V & Giardiello, F. M. Long-term treatment with sulindac in familial adenomatous polyposis: A

prospective cohort study. *Gastroenterology* **122**, 641–645 (2002).

18. Van Stolk, R. *et al.* Phase I trial of exisulind (sulindac sulfone, FGN-1) as a chemopreventive agent in patients with familial adenomatous polyposis. *Clin. Cancer Res.* **6**, 78–89 (2000).
19. Arber, N. *et al.* Sporadic adenomatous polyp regression with exisulind is effective but toxic: A randomised, double blind, placebo controlled, dose-response study. *Gut* **55**, 367–373 (2006).
20. Baron, J. A. *et al.* A randomized trial of aspirin to prevent colorectal adenomas. *N. Engl. J. Med.* **348**, 891–899 (2003).
21. Sandler, R. S. *et al.* A randomized trial of aspirin to prevent colorectal adenomas in patients with previous colorectal cancer. *N. Engl. J. Med.* **348**, 883–890 (2003).
22. Burn, J. *et al.* A randomized placebo-controlled prevention trial of aspirin and/or resistant starch in young people with familial adenomatous polyposis. *Cancer Prev. Res.* **4**, 655–665 (2011).
23. Albouy, B. *et al.* Preliminary results of the Prostacox phase II trial in hormonal refractory prostate cancer. *BJU Int.* **100**, 770–774 (2007).
24. Fabi, A. *et al.* Impact of celecoxib on capecitabine tolerability and activity in pretreated metastatic breast cancer: Results of a phase II study with biomarker evaluation. *Cancer Chemother. Pharmacol.* **62**, 717–725 (2008).
25. Lacourt, T. E. *et al.* Associations of inflammation with symptom burden in patients with acute myeloid leukemia. *Psychoneuroendocrinology* **89**, 203–208 (2018).
26. Fung, F. Y. *et al.* Correlation between cytokine levels and changes in fatigue and

quality of life in patients with acute myeloid leukemia. *Leuk. Res.* **37**, 274–279 (2013).

27. Meyers, C. A., Albitar, M. & Estey, E. Cognitive impairment, fatigue, and cytokine levels in patients with acute myelogenous leukemia or myelodysplastic syndrome. *Cancer* **104**, 788–793 (2005).

28. Ponthan, F. *et al.* Celecoxib prevents neuroblastoma tumor development and potentiates the effect of chemotherapeutic drugs in vitro and in vivo. *Clin. Cancer Res.* **13**, 1036–1044 (2007).

29. Lu, M. *et al.* Aspirin sensitizes cancer cells to TRAIL-induced apoptosis by reducing survivin levels. *Clin. Cancer Res.* **14**, 3168–3176 (2008).

30. Shin, D. M. *et al.* Chemoprevention of head and neck cancer by simultaneous blocking of epidermal growth factor receptor and cyclooxygenase-2 signaling pathways: Preclinical and clinical studies. *Clin. Cancer Res.* **19**, 1244–1256 (2013).

31. Chae, Y. K., Trinh, L. X., Keating, M. J., & Estrov, Z. Concurrent Use of Aspirin with the Fludarabine, Cyclophophamide, Rituximab (FCR) Regimen Improves Outcome in Patients with Relapsed/Refractory CLL. *Blood* (2012).

32. Hanahan, D. & Weinberg, R. A. Hallmarks of cancer: The next generation. *Cell* **144**, 646–674 (2011).

33. Elder, D. J. E., Halton, D. E., Hague, A. & Paraskeva, C. Induction of apoptotic cell death in human colorectal carcinoma cell lines by a cyclooxygenase-2 (COX-2)-selective nonsteroidal anti-inflammatory drug: Independence from COX-2 protein expression. *Clin. Cancer Res.* **3**, 1679–1683 (1997).

34. Totzke, G., Schulze-Osthoff, K. & Jänicke, R. U. Cyclooxygenase-2 (COX-2) inhibitors sensitize tumor cells specifically to death receptor-induced apoptosis independently of COX-2 inhibition. *Oncogene* **22**, 8021–8030 (2003).

35. Piazza, G. A. *et al.* Sulindac sulfone inhibits azoxymethane-induced colon carcinogenesis in rats without reducing prostaglandin levels. *Cancer Res.* **57**, 2909–2915 (1997).

36. Piazza, G. A. *et al.* Apoptosis primarily accounts for the growth-inhibitory properties of sulindac metabolites and involves a mechanism that is independent of cyclooxygenase inhibition, cell cycle arrest, and p53 induction. *Cancer Res.* **57**, 2452–2459 (1997).

37. Bielenberg, D. R. & Zetter, B. R. The Contribution of Angiogenesis to the Process of Metastasis. *Cancer J. (United States)* **21**, 267–273 (2015).

38. Harris, R. E. Cyclooxygenase-2 (cox-2) blockade in the chemoprevention of cancers of the colon, breast, prostate, and lung. *Inflammopharmacology* **17**, 55–67 (2009).

39. Zhang, J., Zhou, Y., Hu, M. & Xie, W. Inhibition effects of Celebrex on the proliferation of Lewis lung cancer cells and growth of transplanted Lewis lung carcinoma. *Med. J. Wuhan Univ.* **29**, 485–488 (2008).

40. Liu, D.-B. *et al.* Celecoxib induces apoptosis and cell-cycle arrest in nasopharyngeal carcinoma cell lines via inhibition of STAT3 phosphorylation. *Acta Pharmacol. Sin.* **33**, 682–690 (2012).

41. Bock, J. M. *et al.* Celecoxib toxicity is cell cycle phase specific. *Cancer Res.* **67**,

3801–3808 (2007).

42. De Kouchkovsky, I. & Abdul-Hay, M. ‘Acute myeloid leukemia: A comprehensive review and 2016 update.’ *Blood Cancer J.* **6**, (2016).

43. Siegel, R. L., Miller, K. D. & Jemal, A. Cancer statistics, 2019. *CA Cancer J. Clin.* **69**, 7–34 (2019).

44. Ganzel, C., Becker, J., Mintz, P. D., Lazarus, H. M. & Rowe, J. M. Hyperleukocytosis, leukostasis and leukapheresis: Practice management. *Blood Rev.* **26**, 117–122 (2012).

45. Creutzig, U. & Kaspers, G. J. L. Revised recommendations of the international working group for diagnosis, standardization of response criteria, treatment outcomes, and reporting standards for therapeutic trials in acute myeloid leukemia [3]. *J. Clin. Oncol.* **22**, 3432–3433 (2004).

46. Li, Y. *et al.* Mutational spectrum and associations with clinical features in patients with acute myeloid leukaemia based on next-generation sequencing. *Mol. Med. Rep.* **49**, 4147–4158 (2019).

47. Ley, T. J. *et al.* DNMT3A mutations in acute myeloid leukemia. *N. Engl. J. Med.* **363**, 2424–2433 (2010).

48. Jaiswal, S. *et al.* Age-related clonal hematopoiesis associated with adverse outcomes. *N. Engl. J. Med.* **371**, 2488–2498 (2014).

49. Rossi, D. J. *et al.* Deficiencies in DNA damage repair limit the function of haematopoietic stem cells with age. *Nature* **447**, 725–729 (2007).

50. Di Nardo, C. D. & Cortes, J. E. Mutations in AML: Prognostic and therapeutic

implications. *Hematology* **2016**, 348–355 (2016).

51. Azari-Yam, A. *et al.* FLT3 Gene Mutation Profile and Prognosis in Adult Acute Myeloid Leukemia. *Clin. Lab.* **62**, 2011–2017 (2016).

52. Schofield, R. The relationship between the spleen colony-forming cell and the haemopoietic stem cell. A hypothesis. *Blood Cells* **4**, 7–25 (1978).

53. Korn, C. & Méndez-Ferrer, S. Myeloid malignancies and the microenvironment. *Blood* **129**, 811–822 (2017).

54. Zambetti, N. A. *et al.* Mesenchymal Inflammation Drives Genotoxic Stress in Hematopoietic Stem Cells and Predicts Disease Evolution in Human Pre-leukemia. *Cell Stem Cell* **19**, 613–627 (2016).

55. Ley, T. J. *et al.* Genomic and epigenomic landscapes of adult de novo acute myeloid leukemia. *N. Engl. J. Med.* **368**, 2059–2074 (2013).

56. Bennett, J. M. *et al.* Proposals for the Classification of the Acute Leukaemias French-American-British (FAB) Co-operative Group. *Br. J. Haematol.* **33**, 451–458 (1976).

57. Manaloor, E. J. *et al.* Immunohistochemistry can be used to subtype acute myeloid leukemia in routinely processed bone marrow biopsy specimens: Comparison with flow cytometry. *Am. J. Clin. Pathol.* **113**, 814–822 (2000).

58. Bennett, J. M. *et al.* Criteria for the diagnosis of acute leukemia of megakaryocyte lineage (M7). A report of the French-American-British Cooperative Group. *Ann. Intern. Med.* **103**, 460–462 (1985).

59. Lee, E. J., Pollak, A., Leavitt, R. D., Testa, J. R. & Schiffer, C. A. Minimally

differentiated acute nonlymphocytic leukemia: A distinct entity. *Blood* **70**, 1400–1406 (1987).

60. Van Der Schoot, C. E., Daams, G. M., Pinkster, J., Vet, R. & Kr.vondem Borne, A. E. G. Monoclonal antibodies against myeloperoxidase are valuable immunological reagents for the diagnosis of acute myeloid leukaemia. *Br. J. Haematol.* **74**, 173–178 (1990).

61. Neame, P. B. *et al.* Classifying acute leukemia by immunophenotyping: A combined FAB-immunologic classification of AML. *Blood* **68**, 1355–1362 (1986).

62. Falini, B., Tiacci, E., Martelli, M. P., Ascani, S. & Pileri, S. A. New classification of acute myeloid leukemia and precursor-related neoplasms: changes and unsolved issues. *Discov. Med.* **10**, 281–292 (2010).

63. Patel, J. P. *et al.* Prognostic relevance of integrated genetic profiling in acute myeloid leukemia. *N. Engl. J. Med.* **366**, 1079–1089 (2012).

64. Dombret, H. & Gardin, C. An update of current treatments for adult acute myeloid leukemia. *Blood* **127**, 53–61 (2016).

65. Appelbaum, F. R. Who should be transplanted for AML? *Leukemia* **15**, 680–682 (2001).

66. Thol, F., Schlenk, R. F., Heuser, M. & Ganser, A. How I treat refractory and early relapsed acute myeloid leukemia. *Blood* **126**, 319–327 (2015).

67. Onder, G., Pellicciotti, F., Gambassi, G. & Bernabei, R. NSAID-related psychiatric adverse events: Who is at risk? *Drugs* **64**, 2619–2627 (2004).

68. Martel-Pelletier, J., Lajeunesse, D., Reboul, P. & Pelletier, J.-P. Therapeutic role of

dual inhibitors of 5-LOX and COX, selective and non-selective non-steroidal anti-inflammatory drugs. *Ann. Rheum. Dis.* **62**, 501–509 (2003).

69. Bacchi, S., Palumbo, P., Sponta, A. & Coppolino, M. F. Clinical pharmacology of non-steroidal anti-inflammatory drugs: A review. *Anti-inflamm. Anti-Allergy Agents Med. Chem.* **11**, 52–64 (2012).

70. Ricciotti, E. & Fitzgerald, G. A. Prostaglandins and inflammation. *Arterioscler. Thromb. Vasc. Biol.* **31**, 986–1000 (2011).

71. Lewis, G. P. Prostaglandins in inflammation. *RES J. Reticuloendothel. Soc.* **22**, 389–402 (1977).

72. Raskin, J. B. Gastrointestinal effects of nonsteroidal anti-inflammatory therapy. *Am. J. Med.* **106**, 3S-12S (1999).

73. DuBois, R. N. *et al.* Cyclooxygenase in biology and disease. *FASEB J.* **12**, 1063–1073 (1998).

74. Hoffmann, C. COX-2 in brain and spinal cord - Implications for therapeutic use. *Curr. Med. Chem.* **7**, 1113–1120 (2000).

75. O'Brien, G. M. & Harris, R. C. Cyclooxygenase-2 and the kidney: Functional and pathophysiological implications. *J. Hypertens.* **20**, S3–S9 (2002).

76. Chandrasekharan, N. V *et al.* COX-3, a cyclooxygenase-1 variant inhibited by acetaminophen and other analgesic/antipyretic drugs: Cloning, structure, and expression. *Proc. Natl. Acad. Sci. U. S. A.* **99**, 13926–13931 (2002).

77. Frölich, J. C. A classification of NSAIDs according to the relative inhibition of cyclooxygenase isoenzymes. *Trends Pharmacol. Sci.* **18**, 30–34 (1997).

78. DeWitt, D. L., Meade, E. A. & Smith, W. L. PGH synthase isoenzyme selectivity: The potential for safer nonsteroidal antiinflammatory drugs. *Am. J. Med.* **95**, S40–S44 (1993).

79. Zarghi, A. & Arfaei, S. Selective COX-2 inhibitors: A review of their structure-activity relationships. *Iran. J. Pharm. Res.* **10**, 655–683 (2011).

80. Vane, J. R. & Warner, T. D. Nomenclature for cox-2 inhibitors. *Lancet* **356**, 1373–1374 (2000).

81. Silverstein, F. E. *et al.* Gastrointestinal toxicity with Celecoxib vs nonsteroidal anti-inflammatory drugs for osteoarthritis and reumatoid arthritis: The CLASS study: A randomized controlled trial. *J. Am. Med. Assoc.* **284**, 1247–1255 (2000).

82. Bombardier, C. *et al.* Comparison of upper gastrointestinal toxicity of rofecoxib and naproxen in patients with rheumatoid arthritis. *N. Engl. J. Med.* **343**, 1520–1528 (2000).

83. Mukherjee, D., Nissen, S. E. & Topol, E. J. Risk of cardiovascular events associated with selective COX-2 inhibitors. *J. Am. Med. Assoc.* **286**, 954–959 (2001).

84. Asirvatham, S., Dhokchawle, B. V & Tauro, S. J. Quantitative structure activity relationships studies of non-steroidal anti-inflammatory drugs: A review. *Arabian Journal of Chemistry* (2016). doi:10.1016/j.arabjc.2016.03.002

85. Shah, K. *et al.* Prodrugs of NSAIDs: A review. *Open Med. Chem. J.* **11**, 146–195 (2017).

86. Day, R. O., Graham, G. G. & Williams, K. M. Pharmacokinetics of non-steroidal

anti-inflammatory drugs. *Baillieres. Clin. Rheumatol.* **2**, 363–393 (1988).

87. Cryer, B. & Feldman, M. Cyclooxygenase-1 and cyclooxygenase-2 selectivity of widely used nonsteroidal anti-inflammatory drugs. *Am. J. Med.* **104**, 413–421 (1998).

88. Shen, S., Marchick, M. R., Davis, M. R., Doss, G. A. & Pohl, L. R. Metabolic activation of diclofenac by human cytochrome P450 3A4: Role of 5-hydroxydiclofenac. *Chem. Res. Toxicol.* **12**, 214–222 (1999).

89. Tang, W., Stearns, R. A., Wang, R. W., Chiu, S.-H. L. & Baillie, T. A. Roles of human hepatic cytochrome P450s 2C9 and 3A4 in the metabolic activation of diclofenac. *Chem. Res. Toxicol.* **12**, 192–199 (1999).

90. Oda, S. *et al.* Toxicological role of an acyl glucuronide metabolite in diclofenac-induced acute liver injury in mice. *J. Appl. Toxicol.* **37**, 545–553 (2017).

91. Diclofenac monograph. *Compend. Pharm. Spec.*

92. FDA label for voltaren tablets. *https://www.accessdata.fda.gov/drugsatfda_docs/label/2009/019201s038lbl.pdf*

93. Castellano, A. E. *et al.* Indomethacin increases the effect of isosorbide dinitrate on cerebral hemodynamic in migraine patients: Pathogenetic and therapeutic implications. *Cephalalgia* **18**, 622–630 (1998).

94. Lucas, S. The Pharmacology of Indomethacin. *Headache* **56**, 436–446 (2016).

95. Helleberg, L. Clinical Pharmacokinetics of Indomethacin. *Clin. Pharmacokinet.* **6**, 245–258 (1981).

96. Alván, G., Orme, M., Bertilsson, L., Ekstrand, R. & Palmér, L. Pharmacokinetics

of indomethacin. *Clin. Pharmacol. Ther.* **18**, 364–373 (1975).

97. Duggan, D. E., Hogans, A. F., Kwan, K. C. & McMahon, F. G. The metabolism of indomethacin in man. *J. Pharmacol. Exp. Ther.* **181**, 563–575 (1972).

98. Ju, C. & Uetrecht, J. P. Oxidation of a metabolite of indomethacin (desmethyldeschlorobenzoylindomethacin) to reactive intermediates by activated neutrophils, hypochlorous acid, and the myeloperoxidase system. *Drug Metab. Dispos.* (1998).

99. Duggan, D. E., Hooke, K. F., Noll, R. M. & Chiu Kwan, K. Enterohepatic circulation of indomethacin and its role in intestinal irritation. *Biochem. Pharmacol.* **24**, 1749–1754 (1975).

100. Duggan, K. C. *et al.* Molecular basis for cyclooxygenase inhibition by the non-steroidal anti-inflammatory drug naproxen. *J. Biol. Chem.* **285**, 34950–34959 (2010).

101. Ageeva, A. A., Khramtsova, E. A., Plyusnin, V. F., Miranda, M. A. & Leshina, T. V. Physico-chemical approach to the study of naproxen enantiomers. in *Naproxen: Chemistry, Clinical Aspects and Effects* 35–66 (2018).

102. Todd, P. A. & Clissold, S. P. Naproxen: A Reappraisal of its Pharmacology, and Therapeutic Use in Rheumatic Diseases and Pain States. *Drugs* **40**, 91–137 (1990).

103. Sevelius, H., Runkel, R., Segre, E. & Bloomfield, S. Bioavailability of naproxen sodium and its relationship to clinical analgesic effects. *Br. J. Clin. Pharmacol.* **10**, 259–263 (1980).

104. Smith, W. L. *et al.* Differential inhibition of human prostaglandin endoperoxide H

synthases-1 and -2 by aspirin and other nonsteroidal anti-inflammatory drugs. *Eur. J. Med. Chem.* **30**, 417s-427s (1995).

105. FDA label of naproxen. *https://www.accessdata.fda.gov/drugsatfda_docs/label/2017/017581s113,018164s063,020067s020lbl.pdf*

106. Pringsheim, T., Davenport, W. J. & Dodick, D. Acute treatment and prevention of menstrually related migraine headache: Evidence-based review. *Neurology* **70**, 1555–1563 (2008).

107. FDA label of mefenamic acid. *https://www.accessdata.fda.gov/drugsatfda_docs/label/2008/015034s040lbl.pdf*

108. https://www.accessdata.fda.gov/drugsatfda_docs/label/2008/015034s040lbl.pdf. (2008).

109. Lashinski, E. M. *Enzymes and enzyme activity: Structure, biology and clinical significance*. *Enzymes and Enzyme Activity: Structure, Biology and Clinical Significance* (2013).

110. Klebanoff, S. J. Myeloperoxidase: Friend and foe. *J. Leukoc. Biol.* **77**, 598–625 (2005).

111. Brown, K. E., Brunt, E. M. & Heinecke, J. W. Immunohistochemical detection of myeloperoxidase and its oxidation products in Kupffer cells of human liver. *Am. J. Pathol.* **159**, 2081–2088 (2001).

112. Nichols, B. A. & Bainton, D. F. Differentiation of human monocytes in bone marrow and blood: sequential formation of two granule populations. *Lab. Investig.*

29, 27–40 (1973).

113. Bainton, D. F. & Farquhar, M. G. Segregation and packaging of granule enzymes in eosinophilic leukocytes. *J. Cell Biol.* **45**, 54–73 (1970).

114. Wagner, D. K., Collins-Lech, C. & Sohnle, P. G. Inhibition of neutrophil killing of Candida albicans pseudohyphae by substances which quench hypochlorous acid and chloramines. *Infect. Immun.* **51**, 731–735 (1986).

115. McKenna, S. M. & Davies, K. J. A. The inhibition of bacterial growth by hypochlorous acid. Possible role in the bactericidal activity of phagocytes. *Biochem. J.* **254**, 685–692 (1988).

116. Panasenko, O. M., Gorudko, I. V & Sokolov, A. V. Hypochlorous acid as a precursor of free radicals in living systems. *Biochem.* **78**, 1466–1489 (2013).

117. Segal, A. W. & Abo, A. The biochemical basis of the NADPH oxidase of phagocytes. *Trends Biochem. Sci.* **18**, 43–47 (1993).

118. Hampton, M. B., Kettle, A. J. & Winterbourn, C. C. Inside the neutrophil phagosome: Oxidants, myeloperoxidase, and bacterial killing. *Blood* **92**, 3007–3017 (1998).

119. Smith, R. M. & Curnutte, J. T. Molecular basis of chronic granulomatous disease. *Blood* **77**, 673–686 (1991).

120. Heinecke, J. W. Tyrosyl radical production by myeloperoxidase: A phagocyte pathway for lipid peroxidation and dityrosine cross-linking of proteins. *Toxicology* **177**, 11–22 (2002).

121. Lehrer, R. I. & Cline, M. J. Leukocyte myeloperoxidase deficiency and

disseminated candidiasis: the role of myeloperoxidase in resistance to Candida infection. *J. Clin. Invest.* **48**, 1478–1488 (1969).

122. Khan, S. R. *et al.* Proteomic profile of aminoglutethimide-induced apoptosis in HL-60 cells: Role of myeloperoxidase and arylamine free radicals. *Chem. Biol. Interact.* **239**, 129–138 (2015).

123. Tesfa, D., Keisu, M. & Palmblad, J. Idiosyncratic drug-induced agranulocytosis: Possible mechanisms and management. *Am. J. Hematol.* **84**, 428–434 (2009).

124. Uetrecht, J., Zahid, N., Tehim, A., Mim Fu, J. & Rakhit, S. Structural features associated with reactive metabolite formation in clozapine analogues. *Chem. Biol. Interact.* **104**, 117–129 (1997).

125. Miyamoto, G., Zahid, N. & Uetrecht, J. P. Oxidation of diclofenac to reactive intermediates by neutrophils, myeloperoxidase, and hypochlorous acid. *Chem. Res. Toxicol.* (1997). doi:10.1021/tx960190k

126. Panousis, C., Kettle, A. & DR Phillips. Myeloperoxidase oxidizes mitoxantrone to metabolites which bind covalently DNA and RNA. *Anticancer Drug Des* (1995).

127. Panousis, C., Kettle, A. J. & Phillips, D. R. Oxidative metabolism of mitoxantrone by the human neutrophil enzyme myeloperoxidase. *Biochem. Pharmacol.* **48**, 2223–2230 (1994).

128. Panousis, C., Kettle, A. J. & Phillips, D. R. Neutrophil-mediated activation of mitoxantrone to metabolites which form adducts with DNA. *Cancer Lett.* **113**, 173–178 (1997).

129. Kagan, V. E. *et al.* Pro-oxidant and antioxidant mechanisms of etoposide in HL-60

cells: Role of myeloperoxidase. *Cancer Res.* (2001).

130. Stiborová, M. *et al.* Mammalian peroxidases activate anticancer drug ellipticine to intermediates forming deoxyguanosine adducts in DNA identical to those found in vivo and generated from 12-hydroxyellipticine and 13-hydroxyellipticine. *Int. J. Cancer* (2007). doi:10.1002/ijc.22247
131. Poljaková, J. *et al.* DNA adduct formation by the anticancer drug ellipticine in human leukemia HL-60 and CCRF-CEM cells. *Cancer Lett.* **252**, 270–279 (2007).
132. Kim, Y. R. *et al.* Myeloperoxidase expression as a potential determinant of parthenolide-induced apoptosis in leukemia bulk and leukemia stem cells. *J. Pharmacol. Exp. Ther.* **335**, 389–400 (2010).
133. Guzman, M. L. *et al.* The sesquiterpene lactone parthenolide induces apoptosis of human acute myelogenous leukemia stem and progenitor cells. *Blood* **105**, 4163–4169 (2005).
134. Ambrosone, C. B. *et al.* Myeloperoxidase genotypes and enhanced efficacy of chemotherapy for early-stage breast cancer in SWOG-8897. *J. Clin. Oncol.* **27**, 4973–4979 (2009).
135. Spasojević, I. Electron paramagnetic resonance - A powerful tool of medical biochemistry in discovering mechanisms of disease and treatment prospects. *J. Med. Biochem.* **29**, 175–188 (2010).
136. OBJOBJAn EPR Primer 2. 1–24 (2000).
137. Janzen, E. G., Stronks, H. J. & Dubose, C. M. Chemistry and biology of spin-trapping radicals associated with halocarbon metabolism in vitro and in vivo.

Environ. Health Perspect. **VOL. 64**, 151–170 (1985).

138. Collins, S. J., Gallo, R. C. & Gallagher, R. E. Continuous growth and differentiation of human myeloid leukaemic cells in suspension culture. *Nature* **270**, 347–349 (1977).

139. Collins, S. J., Ruscetti, F. W., Gallagher, R. E. & Gallo, R. C. Terminal differentiation of human promyelocytic leukemia cells induced by dimethyl sulfoxide and other polar compounds. *Proc. Natl. Acad. Sci. U. S. A.* **75**, 2458–2462 (1978).

140. Gallagher, R. *et al.* Characterization of the continuous, differentiating myeloid cell line (HL-60) from a patient with acute promyelocytic leukemia. *Blood* **54**, 713–733 (1979).

141. Birnie, G. D. The HL60 cell line: A model system for studying human myeloid cell differentiation. *Br. J. Cancer* **58**, 41–45 (1988).

142. Kohram, F. *et al.* Cell type-dependent functions of microRNA-92a. *J. Cell. Biochem.* **119**, 5798–5804 (2018).

143. Breitman, T. R. & He, R. Combinations of Retinoic Acid with Either Sodium Butyrate, Dimethyl Sulfoxide, or Hexamethylene Bisacetamide Synergistically Induce Differentiation of the Human Myeloid Leukemia Cell Line HL60. *Cancer Res.* **50**, 6268–6273 (1990).

144. Hu, Z.-B. *et al.* Myeloperoxidase: Expression and modulation in a large panel of human leukemia-lymphoma cell lines. *Blood* **82**, 1599–1607 (1993).

145. Leukemia and Lymphoma Society, 2013). *www.llscanada.org* 1–3 (2013).

146. Franks, A. L. & Slansky, J. E. Multiple associations between a broad spectrum of autoimmune diseases, chronic inflammatory diseases and cancer. *Anticancer Res.* **32**, 1119–1136 (2012).

147. Schönthal, A. H., Chen, T. C., Hofman, F. M., Louie, S. G. & Petasis, N. A. Celecoxib analogs that lack COX-2 inhibitory function: Preclinical development of novel anticancer drugs. *Expert Opin. Investig. Drugs* **17**, 197–208 (2008).

148. Ding, H. *et al.* Sensitivity to the non-COX inhibiting celecoxib derivative, OSU03012, is p21WAF1/CIP1 dependent. *Int. J. Cancer* **123**, 2931–2938 (2008).

149. Lowenberg, B., Downing, J. R. & Burnett, A. Acute Myeloid Leukemia. *N. Engl. J. Med.* **341**, 1051–1062 (1999).

150. Fan, Y., Schreiber, E. M., Giorgianni, A., Yalowich, J. C. & Day, B. W. Myeloperoxidase-catalyzed metabolism of etoposide to its quinone and glutathione adduct forms in HL60 cells. *Chem. Res. Toxicol.* **19**, 937–943 (2006).

151. Grzelak, A., Rychlik, B. & Bartosz, G. Light-dependent generation of reactive oxygen species in cell culture media. *Free Radic. Biol. Med.* (2001). doi:10.1016/S0891-5849(01)00545-7

152. Pick, E. & Keisari, Y. A simple colorimetric method for the measurement of hydrogen peroxide produced by cells in culture. *J. Immunol. Methods* **38**, 161–170 (1980).

153. Hill, V. L. & Manley, S. L. Release of reactive bromine and iodine from diatoms anfile:///Users/andrewmorgan/Downloads/Hill_et_al-2009-Limnology_and_Oceanography.pdfd its possible role in halogen transfer in polar

and tropical oceans. *Limnol. Oceanogr.* **54**, 812–822 (2009).

154. Ain, R., Tash, J. S. & Soares, M. J. A simple method for the in situ detection of eosinophils. *J. Immunol. Methods* (2002). doi:10.1016/S0022-1759(01)00526-9

155. Jemal, A., Thomas, A., Murray, T. & Thun, M. Cancer Statistics, 2002. *CA. Cancer J. Clin.* **52**, 23–47 (2002).

156. Kumar, B., Koul, S., Khandrika, L., Meacham, R. B. & Koul, H. K. Oxidative stress is inherent in prostate cancer cells and is required for aggressive phenotype. *Cancer Res.* (2008). doi:10.1158/0008-5472.CAN-07-5259

157. Ishikawa, K. ROS-generating mitochondrial DNA mutations can regulate tumor cell metastasis (Science (2008) (661)). *Science (80-.).* **321**, 342 (2008).

158. Traverso, N. *et al.* Role of Glutathione in Cancer Progression and Chemoresistance. *Oxid. Med. Cell. Longev.* (2013). doi:10.1155/2013/972913

159. Yeh, C.-C. *et al.* A study of glutathione status in the blood and tissues of patients with breast cancer. *Cell Biochem. Funct.* **24**, 555–559 (2006).

160. Ho, J. C. man, Zheng, S., Comhair, S. A. A., Erzurum, S. C. & Farver, C. Differential expression of manganese superoxide dismutase and catalase in lung cancer. *Cancer Res.* (2001).

161. Salzman, R. *et al.* Increased activity of superoxide dismutase in advanced stages of head and neck squamous cell carcinoma with locoregional metastases. *Neoplasma* (2007).

162. Chuang, T.-C. *et al.* Human manganese superoxide dismutase suppresses HER2/neu-mediated breast cancer malignancy. *FEBS Lett.* **581**, 4443–4449 (2007).

163. Behrend, L., Mohr, A., Dick, T. & Zwacka, R. M. Manganese Superoxide Dismutase Induces p53-Dependent Senescence in Colorectal Cancer Cells. *Mol. Cell. Biol.* (2005). doi:10.1128/mcb.25.17.7758-7769.2005

164. Castaldo, S. A., Freitas, J. R., Conchinha, N. V. & Madureira, P. A. The Tumorigenic Roles of the Cellular REDOX Regulatory Systems. *Oxidative Medicine and Cellular Longevity* (2016). doi:10.1155/2016/8413032

165. Foa, P. *et al.* Growth pattern of the human promyelocytic leukaemia cell line HL60. *Cell Prolif.* **15**, 399–404 (1982).

166. Maruf, A. Al, Wan, L. & O'Brien, P. J. Evaluation of Azathioprine-Induced Cytotoxicity in an In Vitro Rat Hepatocyte System . *Biomed Res. Int.* (2014). doi:10.1155/2014/379748

167. Reers, M., Smith, T. W. & Chen, L. B. J-Aggregate Formation of a Carbocyanine as a Quantitative Fluorescent Indicator of Membrane Potential. *Biochemistry* **30**, 4480–4486 (1991).

168. Senft, A. P., Dalton, T. P. & Shertzer, H. G. Determining glutathione and glutathione disulfide using the fluorescence probe o-phthalaldehyde. *Anal. Biochem.* (2000). doi:10.1006/abio.2000.4498

169. Duffy, C. P. *et al.* Enhancement of chemotherapeutic drug toxicity to human tumour cells in vitro by a subset of non-steroidal anti-inflammatory drugs (NSAIDS). *Eur. J. Cancer* (1998). doi:10.1016/S0959-8049(98)00045-8

170. Kang, P., Dalvie, D., Smith, E. & Renner, M. Bioactivation of lumiracoxib by peroxidases and human liver microsomes: Identification of multiple quinone imine

intermediates and GSH adducts. *Chem. Res. Toxicol.* (2009). doi:10.1021/tx8002356

171. Matsuo, T. *et al.* The percentage of myeloperoxidase-positive blast cells is a strong independent prognostic factor in acute myeloid leukemia, even in the patients with normal karyotype. *Leukemia* **17**, 1538–1543 (2003).

172. Sawayama, Y. *et al.* Expression of myeloperoxidase enhances the chemosensitivity of leukemia cells through the generation of reactive oxygen species and the nitration of protein. *Leukemia* **22**, 956–964 (2008).

173. Liu, Z. C. & Uetrecht, J. P. Clozapine is oxidized by activated human neutrophils to a reactive nitrenium ion that irreversibly binds to the cells. *J. Pharmacol. Exp. Ther.* **275**, 1476–1483 (1995).

174. Siraki, A. G., Bonini, M. G., Jiang, J., Ehrenshaft, M. & Mason, R. P. Aminoglutethimide-induced protein free radical formation on myeloperoxidase: A potential mechanism of agranulocytosis. *Chem. Res. Toxicol.* **20**, 1038–1045 (2007).

175. Venkataraman, H., Den Braver, M. W., Vermeulen, N. P. E. & Commandeur, J. N. M. Cytochrome P450-mediated bioactivation of mefenamic acid to quinoneimine intermediates and inactivation by human glutathione S-transferases. *Chem. Res. Toxicol.* **27**, 2071–2081 (2014).

176. Morgan, A. G. M., Babu, D., Michail, K. & Siraki, A. G. An evaluation of myeloperoxidase-mediated bio-activation of NSAIDs in promyelocytic leukemia (HL-60) cells for potential cytotoxic selectivity. *Toxicol. Lett.* **280**, (2017).

177. Zhu, B.-Z. *et al.* Unprecedented hydroxyl radical-dependent two-step chemiluminescence production by polyhalogenated quinoid carcinogens and H<inf>2</inf>O<inf>2</inf>. *Proc. Natl. Acad. Sci. U. S. A.* **109**, 16046–16051 (2012).

178. Masubuchi, Y., Saito, H. & Horie, T. Structural Requirements for the Hepatotoxicity of Nonsteroidal Anti-inflammatory Drugs in Isolated Rat Hepatocytes 1. *J. Pharmacol. Exp. Ther.* **287**, 208–213 (1998).

179. Siraki, A. G., Pourahmad, J., Chan, T. S., Khan, S. & O'Brien, P. J. Endogenous and endobiotic induced reactive oxygen species formation by isolated hepatocytes. *Free Radic. Biol. Med.* (2002). doi:10.1016/S0891-5849(01)00764-X

180. Pick, E. & Mizel, D. Rapid microassays for the measurement of superoxide and hydrogen peroxide production by macrophages in culture using an automatic enzyme immunoassay reader. *J. Immunol. Methods* (1981). doi:10.1016/0022-1759(81)90138-1

181. Rana, P., Naven, R., Narayanan, A., Will, Y. & Jones, L. H. Chemical motifs that redox cycle and their associated toxicity. *Medchemcomm* **4**, 1175–1180 (2013).

182. Soares, K. M. *et al.* Profiling the NIH small molecule repository for compounds that generate H2O2 by redox cycling in reducing environments. *Assay Drug Dev. Technol.* **8**, 152–174 (2010).

183. Soedjak, H. S. & Butler, A. Chlorination catalyzed by vanadium bromoperoxidase. *Inorg. Chem.* (1990). doi:10.1021/ic00350a003

184. Das, C. *et al.* Synthesis, characterization, X-ray crystal structure, DFT calculations,

and catalytic properties of a dioxidovanadium(V) complex derived from oxamohydrazide and pyridoxal: A model complex of vanadate-dependent bromoperoxidase. *Inorg. Chem.* (2014). doi:10.1021/ic501216d

185. Sollo, F. W., Larson, T. E. & Mcgurk, F. F. Colorimetric Methods for Bromine. *Environ. Sci. Technol.* (1971). doi:10.1021/es60050a009

186. Nauseef, W. M. Myeloperoxidase biosynthesis by a human promyelocytic leukemia cell line: Insight into myeloperoxidase deficiency. *Blood* **67**, 865–872 (1986).

187. Van Der Vliet, A., Eiserich, J. P., Halliwell, B. & Cross, C. E. Formation of reactive nitrogen species during peroxidase-catalyzed oxidation of nitrite: A potential additional mechanism of nitric oxide- dependent toxicity. *J. Biol. Chem.* (1997). doi:10.1074/jbc.272.12.7617

188. Winterbourn, C. C. & Kettle, A. J. Biomarkers of myeloperoxidase-derived hypochlorous acid. *Free Radic. Biol. Med.* (2000). doi:10.1016/S0891-5849(00)00204-5

189. Gaut, J. P. *et al.* Neutrophils employ the myeloperoxidase system to generate antimicrobial brominating and chlorinating oxidants during sepsis. *Proc. Natl. Acad. Sci. U. S. A.* **98**, 11961–11966 (2001).

190. Senthilmohan, R. & Kettle, A. J. Bromination and chlorination reactions of myeloperoxidase at physiological concentrations of bromide and chloride. *Arch. Biochem. Biophys.* (2006). doi:10.1016/j.abb.2005.07.005

191. Sawahata, T. & Neal, R. A. Horseradish peroxidase-mediated oxidation of phenol.

Biochem. Biophys. Res. Commun. **109**, 988–994 (1982).

192. Garner, C. E., Matthews, H. B. & Burka, L. T. Phenolphthalein metabolite inhibits catechol-O-methyltransferase- mediated metabolism of catechol estrogens: A possible mechanism for carcinogenicity. *Toxicol. Appl. Pharmacol.* (2000). doi:10.1006/taap.1999.8830

193. IARC Working Group on the Evaluation of Carcinogenic Risks to Humans, Some antiviral and antineoplastic drugs, and other pharmaceutical agents, in IARC Monographs of the Identification of Carcinogenic Hazards to Humans. *Int. Agency Res. Cancer Lyon, Fr.* 387–416 (2000).

194. Fiolet, J. W. T. & Van De Vlugt, F. C. The pH indicator phenol red as an artificial electron acceptor in spinach chloroplasts. *FEBS Lett.* (1975). doi:10.1016/0014-5793(75)80038-X

195. Morgan, A. G. M., Babu, D., Michail, K. & Siraki, A. G. An evaluation of myeloperoxidase-mediated bio-activation of NSAIDs in promyelocytic leukemia (HL-60) cells for potential cytotoxic selectivity. *Toxicol. Lett.* (2017). doi:10.1016/j.toxlet.2017.07.894

196. Ramakrishna Rao, D. N., Fischer, V. & Mason, R. P. Glutathione and ascorbate reduction of the acetaminophen radical formed by peroxidase. Detection of the glutathione disulfide radical anion and the ascorbyl radical. *J. Biol. Chem.* (1990).

197. Stoyanovsky, D. A. *et al.* Detection and characterization of the electron paramagnetic resonance-silent glutathionyl-5,5-dimethyl-1-pyrroline N-oxide adduct derived from redox cycling of phenoxyl radicals in model systems and HL-

60 cells. *Arch. Biochem. Biophys.* (1996). doi:10.1006/abbi.1996.0219

198. Hur, S.-J., Toda, H. & Yamada, M. Isolation and characterization of an unprocessed extracellular myeloperoxidase in HL-60 cell cultures. *J. Biol. Chem.* **264**, 8542–8548 (1989).

199. Selassie, C. D., Kapur, S., Verma, R. P. & Rosario, M. Cellular apoptosis and cytotoxicity of phenolic compounds: A quantitative structure-activity relationship study. *J. Med. Chem.* **48**, 7234–7242 (2005).

200. Khan, S. & O'Brien, P. J. 1-Bromoalkanes as new potent nontoxic glutathione depletors in isolated rat hepatocytes. *Biochem. Biophys. Res. Commun.* (1991). doi:10.1016/0006-291X(91)91389-T

201. Mitchell, J. B., Russo, A., Biaglow, J. E. & McPherson, S. Cellular Glutathione Depletion by Diethyl Maleate or Buthionine Sulfoximine: No Effect of Glutathione Depletion on the Oxygen Enhancement Ratio. *Radiat. Res.* (2006). doi:10.2307/3576226

202. Han, S. S. *et al.* Arsenic trioxide represses constitutive activation of NF-κB and COX-2 expression in human acute myeloid leukemia, HL-60. *J. Cell. Biochem.* (2005). doi:10.1002/jcb.20337

203. Kuntz, E. M. *et al.* Targeting mitochondrial oxidative phosphorylation eradicates therapy-resistant chronic myeloid leukemia stem cells. *Nat. Med.* **23**, 1234–1240 (2017).

204. Moschoi, R. *et al.* Protective mitochondrial transfer from bone marrow stromal cells to acute myeloid leukemic cells during chemotherapy. *Blood* **128**, 253–264

(2016).

205. Ichimori, S. *et al.* Development of a highly responsive needle-type glucose sensor using polyimide for a wearable artificial endocrine pancreas. *J. Artif. Organs* **9**, 105–113 (2006).

206. Lennicke, C., Rahn, J., Lichtenfels, R., Wessjohann, L. A. & Seliger, B. Hydrogen peroxide - Production, fate and role in redox signaling of tumor cells. *Cell Commun. Signal.* **13**, (2015).

207. Szatrowski, T. P. & Nathan, C. F. Production of Large Amounts of Hydrogen Peroxide by Human Tumor Cells. *Cancer Res.* **51**, 794–798 (1991).

208. Sattler, M. *et al.* Hematopoietic growth factors signal through the formation of reactive oxygen species. *Blood* **93**, 2928–2935 (1999).

209. Behrend, L., Henderson, G. & Zwacka, R. M. Reactive oxygen species in oncogenic transformation. *Biochem. Soc. Trans.* **31**, 1441–1444 (2003).

210. Lisanti, M. P. *et al.* Hydrogen peroxide fuels aging, inflammation, cancer metabolism and metastasis: The seed and soil also needs "fertilizer." *Cell Cycle* **10**, 2440–2449 (2011).

211. Sallmyr, A. *et al.* Internal tandem duplication of FLT3 (FLT3/ITD) induces increased ROS production, DNA damage, and misrepair: Implications for poor prognosis in AML. *Blood* **111**, 3173–3182 (2008).